

UNIVERSITÉ DU QUÉBEC À RIMOUSKI

**Étude paléomagnétique des sédiments holocènes de la Fosse du  
Mackenzie, mer de Beaufort**

Mémoire présentée

dans le cadre du programme de maîtrise en Océanographie  
en vue de l'obtention du grade de maître ès sciences

PAR

© Elissa Barris

Janvier 2014

UNIVERSITÉ DU QUÉBEC À RIMOUSKI  
Service de la bibliothèque

Avertissement

La diffusion de ce mémoire ou de cette thèse se fait dans le respect des droits de son auteur, qui a signé le formulaire « Autorisation de reproduire et de diffuser un rapport, un mémoire ou une thèse ». En signant ce formulaire, l'auteur concède à l'Université du Québec à Rimouski une licence non exclusive d'utilisation et de publication de la totalité ou d'une partie importante de son travail de recherche pour des fins pédagogiques et non commerciales. Plus précisément, l'auteur autorise l'Université du Québec à Rimouski à reproduire, diffuser, prêter, distribuer ou vendre des copies de son travail de recherche à des fins non commerciales sur quelque support que ce soit, y compris l'Internet. Cette licence et cette autorisation n'entraînent pas une renonciation de la part de l'auteur à ses droits moraux ni à ses droits de propriété intellectuelle. Sauf entente contraire, l'auteur conserve la liberté de diffuser et de commercialiser ou non ce travail dont il possède un exemplaire.



**Composition du jury :**

**Jean-Carlos Montero Serrano, président du jury, Université du Québec à Rimouski**

**Guillaume St-Onge, directeur de recherche, Université du Québec à Rimouski**

**André Rochon, codirecteur de recherche, Université du Québec à Rimouski**

**Stefanie Brachfeld, examinateur externe, Montclair State University**

Dépôt initial le 13 janvier 2014

Dépôt final le 23 mai 2014



"The ocean is a desert with its  
life underground and the perfect  
disguise above." - Dewey Bunnell



## ***REMERCIEMENTS***

Je remercie sincèrement Guillaume St-Onge pour la direction de cette maîtrise, pour sa disponibilité pour la discussion, et pour son encouragement au cours des dernières deux années. En plus, je suis reconnaissante pour les opportunités intéressantes et enrichissantes d'aider sur le terrain et pour les divers congrès et cours spécialisés auxquels j'ai eu la chance de participer. Je remercie aussi André Rochon pour ses conseils qui ont été nécessaires à la réalisation et la réussite de ce projet. Je remercie également Jean-Carlos Montero-Serrano et Stefanie Brachfeld pour avoir accepté d'évaluer mon mémoire.

Je dois aussi des remerciements au capitaine, à l'équipage et aux scientifiques à bord du NGCC *Amundsen* pendant la mission d'échantillonnage du projet Malina en 2009. Merci aussi au GEOTOP pour la bourse d'études supérieures de 2013, et à l'UQAR pour les bourses d'exemption des droits de scolarité supplémentaires exigés des étudiants étrangers qui ont grandement facilité mes travaux à Rimouski.

J'adresse un très grand merci à Jacques Labrie pour son aide avec les obstacles qui ont été rencontrés au cours du sous-échantillonnage, des mesures aux divers instruments au laboratoire, et avec des logiciels qui ont facilité l'analyse de mes données. Je remercie également Marie-Pier St-Onge pour sa disponibilité constante à mes questions techniques et pour les discussions théorétiques. Merci aussi à Sylvain Leblanc pour les analyses granulométriques et à Guillaume Massé pour les âges radiocarbone supplémentaires.

Finalement, je tiens à remercier tous mes camarades de laboratoire pour toutes les bonnes conversations sur la géologie et le paléomagnétisme qui ont inspirés des idées et soutenus l'intérêt au cours de l'analyse des données et lors de la rédaction du mémoire, aussi bien que pour leur appui moral et les nombreux cafés et bières partagés !



## **RÉSUMÉ**

Les études paléomagnétiques à haute résolution sont d'importance en magnétostratigraphie et géomagnétisme, particulièrement dans l'Arctique en raison de l'inaccessibilité et des faibles vitesses de sédimentation dans plusieurs secteurs. Deux carottes sédimentaires représentant l'Holocène récent ont été récoltées dans la Fosse du Mackenzie, une région avec des vitesses de sédimentation relativement élevées. Une carotte boîte et un *Calypso square core* ont été prélevés à deux sites (690 et 680). Les propriétés physiques et magnétiques et la granulométrie ont été mesurées, ainsi que les aimantations remanentes naturelle, anhystérétique, isothermale et isothermale saturée (NRM, ARM, IRM et SIRM). L'hystérésis magnétique indique une forte concentration de magnétite de type *pseudo-single domain*, un porteur idéal de rémanence, alors que les mesures de la susceptibilité magnétique suggèrent une concentration uniforme. Les valeurs de déviation angulaire maximale (MAD) et du champ médian destructif (MDF) indiquent des données de direction d'excellente qualité et une coercivité typique de la magnétite, respectivement. Finalement, dans la carotte 690 et la partie intermédiaire de la 680, l'inclinaison varie autour des valeurs d'un dipôle axial géocentrique (GAD) pour la latitude des sites, renforçant la fiabilité du signal paléomagnétique. Finalement, des *proxies* de la paléointensité relative ont été construits pour les carottes 690 et 680 en normalisant la NRM par l'IRM et l'ARM, respectivement.

Vingt-et-une coquilles de pélicypodes réparties dans les deux carottes ont été récoltées pour construire un modèle d'âge au radiocarbone à chaque site, une tâche nécessaire pour la mise en contexte d'un enregistrement paléomagnétique, mais souvent difficile dans l'Arctique. En utilisant ces modèles d'âge, les enregistrements paléomagnétiques ont été comparés avec d'autres provenant du bas-Arctique et des moyennes latitudes, soulignant leur potentiel pour des études magnétostratigraphiques

régionales et soutenant l'hypothèse que le cylindre tangentiel n'influence que le comportement du champ géomagnétique dans le Haut Arctique. De plus, des cycles quasi-périodiques ont été retrouvés dans les enregistrements de la susceptibilité magnétique et pourraient refléter l'influence du cycle solaire de Suess sur les oscillations Arctique et Pacifique décennale. Finalement, les mesures granulométriques indiquent une différence de provenance entre les deux sites, spécifiquement une source additionnelle de sédiments côtiers plus grossiers au site distal.

*Mots clés* : fosse du Mackenzie, mer de Beaufort, Arctique, Holocène, paléointensité relative, variations paléomagnétiques séculaires, variations solaires, oscillation Pacifique décennale



### ***ABSTRACT***

High-resolution paleomagnetic studies are of great importance to magnetostratigraphy and geomagnetism, especially in the Arctic due to the inaccessibility and slow sedimentation rates observed in many regions. Two sediment cores representing the late Holocene were sampled in the Mackenzie Trough, a site of relatively high sedimentation rates. One box core and one Calypso square core were recovered at each site (690 and 680). Physical and magnetic properties and grain size were measured, as well as natural, anhysteretic, isothermal and saturated remanent magnetizations (NRM, ARM, IRM and SIRM). Magnetic hysteresis parameters indicate a high concentration of pseudo-single domain magnetite, an ideal remanence carrier, while magnetic susceptibility and remanence measurements suggest a uniform concentration of these grains. Additionally, the maximum angular deviation (MAD) and median destructive field (MDF) values indicate excellent quality directional data and a coercivity typical of magnetite, respectively. In the entirety of core 690 and the middle section of core 680, inclination varies around the local geocentric axial dipole (GAD), supporting the reliability of the paleomagnetic signal. Relative paleointensity (RPI) proxies were successfully constructed for core 690 and 680 by normalizing the NRM by IRM and ARM, respectively.

A total of 21 pelecypod shells, distributed throughout both cores, were collected for the construction of radiocarbon-based age models at each site. This task is necessary for the placement of paleomagnetic records in their appropriate temporal contexts, though often challenging in the Arctic. Using their respective age models, the full-vector paleomagnetic records were compared with other low Arctic and mid-latitude records, highlighting their potential in regional magnetostratigraphic studies and furthermore supporting the hypothesis that the influence of the tangent cylinder on magnetic field behavior is limited to the High Arctic. Additionally, quasi-periodic cycles were found in the magnetic susceptibility records and could reflect the influence of the Suess solar cycle on the Arctic

and Pacific Decadal Oscillations. Finally, grain size measurements suggest a difference in provenance between the two sites, specifically a possible additional supply of larger-grained, coastal sediments to the more distal site.

*Key words:* Mackenzie Trough, Beaufort Sea, Arctic, Holocene, relative paleointensity, paleomagnetic secular variation, solar variations, Pacific Decadal Oscillation



*TABLE DES MATIÈRES*

REMERCIEMENTS .....	IX
RÉSUMÉ .....	XI
ABSTRACT .....	XIV ✓
TABLE DES MATIÈRES.....	XVII
LISTE DES TABLEAUX.....	XIX
LISTE DES FIGURES .....	XXI
INTRODUCTION GÉNÉRALE.....	26 ✓
PALEOMAGNETIC STUDY OF HOLOCENE SEDIMENTS FROM THE MACKENZIE RIVER TROUGH, BEAUFORT SEA.....	35
CONCLUSION .....	85
RÉFÉRENCES BIBLIOGRAPHIQUES .....	88 ✓



*LISTE DES TABLEAUX*

Tableau 1 : Core locations .....43

Tableau 2 : Radiocarbon dates from cores 690 and 680.....45



## *LISTE DES FIGURES*

Figure 1: Location of cores 690 (green) and 680 (red) in the Mackenzie Trough, Beaufort Sea .....	42
Figure 2: Subsampling of u-channels from an open CASQ core on the deck of the CCGS Amundsen; u-channels in core 680 were overlapped by at least 10 cm in order to avoid the loss of paleomagnetic data due to the 4.5 cm smoothing function of the magnetometer .....	47
Figure 3A: CT-scan images, average grain size and sorting, and percentages of clay and silt core 690 .....	50
Figure 3B: CT-scan images, average grain size and sorting, and percentages of clay, silt and sand for core 680 .....	51
Figure 4: Examples of the correlation of physical properties, $L^*$ , $a^*$ , and Ti content, between the CASQ cores and their associated box cores for A) core 690 and B) core 680 .....	52
Figure 5: Demagnetization of NRM, ARM, IRM, and SIRM for A) core 690 and B) core 680 .....	53
Figure 6A: Orthogonal projections (Zijderveld diagrams) of demagnetization at various depths in core 690, with open diamonds representing the vertical projection of the magnetization vector and closed diamonds the horizontal projection. Also shown are AF demagnetization plots with the MDF indicated .....	54

- Figure 6B: Orthogonal projections (Zijderveld diagrams) of demagnetization at various depths in core 680, with open diamonds representing the vertical projection of the magnetization vector and closed diamonds the horizontal projection. Also shown are AF demagnetization plots with the MDF indicated ..... 55
- Figure 7: Measured inclination shown with the geocentric axial dipole (GAD), relative declination, maximum angular deviation (MAD), median destructive field (MDF), and  $IRM_{10mT}/SIRM_{10mT}$  (pseudo S-ratio) for A) core 690 and B) core 680. Unreliable intervals in core 680 are shaded in gray and correspond to the upper and lower sections of the core (see text for details) ..... 57
- Figure 8: Magnetic hysteresis measurements (corrected to remove the paramagnetic component) from the top, near middle, and bottom of A) core 690 and B) core 680, with the raw measurement shown by the dashed curve. These examples are representative of hysteresis properties measured throughout the cores ..... 58
- Figure 9: Day plot visualizing hysteresis parameters for core 690 (green) and core 680 (red), delimiting the single domain (SD), pseudo-single domain (PSD), and multi domain (MD) particle size ranges ..... 59
- Figure 10: NRM, ARM, IRM and SIRM over the characteristic range (20-60 mT), median destructive field (MDF), low-field magnetic susceptibility ( $k_{LF}$ ), and grain size parameters  $SIRM_{30-50mT}/k_{LF}$  and  $k_{ARM}/k_{LF}$  for A) core 690 and B) core 680 ..... 61
- Figure 11: Age models, with A) three linked linear fits for core 690 and B) a 4th order polynomial fit for core 680, with open points representing excluded ages (see text for details) ..... 63

Figure 12: Inclination of core 690 and core 680 shown with the <i>CALS3k.4</i> geomagnetic field model output at station 690, as well as cores 5JPC and 6JPC from the Chukchi Sea, core 803PC from the Beaufort Sea, core 006PC from the Northwest Passage, and a core from Mara Lake in British Columbia. Also shown is the Western U.S. PSVL record .....	66
Figure 13: Relative declination of core 690 and core 680 shown with the <i>CALS3k.4</i> geomagnetic field model output at station 690, as well as cores 5JPC and 6JPC from the Chukchi Sea, core 803PC from the Beaufort Sea, core 006PC from the Northwest Passage, a core from Mara Lake in British Columbia, and the Western U.S. PSVL record .....	67
Figure 14: Demagnetization curves showing magnetization normalized by maximum magnetization for NRM, ARM, IRM, and SIRM versus the applied field .....	69
Figure 15: Coherence of different RPI calculations with their respective normalizers for A) core 690, B) core 680, and C) the middle section of core 680. The gray lines mark a confidence level of 95% .....	70
Figure 16: RPI of core 690 and core 680 shown with the <i>CALS3k.4</i> geomagnetic field model output at station 690, as well as cores 5JPC and 6JPC from the Chukchi Sea, and core 803PC from the Beaufort Sea .....	71
Figure 17: NRM, MDF, $k_{LF}$ , and $k_{ARM}/k_{LF}$ versus age for A) core 690 and B) core 680. Possible high-frequency variations are visible in the $k_{LF}$ record, especially for core 690; corresponding bands of higher magnetic susceptibility between the two cores are suggested by shaded intervals .....	75
Figure 18: Wavelet analysis of A) unsmoothed and B) smoothed (sf = 3) $k_{LF}$ in core 690 .....	76
Figure 19: Wavelet analysis of A) unsmoothed and B) smoothed (sf = 3) $k_{LF}$ in core 680 .....	77

Figure 20: Cross-wavelet coherence between core 690 and core 680 for A) unsmoothed and  
B) smoothed ( $sf = 3$ )  $k_{LF}$  ..... 78

Figure 21: Comparison of  $k_{LF}$  with  $\delta^{18}O$  records from New Mexico and Colorado, and a  
precipitation reconstruction from Washington..... 81



## *INTRODUCTION GÉNÉRALE*

Ce projet de maîtrise se concentre sur l'étude paléomagnétique, paléoclimatique et océanographique des sédiments marins de l'ouest de l'Arctique, près de la côte des Territoires du Nord-Ouest et du Yukon dans le mer de Beaufort. Deux carottes sédimentaires ont été échantillonnées dans la Fosse du Mackenzie, un secteur où les vitesses de sédimentation sont exceptionnellement élevées et qui incise la partie ouest de la marge continentale du bassin Beaufort-Mackenzie. Le projet se divise en deux objectifs principaux : 1) reconstruire l'évolution récente du champ magnétique terrestre dans l'Arctique de l'ouest, et 2) reconstituer l'histoire climatique et environnementale de l'Arctique de l'ouest au cours de l'Holocène récent.

### *Échantillonnage et mesures*

Afin de répondre à ces deux objectifs principaux, deux sites ont été sélectionnés dans la Fosse du Mackenzie, à environ 150 km de l'embouchure du fleuve. Les sites ont été choisis en raison des vitesses de sédimentation élevées dans la fosse (e.g., Hill et al., 1991; Macdonald et al., 1998; Bringué et Rochon, 2012). Les échantillons utilisés proviennent de deux carottes boîtes et deux carottes de type *Calypso square core* (CASQ). Le CASQ, un carottier à gravité de grand volume, a l'avantage de permettre la récolte d'une grande quantité de sédiment peu perturbé et de préserver l'interface eau-sédiment qui est habituellement détruite par le carottage à piston. Une carotte CASQ et une carotte boîte ont été prélevées à chaque site.

Les analyses de laboratoire comportant des mesures physiques et magnétiques ont été effectuées sur les *u-channels* prélevés dans les carottes CASQ et boîte. Dans un premier temps, les observations visuelles ainsi que la mesure de la composition chimique

par fluorescence X (XRF), la réflectance (spectrophotométrie) et la susceptibilité magnétique ont été effectuées à chaque centimètre. Suite à l'analyse de ces propriétés physiques, l'aimantation rémanente naturelle (NRM) a été mesurée et démagnétisée à l'aide d'un champ magnétique alternatif afin de déterminer le spectre de coercivité des minéraux magnétiques et d'isoler l'aimantation caractéristique. Le même processus a été répété avec les aimantations induites artificiellement, dont l'aimantation rémanente anhystérétique (ARM), isothermale (IRM), et isothermale saturée (SIRM). Des analyses tomographiques au CAT-scan ont également été effectuées pour visualiser les structures sédimentaires et obtenir une mesure de densité. Finalement, les *u-channels* ont été sous-échantillonnés à des intervalles de 5 cm pour les analyses granulométriques alors que d'autres échantillons ponctuels ont été prélevés aux limites de sections pour les mesures de l'hystérésis magnétique qui fournit de l'information sur la granulométrie et la minéralogie magnétique.

### *L'étude paléomagnétique*

Les enregistrements paléomagnétiques à haute résolution sont nécessaires dans la compréhension des variations paléomagnétiques séculaires et des changements de paléointensité à haute fréquence. Néanmoins, ils restent particulièrement rares dans l'Arctique où des vitesses de sédimentation assez élevées pour révéler les traits géomagnétiques aux échelles millénaires et séculaires sont plus difficiles à trouver. Une connaissance plus développée de ces variations est exigée particulièrement aux hautes latitudes pour la mise en contexte des événements récents observés dans le champ magnétique dont, par exemple, la migration rapide du pôle Nord magnétique du Canada vers la Sibérie (e.g., Jackson et al., 2000; Olsen et Mandeia, 2007; St-Onge et Stoner, 2011). Les variations spatiales, telle que l'évolution des *lobes de flux* (Figure 1), des régions de flux magnétique plus intense également situées sous le Canada et la Sibérie, peuvent être mieux comprises par l'inter-comparaison avec d'autres enregistrements environnants (e.g., Bloxham et Gubbins, 1985; Jackson et al., 2000; Stoner et al., 2013).

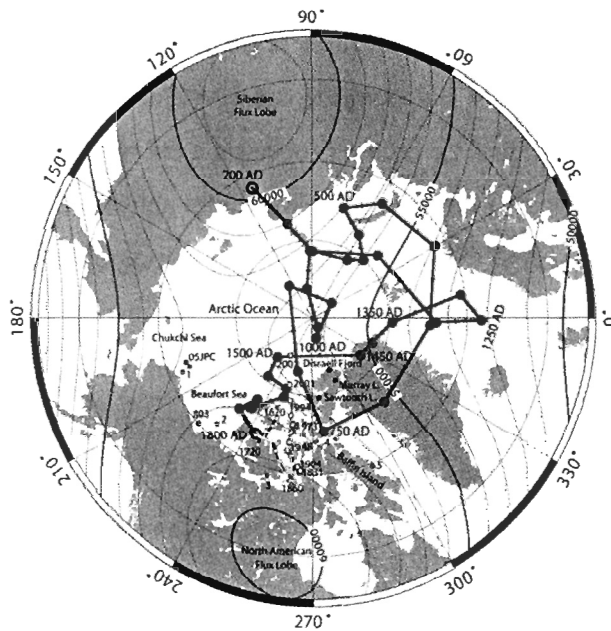


**Figure 1** : Reconstitution de la migration récente du pôle Nord magnétique à partir de données paléomagnétiques (points rouges), de données historiques (points bleus) et de données observées (points jaunes), avec la délimitation des lobes de flux actuels (cercles rouges). Tiré de St-Onge et Stoner (2011).

Les enregistrements de résolution temporelle élevée sont aussi nécessaires pour contribuer à la magnétostratigraphie et potentiellement servir à dater les enregistrements sédimentaires arctiques. La chronostratigraphie est une partie essentielle de toute étude temporelle, qu'elle soit paléomagnétique ou environnementale. Cependant, les méthodes de datation conventionnelles pour établir un modèle d'âge dans les études holocènes, notamment la datation à l'aide du  $^{14}\text{C}$ , peut parfois représenter un défi de taille. Cette problématique est particulièrement commune dans l'Arctique, alors que les matériaux datables sont généralement rares en raison d'une dissolution du matériel carbonaté plus rapide dans les eaux froides (Jutterström et Anderson, 2005). De plus, le temps de résidence du carbone inorganique dissous dans l'eau, qui rend le matériel daté plus ancien, contrôle le degré auquel les âges mesurés doivent être corrigés et peut varier significativement entre différentes régions des océans. Le manque de mesures précises de cet *effet réservoir* dans l'Arctique produit une fiabilité limitée de la calibration des âges  $^{14}\text{C}$  au cours de l'Holocène. Dans ce contexte, la magnétostratigraphie à haute résolution est particulièrement utile dans l'Arctique. En effet, cette technique propose une façon alternative pour déterminer l'âge relatif d'un enregistrement récent en le corrélant avec d'autres enregistrements paléomagnétiques bien datés de la même région (e.g., Lisé-

Pronovost et al., 2009; Barletta et al., 2010; St-Onge et Stoner, 2011; Ólafsdóttir et al., 2013). Cette technique permet la vérification des modèles d'âge existant et peut également aider à l'établissement de marqueurs chronostratigraphiques régionaux additionnels pour une utilisation conjointe avec les dates du radiocarbone.

L'emplacement des carottes a également une valeur potentielle pour les modèles géomagnétiques. Actuellement, les modèles du champ magnétique sont basés sur des données obtenues en majorité dans l'hémisphère nord, mais principalement au sud de 60° latitude (e.g., Stoner et al., 2007; Barletta et al., 2008; Lisé-Pronovost et al., 2009; Ólafsdóttir et al., 2013; Korte et al., 2011; Figure 2). Cette lacune de données paléomagnétiques dans les hautes latitudes doit être comblée afin de vérifier le niveau de précision des modèles existants dans les régions telle que l'Arctique qui sont éloignées des sources de données. Les enregistrements fiables à haute résolution ont aussi le potentiel de contribuer à la calibration et à la contrainte des futurs modèles géomagnétiques.

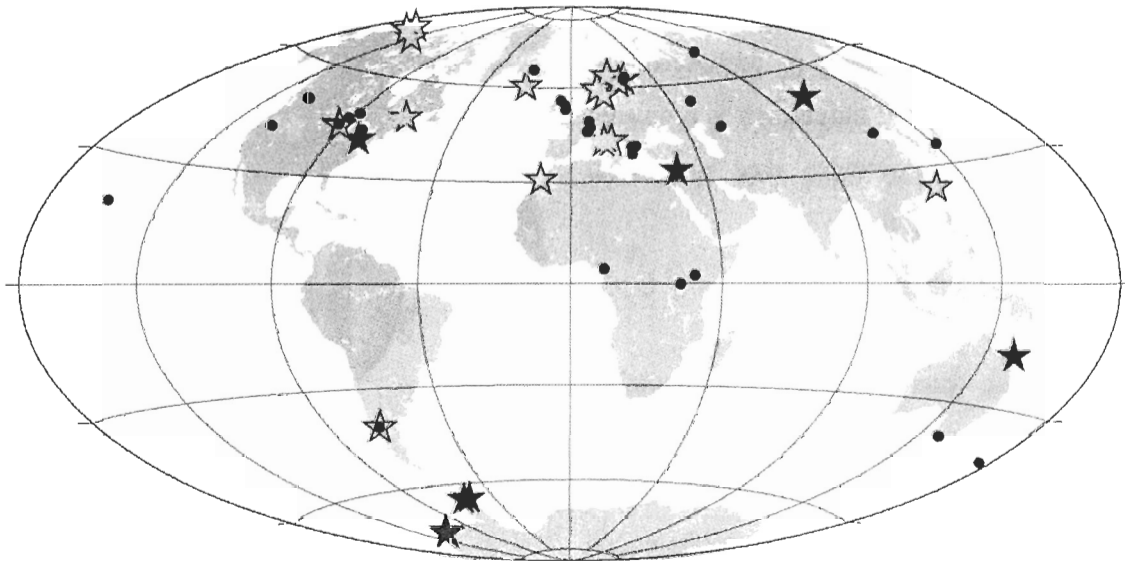
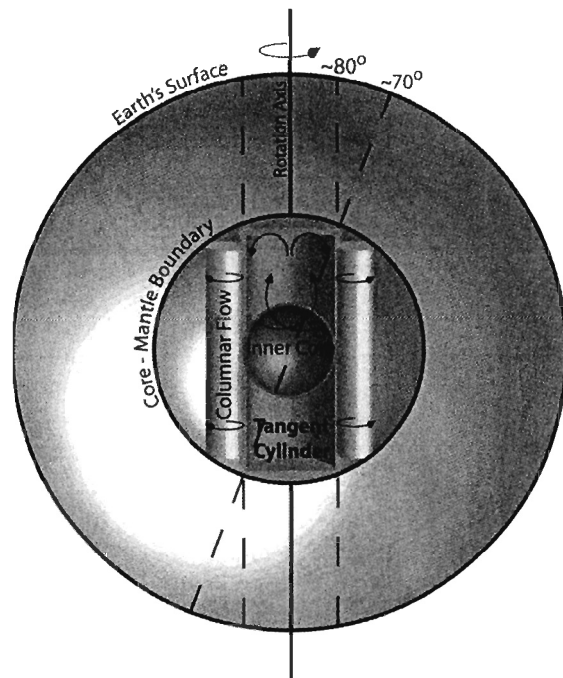


**Figure 2** : Carte illustrant le manque de données aux latitudes supérieures à 60°N dans le dernier modèle géomagnétique *CALS3k.4* (Korte et al., 2011). Les données de direction sont représentées par les étoiles jaunes, les données d'intensité par les étoiles rouges et les étoiles jaunes avec le contour rouge, alors que les données provenant des modèles géomagnétiques antérieurs sont illustrées par les points bleus. Tiré de Korte et al. (2011).

Le comportement du champ magnétique aux hautes latitudes est actuellement très peu documenté. Or, il y présente un comportement différent au niveau des pôles magnétiques contrairement aux latitudes plus basses. En raison des caractéristiques de convection dans le noyau externe qui génère le champ magnétique, une région avec un comportement différent existe potentiellement au sein du *cylindre tangentiel*, un régime cylindrique hypothétique tangent au noyau interne et parallèle à l'axe de rotation (Figure 3). Ce régime est supposé être représenté à la surface de la Terre à environ 69.5°N, mais plus d'enregistrements à haute résolution doivent être étudiés afin de savoir si des différences se manifestent au niveau de la surface et de comprendre d'autres caractéristiques tels que les lobes de flux et la migration des pôles magnétiques (St-Onge et Stoner, 2011).

**Figure 3** : Schéma représentant les régimes de convection dans le noyau externe soulignant la différence de comportement au sein du cylindre tangentiel et montrant l'intersection du cylindre avec la surface. Tiré de Lawrence et al. (2009).



Ainsi, dans ce mémoire de maîtrise, deux nouveaux enregistrements des changements de direction et d'intensité du champ géomagnétique pendant l'Holocène récent seront présentés dans l'optique de :

- développer l'utilité de la magnétostratigraphie régionale dans l'ouest de l'Arctique ;
- vérifier les modèles géomagnétiques dans une région sous-représentée par les données ;
- améliorer notre compréhension du comportement du champ aux hautes latitudes.

À cette fin, les enregistrements géomagnétiques seront comparés avec d'autres enregistrements voisins ainsi qu'avec les résultats du dernier modèle de Korte et al. (2011) afin de tester leur intérêt en magnétostratigraphie et de déterminer l'étendue de l'influence du cylindre tangentiel et des lobes du flux dans le bas-Arctique.

### *L'étude environnementale*

Le deuxième objectif du projet est d'analyser l'histoire climatique, environnementale, et océanographique de la région lors de l'Holocène récent, particulièrement les derniers  $\approx$  2500 ans, en utilisant les mesures magnétiques, physiques et granulométriques des carottes. En raison des vitesses de sédimentation élevées des sites d'échantillonnage, mesurées entre 220 et 320 cm/ka dans une étude récente au même emplacement mené par Durantou et al. (2012), cette étude présente des archives climatiques et océanographiques de résolution temporelle exceptionnelle en comparaison avec les autres régions de l'Arctique. Comme c'est le cas pour le paléomagnétisme, une résolution temporelle élevée est nécessaire pour investiguer les variations environnementales qui ont lieu à des échelles de temps plus courtes ou lors des processus cycliques séculaires à décennaux.

L'emplacement des deux carottes promet une perspective intéressante concernant les processus océanographiques de la région puisque ce secteur n'est pas uniquement sous l'influence du fleuve Mackenzie, mais également des courants marins profonds et de surface (Figure 4). La carotte la plus au large du delta présente un intérêt particulier car cette zone est connue pour être affectée par le courant profond de Beaufort. Ce courant originaire de l'océan Pacifique par l'intermédiaire du détroit de Béring s'écoule typiquement vers l'est le long de la marge continentale de Beaufort (Aagaard, 1984; Carmack et Macdonald, 2002; Pickart, 2004). De plus, la sédimentation du site le plus profond est potentiellement sensible à certains traits de la circulation de surface, notamment le tourbillon cyclonique de Beaufort dominant dans la région (e.g., Pickart, 2004). En revanche, le site moins profond est plus influencé par des courants de surface poussés par le vent. Il y a ainsi deux régimes distincts, le premier s'écoulant vers le nord-est en suivant la côte et le second orienté vers l'ouest en direction du delta et de la Fosse du

Mackenzie (e.g., Harper et Penland 1982; Hill et al., 1991; Carmack et Macdonald, 2002). Le panache (*plume*) de sédiment créé à l'embouchure du fleuve n'occupe que la partie sommitale de la colonne d'eau (les 2-3 premiers mètres). Ce dernier est ensuite poussée vers l'est par les courants de surface provenant du remplissage préférentiel dans la partie est de la fosse (e.g., Doraxan et al., 2012). Un des objectifs de ce projet de maîtrise est donc d'étudier les diverses caractéristiques océanographiques et hydrographiques relatives aux deux sites et d'évaluer ainsi l'importance des variations de profondeur et de distance à la côte.

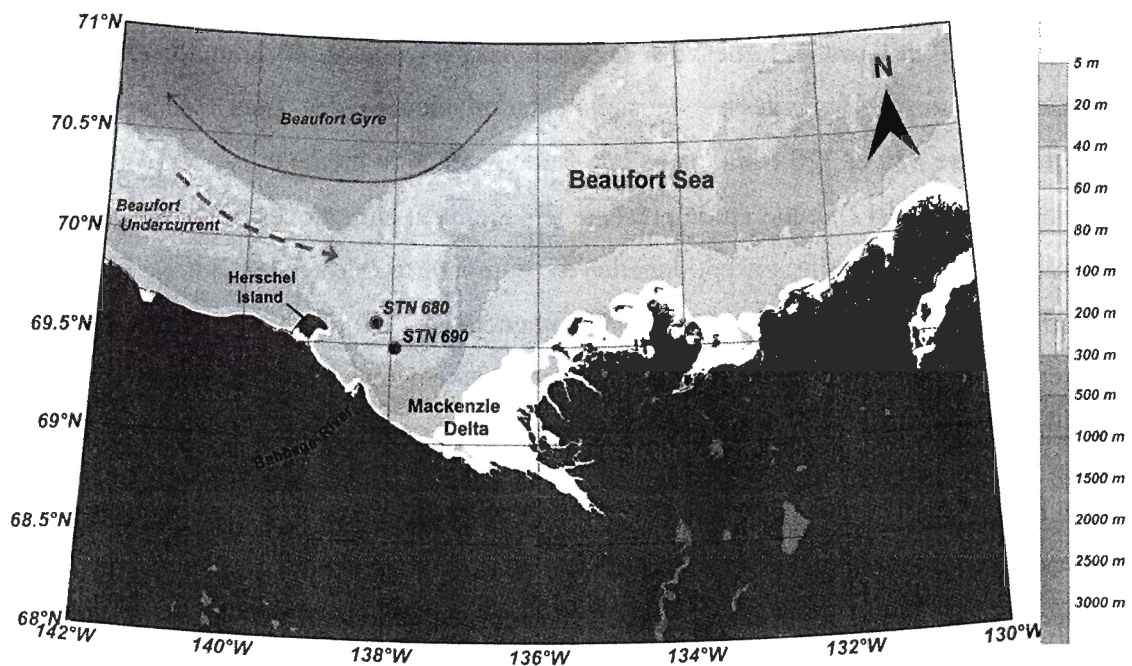


**Figure 4 :** Localisation de la carotte 690 (vert) et 680 (rouge) dans la fosse du Mackenzie, mer de Beaufort.

Les deux carottes présentent également l'opportunité d'investiguer la présence des différents régimes d'accumulations sédimentaires. La sédimentation est principalement dominée par les apports silteux et argileux du fleuve Mackenzie, mais d'autres sources de sédiment sont potentiellement présentes plus au large dans le delta. Les deux sources les plus tangibles étant la rivière Babbage au Yukon et l'érosion côtière, spécialement

provenant de l'île Herschel, connue pour accumuler des sédiments plus grossiers d'origine continentale (Hill et al., 1991; Lantuit et Pollard, 2008). Ces sources additionnelles pourraient constituer des différences dans le triage et la granulométrie entre les deux archives et de plus révéler le rôle des courants marins et atmosphériques dans le transport de sédiments dans la fosse. De tels assemblages apporteront ainsi des précisions sur l'histoire hydrologique et l'évolution côtière de la région.

D'autres études menées dans l'Arctique ont mis en évidence dans des séquences sédimentaires des cycles climatiques telles que l'oscillation Pacifique décennale, l'oscillation Arctique et l'oscillation nord-Atlantique (e.g., Bringué et Rochon, 2012; Durantou et al., 2012). Des archives enregistrant des cycles solaires existent également et peuvent indirectement influencer les divers processus environnementaux en raison de leurs impacts sur les cycles atmosphériques et océaniques (e.g., Bond et al., 2001; Hu et al., 2003; Bringué et Rochon, 2012). Un dernier objectif important de ce projet de maîtrise est de déterminer si de tels oscillations sont observables dans l'enregistrement sédimentaire de la Fosse du Mackenzie, et dans le cas présent, de les replacer dans le contexte climatique de tout l'ouest de l'Arctique pour évaluer les limites spatiales des différentes oscillations atmosphériques et investiguer les possibles interactions entre plusieurs de ces processus.

### *Objectifs et organisation du mémoire*

Pour mieux comprendre le comportement du champ magnétique terrestre, il est nécessaire d'avoir accès à des enregistrements paléomagnétiques continus, de haute résolution temporelle, et surtout provenant de régions polaires pour évaluer la dynamique du champ près du cylindre tangentiel. De tels enregistrements présentent également un intérêt particulier en magnétostratigraphie. Cette méthode est souvent exigée en conjonction avec, ou en remplacement de, la datation au radiocarbone dans les sédiments arctiques difficiles à dater. Finalement, différencier les divers sources de sédiments, déterminer les différents processus contrôlant la sédimentation, et extraire les signaux naturels et anthropogéniques font partie des plus grands défis se présentant dans le domaine de la paléoclimatologie. Les régimes océaniques et systèmes hydrologiques de

l'Arctique restent des régions insuffisamment étudiées à cet égard alors que la gamme naturelle des variations, notamment dans les cycles solaires et atmosphériques, les précipitations et les réponses hydrologiques, est une partie essentielle pour la compréhension des changements environnementaux actuellement observés dans l'Arctique.

Ce mémoire est présenté sous forme d'un article scientifique, rédigé en anglais avec l'intention de le soumettre à une revue internationale (à déterminer). Il cherche d'une part à reconstruire les variations du champ géomagnétique à haute résolution, mais aussi à évaluer les processus climatiques, environnementaux et océanographiques qui influencent la sédimentation dans la Fosse du Mackenzie. Je suis l'auteure principale, rédigeant sous la supervision des professeurs Guillaume St-Onge et André Rochon de l'ISMER. Je suis aussi responsable de la majeure partie des travaux de laboratoire, excluant la granulométrie qui a été réalisée par Sylvain Leblanc (ISMER) et la datation au radiocarbone qui a été effectuée à l'Université Laval (Québec, Canada), l'Université de Géorgie (Athens, É.U.) et à l'Université de Californie à Irvine (Irvine, É.U.). Quatre âges au radiocarbone additionnels ont été obtenus au Commissariat de l'énergie atomique et aux énergies alternatives (Saclay, France) et fournies par le professeur Guillaume Massé (Takuvik). J'ai effectué l'interprétation de toutes les données et créé les figures présentées dans l'article avec l'aide technique de Jacques Labrie et Marie-Pier St-Onge (ISMER). L'échantillonnage a été menée en août 2009 dans le cadre du projet international *Malina* à bord le brise-glace NGCC *Amundsen*.

# PALEOMAGNETIC STUDY OF HOLOCENE SEDIMENTS FROM THE MACKENZIE RIVER TROUGH, BEAUFORT SEA

ELISSA BARRIS<sup>1,2</sup>, GUILLAUME ST-ONGE<sup>1,2,3</sup>, ANDRÉ ROCHON<sup>1,3</sup>

<sup>1</sup>Institut des sciences de la mer de Rimouski (ISMER)

<sup>2</sup>Chaire de recherche du Canada en géologie marine/Canada Research Chair in Marine Geology

<sup>3</sup>GEOTOP

## ABSTRACT

High-resolution paleomagnetic studies are of great importance to magnetostratigraphy and geomagnetism, especially in the Arctic due to the inaccessibility and slow sedimentation rates observed in many regions. Two sediment cores representing the late Holocene were sampled in the Mackenzie Trough, a site of relatively high sedimentation rates. One box core and one Calypso square core were recovered at each site (690 and 680). Physical and magnetic properties and grain size were measured, as well as natural, anhysteretic, isothermal and saturated remanent magnetizations (NRM, ARM, IRM and SIRM). Magnetic hysteresis parameters indicate a high concentration of pseudo-single domain magnetite, an ideal remanence carrier, while magnetic susceptibility and remanence measurements suggest a uniform concentration of these grains. Additionally, the maximum angular deviation (MAD) and median destructive field (MDF) values indicate excellent quality directional data and a coercivity typical of magnetite, respectively. In the entirety of core 690 and the middle section of core 680, inclination varies around the local geocentric axial dipole (GAD), supporting the reliability of the paleomagnetic signal. Relative paleointensity (RPI) proxies were successfully constructed for core 690 and 680 by normalizing the NRM by IRM and ARM, respectively.

A total of 21 pelecypod shells, distributed throughout both cores, were collected for the construction of radiocarbon-based age models at each site. This task is necessary for the placement of paleomagnetic records in their appropriate temporal contexts, though

often challenging in the Arctic. Using their respective age models, the full-vector paleomagnetic records were compared with other low Arctic and mid-latitude records, highlighting their potential in regional magnetostratigraphic studies and furthermore supporting the hypothesis that the influence of the tangent cylinder on magnetic field behavior is limited to the High Arctic. Additionally, quasi-periodic cycles were found in the magnetic susceptibility records and could reflect the influence of the Suess solar cycle on the Arctic and Pacific Decadal Oscillations. Finally, grain size measurements suggest a difference in provenance between the two sites, specifically a possible additional supply of larger-grained, coastal sediments to the more distal site.

*Key words:* Mackenzie Trough, Beaufort Sea, Arctic, Holocene, relative paleointensity, paleomagnetic secular variation, solar variations, Pacific Decadal Oscillation

## **1. Introduction**

High-resolution (centennial- to millennial-scale) paleomagnetic records offer valuable insight on short-term variations of the Earth's magnetic field, and are additionally useful as a regional stratigraphic tool. Many continuous, sedimentary paleomagnetic records representing the Holocene have been developed in recent decades, contributing to a more complete understanding of geomagnetic field variability (e.g. Turner and Thompson, 1981; Creer and Tucholka, 1982; Lund and Banerjee, 1985; Verosub et al., 1986; Lund, 1996; Brachfeld et al., 2000; Gogorza et al., 2000; St-Onge et al., 2003; Snowball et al., 2007; Barletta et al., 2010b). Paleomagnetic records, derived from generally continuous, high-resolution lacustrine and marine sedimentary sequences (e.g., Turner and Thompson, 1981; Verosub et al., 1986; Barletta et al., 2008; Lisé-Pronovost et al., 2009), among absolute paleomagnetic data from archeomagnetic and volcanic studies (e.g., Gallet et al., 2002; Hagstrum and Champion, 2002), have enabled the calibration of global geomagnetic field models such as *CALS3K.4*, *CALS7K.2*, and *CALS10K.1b* (Korte et al., 2005; Korte and Constable, 2005; Korte and Constable, 2011; Korte et al., 2011). These models have so far been demonstrated to generally reproduce the centennial- and millennial-scale variability observed in paleomagnetic records (e.g., Lisé-Pronovost et al., 2009; Barletta et

al., 2010a; Haberzettl et al., 2012). However, more paleomagnetic data from sparsely studied regions, such as the Northern high latitudes (i.e.  $> 60^\circ$  N), are needed to provide additional constraints on the aforementioned models, so as to reduce regional biases on global estimates of direction and intensity (Snowball et al., 2007; Genevey et al., 2008; Knudsen et al., 2008; Sagnotti et al., 2011; Korte and Muscheler et al., 2012). In this study, two high-latitude, high-resolution, full-vector paleomagnetic records are developed from the Mackenzie Trough, offshore of the Mackenzie River delta on the Beaufort Sea Shelf (Northwest and Yukon Territories, Canada). Recent, i.e. Late Holocene, datasets such as these offer a means of testing the accuracy of, as well as potentially better constraining, geomagnetic field models over regions underrepresented by real data. They may also give valuable insight on high-latitude geomagnetic field behavior, which is key to further developing geodynamo theory. Studies such as this specifically address the "tangent cylinder" feature of the geodynamo, a probable convection regime in the outer core theorized to lie tangent to the inner core along the Earth's rotational axis, and projected to intersect the Earth's surface at approximately  $69.5^\circ$  N and S (e.g., Kono and Roberts, 2003; St-Onge and Stoner, 2011). It is thought that differences in outer core convection within this regime could be manifested in geomagnetic field behavior at high latitudes, which would additionally have important implications for magnetic pole migration and magnetic flux lobe evolution, though more paleomagnetic data from both the High and Low Arctic are needed to support this hypothesis (e.g., Bloxham and Gubbins, 1985; Kono and Roberts, 2003; St-Onge and Stoner, 2011).

Continuous paleomagnetic records can also aid in developing relative chronologies using magnetostratigraphy, in which paleomagnetic secular variations and sometimes relative paleointensity features of proximal sediment records are synchronized with one another in order to establish regional chronostratigraphic markers (e.g., Stoner and St-Onge, 2007; Stoner et al., 2007; Roberts et al., 2013). Directional correlation between sites can be more powerful in the Arctic than at lower latitudes, since high-latitude records, by nature of their proximity to the North magnetic pole, have the potential to exhibit higher amplitude variations in inclination and declination (Lisé-Pronovost et al., 2009; Barletta et al., 2010a). Furthermore, Holocene radiocarbon-based chronostratigraphy can be more challenging in the marine Arctic due to the rarity of datable material, as well as the often

poorly constrained reservoir effect. A reliable age model is a central requirement of any paleoclimatic or paleomagnetic study, making magnetostratigraphy vital as a means of independently supporting radiocarbon-based chronologies, especially where datable material is sparser than desired or calibration accounting for the reservoir effect is questionable (e.g., Lisé-Pronovost et al., 2009; Barletta et al., 2010a; St-Onge and Stoner, 2011; Ólafsdóttir et al., 2013). However, due to the inaccessibility and low sedimentation rates of many Arctic marine locations, high-resolution Holocene paleomagnetic records representing the northern high latitudes ( $> 60^\circ$  N) are also sparse (e.g., Andrews and Jennings, 1990; Snowball and Sandgren, 2002; Geiss and Banerjee, 2003; Snowball and Sandgren, 2004; Snowball et al., 2007; Stoner et al., 2007; Barletta et al., 2008; Lisé-Pronovost et al., 2009; Barletta et al., 2010b; Sagnotti et al., 2011; Ólafsdóttir et al., 2013). Thus the continental shelves and slopes of Arctic marginal seas, many of which, such as the Beaufort Sea, have relatively high sedimentation rates (Darby, 2006), present promising sampling realms for the investigation of centennial- and millennial-scale variability of the high latitude geomagnetic field.

High-resolution sediment records play a similarly valuable role in the study of Arctic paleoenvironments. The magnetic and physical properties of Arctic sediments (i.e. magnetic susceptibility, grain size, and mineralogy) can be interpreted as signals of variations in the regional environment as well as possible climatic processes (e.g., Liu et al., 2012; Simon et al., 2013; St-Onge and St-Onge, in press). Recent marine records from the Arctic provide insight on late Holocene regional environmental changes, such as variations in sediment output, precipitation and runoff (e.g., Dean, 1997; Lisé-Pronovost et al., 2009; Habertzettl et al., 2010; Durantou et al., 2012). They can also shed light on periodic or quasi-periodic atmospheric processes occurring on decadal, centennial, and millennial scales (Zachos et al., 2001; Bringué and Rochon, 2012; Boyer-Villemare et al., 2013). Multi-annual to multi-decadal cycles such as the Arctic Oscillation, closely related to the North Atlantic Oscillation, play a strong role in controlling Arctic surface currents (including intake from the Pacific Ocean through the Bering Strait), as well as precipitation and continental runoff (Niebauer and Day, 1989; Thompson and Wallace, 1998; Ambaum et al., 2001; Déry and Wood, 2004; Macdonald et al., 2005). The importance of the Arctic Oscillation as a leading control on natural climate variability in the Arctic has been

demonstrated by previous high-resolution paleoceanography studies in the Mackenzie Trough and nearby sites in the southern Beaufort Sea (e.g., Bringué and Rochon, 2012; Durantou et al., 2012). Additionally, the interrelated Pacific Decadal Oscillation, Aleutian Low, and El Niño Southern Oscillation have also been proposed to influence the Western Arctic in particular (Niebauer and Day, 1989; Overland et al., 1999; Macdonald et al., 2005; Carmack et al., 2006). Impacts of the Pacific Decadal Oscillation were identified in a previous study at the same site as this one over the last  $\approx$  150 yrs, which linked positive phases of the oscillation to relatively warm, high-salinity periods governed by increased supplies of Pacific waters to the Beaufort Shelf (Durantou et al., 2012).

Finally, the relationship between solar activity and climate is also an important subject of investigation; whether and how sedimentary records may indirectly record solar cycles could provide key insights on their influence over regional climate variability (Bond et al., 2001; Shindell et al., 2001; Hu et al., 2003; Wiles et al., 2004). Evidence for a possible link between paleoceanography records and solar activity in the Beaufort region has been previously proposed: for example, Bringué and Rochon (2012) identified several cool periods in a core from the southern Beaufort Sea, near the Mackenzie Trough. The most recent of these periods could be correlated to the Little Ice Age, which, is thought to be related to the consecutive Wolf, Spörer, and Maunder solar minima (e.g., Lean and Rind, 1999; Bond et al., 2001; Wiles et al., 2004; Koch et al., 2007). The two records of magnetic and physical properties evaluated here were obtained at exceptionally high resolutions relative to many Arctic sediment records, and they not only present important information to high latitude geomagnetic and magnetostratigraphic studies, but may also provide further evidence of the influence of solar or atmospheric cycles on regional climate.

## **2. Regional Geologic Setting**

### *2.1. Sedimentology*

The continental seas and marginal shelves of the Western Arctic are ideal locations for paleomagnetic and paleoclimatic studies due to their high levels of sedimentation

relative to much of the Arctic Ocean (Darby et al., 2006). The Mackenzie River, the fourth largest Arctic river in terms of freshwater discharge (largest in the North American Arctic), is the largest single source of sediment to the Arctic and dominates sedimentation on the Beaufort Shelf, carrying an annual load of  $\approx 125$  Mt of sediment (Hill et al., 1991; Carson et al., 1998; Macdonald et al., 1998). The Mackenzie Trough itself exhibits the highest rate of sediment accumulation in the region, often reaching a few millimeters per year (e.g., Hill et al., 1991; Macdonald et al., 1998; Richerol et al., 2008; Scott et al., 2009; Bringué and Rochon, 2012; Durantou et al., 2012), making the feature an attractive candidate for recent, high-resolution studies such as this, as compared to many other Arctic regions having generally lower sedimentation rates (e.g., Rochon and de Vernal, 1994; Ledu et al., 2008). In fact, rates ranging from 220 to 320 cm/ka through the late Holocene were recently measured at the location of this study (Durantou et al., 2012). The trough holds between 30 and 50 m of Holocene sediment overlying late Pleistocene deglacial deposits (Blasco et al., 1990; Hill et al., 1991; Batchelor et al., 2013). High-resolution seismic reflection data reveal the continuous, parallel, and low-amplitude internal reflectors of this uppermost sequence, suggesting deposition primarily from the vertical accretion of sediments out of suspension (Elverhøi et al., 1980; Dowdeswell et al., 1997; Kleiber et al., 2000; Batchelor et al., 2013). Signs of gentle progradation are also apparent, and support previous suggestions by Hill et al. (1991, 1996) of a preferential eastward infilling of the trough (Batchelor et al., 2013).

The postglacial sediment load of the Mackenzie River consists primarily of silt and some clay with a minimal percentage of fine sand, in contrast to the significantly sandier sediments of the Mackenzie Shelf (Blasco et al., 1990; Carson et al., 1998; Hill et al., 1996, 2001; Barletta et al., 2008; Scott et al., 2009). Sedimentation offshore of the delta, i.e. at depths greater than  $\approx 10$  m, occurs principally through the deposition of fine particles out of suspension (Hill et al., 1991), and cores at these depths reveal sediment facies consisting almost entirely of fine, bioturbated mud, breaking down into a silt/clay ratio of  $\approx 2$  (e.g., Vilks et al., 1979; Pelletier, 1984; Hill et al., 2001; Richerol et al., 2008; Scott et al., 2009; Jerosch et al., 2012; Durantou et al., 2012). In general, postglacial sedimentation on much of the North American Arctic continental margin is dominated by fine-grained, fluvially and glacially eroded sediments of continental terrain, which is often rich in ideal

magnetic remanence carriers such as magnetite and titanomagnetite (Bischof and Darby, 1997, 1999; Darby, 2003; Darby and Bischof, 2004; Stoner and St-Onge, 2007; Barletta et al., 2008).

The Mackenzie River accounts for  $\approx 95\%$  of sedimentation on the Beaufort Shelf, though other significant contributions are derived from coastal erosion and several Yukon rivers (Hill et al., 1991). Two features in particular, the highly erosive Herschel Island and the Babbage River in northern Yukon, could provide minor additional sources of sediment to the study area, and are especially close to site 680. Coastal erosion, though a small contribution to overall sedimentation by volume, accounts for the majority of sand and gravel found on the Beaufort Shelf, and is also known to be the source of larger-grained deposits on Herschel Island (Hill et al., 1991; Lantuit and Pollard, 2008).

## *2.2. Hydrology and oceanography*

The Mackenzie Delta is a vast, complex system of distributary channels extending about 210 km from the mouth of the river and spanning a width of about 87 km (Lewis, 1988). It forms a shallow shelf roughly 120 km wide and 530 km long, with the Mackenzie Trough carved along its western side (Carmack et al., 2004). The head of the Mackenzie Trough lies about 80 km farther to the northwest from the lower delta plain, converging gradually with the long pro-delta slope. The high rates of freshwater discharge (ranging from 249 to 333 km<sup>3</sup> annually), which fluctuate strongly seasonally, contribute strongly to the highly variable quality of surface circulation patterns near the delta (Macdonald et al., 1998; Hill et al., 2001; Dittmar and Kattner, 2003). However, offshore of the delta other Arctic circulation patterns play an increasingly dominant role. One of the more prominent features in surface circulation in the Western Arctic is the Beaufort Gyre, an anticyclonic gyre (dominated by westward flow) along the northern edge of the Mackenzie and Beaufort shelves (Pickart, 2004). Beneath the Beaufort Gyre, halocline waters flow along the continental margin from the Pacific Ocean in Beaufort Undercurrent, which is generally cyclonic (dominated by eastward flow) but known to reverse its direction (Carmack and Macdonald, 2002; Pickart, 2004). Sedimentation on the continental shelf largely occurs through the transport of fine particles in suspension in the Mackenzie plume, which occupies a thick (2-3 m) surface-layer and is therefore strongly influenced by

wind-driven surface currents. There are two dominant regimes: one characterized by an along-shore east-northeastward flow and another by a westward flow toward the Mackenzie Trough (Harper and Penland, 1982; Hill et al., 1991; Carmack and Macdonald, 2002; Macdonald et al., 2002; Doraxan et al., 2012). These currents grow weaker with depth, but on the outer shelf, i.e. at depths  $> 60$  m, a stronger current regime is again observed due to the added influence of another easterly current, possibly an extension of the Beaufort Undercurrent from the Alaskan shelf (Aagaard, 1984; Hill et al., 1991; Pickart, 2004). This contribution, along with that of wind-driven surface currents flowing in the same direction, results in a net eastward drift of the Mackenzie River's plume of suspended sediment, and therefore a preferential eastward infilling of sediment in the Trough (Hill et al., 1991, 1996, 2001; Carmack and Macdonald, 2002). These deposition patterns are readily apparent in the bathymetry of the area, with the Trough axis visibly curving from northwest to north (Figure 1).

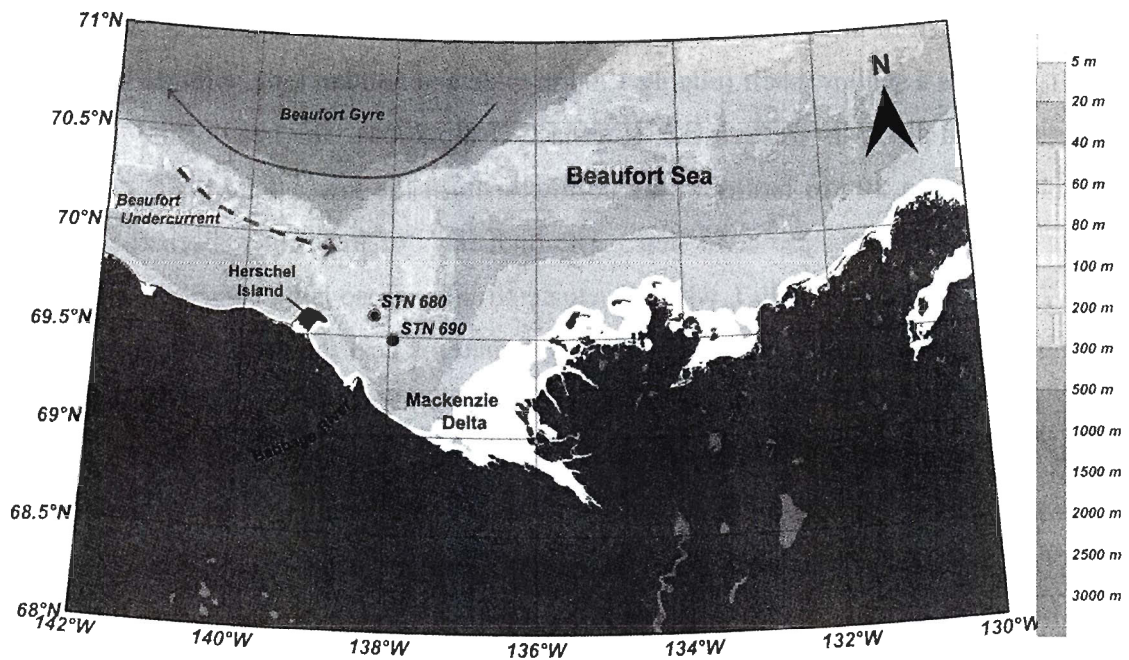


**Figure 1:** Locations of core 690 (green) and 680 (red) in the Mackenzie Trough, Beaufort Sea.

### 3. Materials and Methods

#### 3.1 Coring sites

Calypso square (CASQ) sediment cores, large gravity cores with a 25 x 25 cm cross-section, along with corresponding box cores, were recovered from two sites, STN 690 and STN 680, in the Mackenzie River Trough (Figure 1). Sampling was conducted in August 2009 aboard the Canadian research ice-breaker the CCGS *Amundsen* during a leg of the international Malina project. Two nearby coring sites were selected based on previous studies demonstrating the high rates of sedimentation in the Mackenzie Trough (e.g., Hill et al., 1991; Macdonald et al., 1998; Rochon et al., 2003). Core 690 was located at 69.49° N, 137.94° W, about 100 km from the mouth of the Mackenzie River in a water depth of 54 m, and was 3.60 m long. Core 680, at 69.61° N, 138.21° W, was located about 17 km farther down the trough in a water depth of 122 m, and was 5.06 m long (Table 1, Figure 1). The Calypso square (CASQ) corers are advantageous for recent studies such as this one, as they result in minimal sediment perturbation and are designed to preserve the sediment-water interface, permitting the comparison of results with historical and observational records.

**Table 1:** Core locations.

Core	Latitude (°N)	Longitude (°W)	Depth (m)	Length (m)
690, box/CASQ	69.49	137.94	54	3.60
680, box/CASQ	69.61	138.21	122	5.06

#### 3.2 Physical Analysis

U-channels (u-shaped plastic liners of 2 x 2 cm cross-section) were subsampled from the upper 4.00 m of the station 680 CASQ core on deck. The lowermost section of the CASQ was unrecoverable due to implosion of the CASQ liner. U-channels were also sampled from push cores sampled at sea in both companion box cores. In the Paleo and Environmental Magnetism Laboratory at the *Institut des sciences de la mer de Rimouski* (ISMER), u-channels were subsampled from the individual sections of the station 690 CASQ core, except for the top 10 cm which were too soupy.

All u-channels were analyzed at 1 cm intervals with a GEOTEK Multi-Sensor Core Logger (MSCL) at ISMER enabling the continuous and simultaneous measurement of X-ray fluorescence using an Innov-X XRF spectrometer, diffuse spectral reflectance using a Konika Minolta model here color spectrophotometer, and low-field volumetric magnetic susceptibility using a Barlington MS2E point sensor (e.g., St-Onge et al., 2007). X-ray fluorescence measures the bulk concentration of individual elements, some of which, namely iron and titanium, can reflect variations in the overall magnetic mineralogy of the sediment. Even though the XRF results are presented as ppm, only relative changes are used as an absolute calibration of the sediment was not performed. Diffuse spectral reflectance can also offer insight on changes in mineralogy, with redness in particular evidencing the presence of hematite. It is recorded in the CIE 1979 ( $L^*$ ,  $a^*$ ,  $b^*$ ) color space, where the parameter  $L^*$  represents a scale from black (0) to diffuse white (100),  $a^*$  from green (-) to red (+), and  $b^*$  from blue (-) to yellow (+) (e.g. St-Onge et al., 2007). Finally, low-field magnetic susceptibility ( $k_{LF}$ ) primarily reflects changes in the concentration of ferrimagnetic minerals, as well as to a lesser degree the size of magnetic grains, with larger grains resulting in a greater  $k_{LF}$  (e.g., Stoner and St-Onge, 2007). U-channels were also photographed by a high-resolution digital camera mounted on the MSCL. Some MSCL data measured from core 680 should be treated with caution, as many thin cracks occurred in the sediment due to drying, some large enough to produce gaps in discrete measurements such as  $k_{LF}$  and color.

In order to identify sedimentary structures and check for signs of possible core deformation, all the u-channels were then passed through a Computerized Axial Tomography Scan (CAT-scan) at the *Institut national de la recherche scientifique, Centre Eau Terre Environnement (INRS-ETE)* in Québec City, Canada. This allows imaging at a cross-sectional resolution of 0.23 mm and an axial resolution of 0.6 mm. Additionally, the computed tomography (CT) numbers, which serve as a measure of bulk density (St-Onge et al., 2007; Fortin et al., 2003), were extracted from the images at 1 mm intervals.

### 3.3 Radiocarbon Analysis

On board, 8 pelecypod shells or shell fragments and three mixed benthic-planktonic foraminifera samples were collected from the station 680 CASQ core for radiocarbon

analysis. The samples were sent to the Center for Applied Isotope Studies at the University of Georgia in Athens, Georgia and the Radiochronology Laboratory, *Centre d'études nordiques* at Université Laval in Quebec City, Quebec for Accelerator Mass Spectroscopy (AMS) radiocarbon dating (Table 2).

**Table 2:** Radiocarbon dates from cores 690 and 680.

Core	Sample	Lab No.	Depth (cm)	Composite Depth (cm)	Material	<sup>14</sup> C Age (yr BP)	Calibrated Age* (cal BP)
690 BC2	690-5	ULA-3410	0	0	Bivalve	<i>modern</i>	<i>modern</i>
690 CASQ	690-1	SacA-18295	4	14	Bivalve	1230 ± 30	489 ± 158
690 CASQ	690-6	ULA-3411	15	25	Bivalve	1565 ± 15	788 ± 154
680 CASQ	680-2	ULA-3002	47.5	47.5	Bivalve	1250 ± 20	513 ± 149.5
680 CASQ	680-10	ULA-3010	80	80	foraminifera	1490 ± 25	722 ± 167.5 **
690 CASQ	690-7	ULA-3412	102	112	Bivalve	1835 ± 15	1070 ± 179
690 CASQ	690-3	SacA-18297	123	133	Bivalve	1990 ± 35	1188 ± 194
690 CASQ	690-8	ULA-3413	146	156	Bivalve	1945 ± 20	1141 ± 177
680 CASQ	680-1	ULA-3001	174	174	Bivalve	1545 ± 30	776 ± 163.5
690 CASQ	690-4	SacA-18298	175	185	Bivalve	2020 ± 30	1226 ± 196
690 CASQ	690-9	ULA-3414	179.5	189.5	Bivalve	2320 ± 20	1549.5 ± 209.5 ***
690 CASQ	690-10	ULA-3415	185.5	195.5	Bivalve	2210 ± 20	1441.5 ± 184.5
690 CASQ	690-11	ULA-3416	209	219	Bivalve	2250 ± 20	1481.5 ± 191.5
680 CASQ	680-9	ULA-3009	210	210	foraminifera	2325 ± 25	1560 ± 94 **
680 CASQ	680-7	ULA-3007	251.5	251.5	Bivalve <i>Nuculana</i>	2015 ± 25	1219 ± 190
690 CASQ	690-12	ULA-3417	266	276	Bivalve	2790 ± 20	2102.5 ± 208.5 ***
680 CASQ	680-3	ULA-3003	291.5	291.5	Bivalve <i>Macoma</i>	2060 ± 30	1279 ± 200
680 CASQ	680-4	ULA-3004	315.5	315.5	Bivalve <i>Bathyrca</i> Gastropod <i>Naticidae</i>	2035 ± 30	1245 ± 198
690 CASQ	690-13	ULA-3418	320.5	320.5	Bivalve	2640 ± 20	1920 ± 218
680 CASQ	680-5	ULA-3005	337.5	337.5	Bivalve <i>Macoma</i>	2430 ± 20	1674 ± 212
690 CASQ	690-14	ULA-3419	355	355	Bivalve	2800 ± 20	2112 ± 207
680 CASQ	680-8	ULA-3008	405	405	foraminifera	2860 ± 25	2167 ± 223 **
680 CASQ	680-6	ULA-3006	482.4	482.4	Bivalve	2990 ± 20	2388.5 ± 261.5

\*Calibrated with CALIB6.0 online software (Stuiver et al., 2005),  $\Delta R = 335 \pm 85$  yrs (Coulthard et al., 2010).

\*\*Mixed foram ages excluded from the final age model (see text for details).

\*\*\*Bivalve ages excluded from the final age model (see text for details).

In the laboratory, during the sampling of u-channels from the station 690 core, 9 pelecypod shells were collected and analyzed at the KECK Carbon Cycle AMS Facility at the University of California in Irvine, California and once again the Radiochronology Laboratory at Université Laval (Table 2). One shell collected from the surface of the station 690 box core was confirmed to be modern (i.e., containing bomb <sup>14</sup>C), and the top of the core was assigned the assumed age of -59 cal BP, corresponding to the year of

sampling in 2009. Additionally, four pelecypod shells were collected from a second set of u-channels, subsampled on deck from the station 690 CASQ core by Guillaume Massé (*Laboratoire d'océanographie et du climat à Paris*) in collaboration with the Malina project, and analyzed at the *Laboratoire de Mesure du Carbone 14, Commissariat à l'énergie atomique et aux énergies alternatives* (CEA) in Saclay, France (Table 2).

Radiocarbon analyses were conducted using Libby's half life (i.e. 5568 yrs) and corrected for isotopic fractionation after the convention established by Stuiver and Polach (1977). All dates were reported initially in conventional radiocarbon age ( $^{14}\text{C}$  yrs BP), and converted to calibrated years (cal BP) using the online calibration software CALIB6.0 developed by Stuiver et al. (2005) with the Marine09.14c dataset. A  $\Delta R$  value of  $335 \pm 85$  yrs was used for calibration, based on a regional marine reservoir offset measured for the nearby Northwest Canadian Arctic archipelago by Coulthard et al. (2010).

#### 3.4 Rock Magnetic and Paleomagnetic Analysis

Paleomagnetic data were measured along all u-channels at ISMER using a 2G Enterprises cryogenic magnetometer. Because of the edge effect associated with the response function of the cryogenic magnetometer pick-up coils (Weeks et al., 1993), the upper and lowermost 5 cm of data from each u-channel were excluded from the ends of u-channels at section breaks to eliminate the edge effects effectuated by this response function, except for cases where on-deck sampling allowed for overlap, as for the bulk of core 680 (Figure 2). In addition, because of this edge effect, the thin cracks seen in core 680 did not cause a problem in the magnetic measurements as they did in the MSCL measurements. Data were omitted due to edge effects in core 690 from 157 to 166 cm and from 260 to 269 cm. The first 15 cm of box core data were merged with the CASQ record to account for the fact that the top 10 cm of the CASQ was too soupy to effectively sample. The only data which had to be excluded due to edge effect in core 680 are from 8 to 17 cm, since other u-channels were overlapped by 10 cm during sampling.

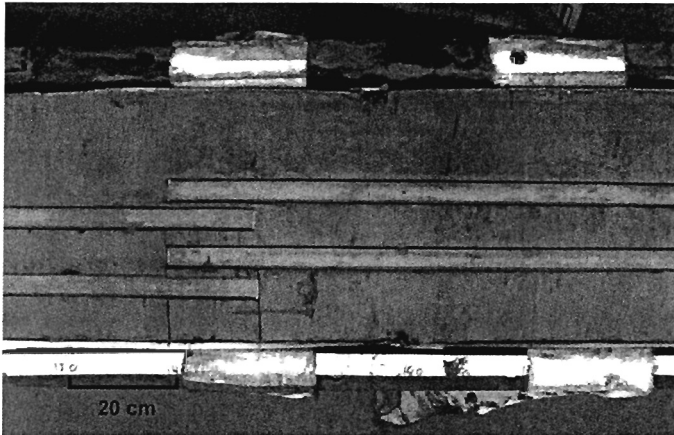


**Figure 2:** Subsampling of u-channels from an open CASQ core on the deck of the CCGS *Amundsen*; u-channels in core 680 were overlapped by at least 10 cm in order to avoid the loss of paleomagnetic data due to the 4.5 cm smoothing function of the magnetometer.

The natural remanent magnetization (NRM) was determined by applying stepwise alternating field (AF) demagnetization at peak fields increasing from 0 to 80 mT in 5 mT increments and measuring after each step. Data for demagnetization steps between 20 and 60 mT were selected to represent the characteristic remanent magnetization (ChRM), excluding components representing any possible viscous remanent magnetization (VRM). Inclination and declination were calculated over the characteristic range, as well as maximum angular deviation (MAD), a measure of the precision of the magnetization vector at any one step relative to the geometry of the overall magnetization, using the Mazaud (2005) software, which employs a principal component analysis (PCA) routine using a least-square line fitting technique (Kirschvink, 1980). Also computed is the median destructive field (MDF), the demagnetizing peak field needed to reduce the initial magnetic remanence by half.

After measuring the NRM, an anhysteretic remanent magnetization (ARM) was induced using a peak AF of 100 mT and a 0.05 mT direct current (DC) biasing field, and subsequently stepwise demagnetized and measured following the same procedure as for the NRM. Next, an isothermal remanent magnetization (IRM) was imparted using a pulse magnetizer module to induce a 0.3 T DC pulse field. After demagnetization and measurement, again along the same increments as the NRM and ARM, a saturated isothermal remanent magnetization (SIRM) was imparted by a 0.95 T DC pulse field. The SIRM was demagnetized and measured at 0, 10, 30, and 50 mT.

Magnetic hysteresis properties, which primarily relate to magnetic mineralogy and granulometry, were measured under a field (and equal back-field) applied in 10 mT increments to a maximum of 1 T using a Princeton Measurements Corp alternating gradient force magnetometer (AGM) at ISMER. Sediment for these measurements was sampled from the section breaks of each core (at the top or bottom of each u-channel), yielding 10 measurements for core 690 and 8 measurements for core 680, including box core samples. Magnetic hysteresis parameters, saturation magnetization ( $M_s$ ), saturation remanence ( $M_{rs}$ ), coercivity ( $H_c$ ), and coercivity of remanence ( $H_{cr}$ ), were derived from the measured hysteresis and IRM backfield curves.

The NRM acquired by the sediment as well as the various laboratory-induced magnetizations are, like magnetic susceptibility, strongly dependent upon the concentration of magnetic minerals present. However, different types of magnetization activate different assemblages of magnetic grains, and can therefore be normalized by other magnetic parameters to characterize magnetic grain size and mineralogy (e.g., King et al., 1982; Thompson and Oldfield, 1986; Brachfeld and Banerjee, 2000; Maher et al. 1999; Stoner and St-Onge, 2007). When normalized by a concentration-dependent magnetic parameter, commonly a laboratory-induced magnetization (ARM, IRM, or SIRM), the NRM can be regarded as a proxy of relative paleointensity (RPI) independent of changes in the concentration of magnetic grains downcore (e.g., Tauxe, 1993; Valet, 2003; Stoner and St-Onge, 2007). The stability of the NRM can be ascertained by low MAD values; values  $< 5^\circ$  are generally considered to represent a high precision directional record (Stoner and St-Onge, 2007). Variations in magnetic grain size can be deduced by normalizing SIRM by  $k_{LF}$ , which is inversely proportional to the size of the remanence carrying grains and most sensitive among particles  $> 10 \mu\text{m}$  (Thompson and Oldfield, 1986). Anhysteretic susceptibility ( $k_{ARM}$ : the ARM divided by the intensity of the DC biasing field applied during magnetization) normalized by  $k_{LF}$  also varies inversely with magnetic grain size if the magnetic assemblage consists predominantly of magnetite; this ratio is more sensitive to particles between 1 and  $10 \mu\text{m}$  (King et al., 1982). Information about magnetic mineralogy can be obtained by normalizing IRM by SIRM (the pseudo S-ratio); values close to 1 indicate primarily low-coercivity remanence carriers such as magnetite (e.g., St-Onge et al., 2003). The MDF is also dependent on mean coercivity, with values between  $\approx$

20 and 40 mT corresponding to magnetite (Dankers, 1981). In cases of uniform mineralogy, variations in MDF are inversely proportional to magnetic grain size as coercivity decreases for coarser grains (Dankers, 1981).

### *3.5 Grain Size Analysis*

All u-channels were sampled at 5 cm intervals for physical grain size analysis, which, together with magnetic grain size, can offer information on the consistency of river discharge and whether multiple sediment sources or currents influencing deposition are at play. Samples were added to a Calgon<sup>®</sup> electrolytic solution, sodium hexametaphosphate, and mixed for about 3 hours using an in-house rotator, prior to being disaggregated in an ultrasonic bath for 90 seconds in preparation for analysis. Sieving was not necessary for any samples, since the sediment was visibly composed of fine silt with minimal amounts of very fine sand, all particles being smaller than 2 mm in diameter. Grain size and sorting measurements were conducted on the disaggregated samples using a Beckman-Coulter LS-13320 laser diffractometer (0.04-2000  $\mu\text{m}$ ). The grain size data were processed using the GRADISTAT software for analyzing sediment parameters (Blott and Pye, 2001).

## **4. Results**

### *4.1 Lithology and Stratigraphy*

Both cores consist almost entirely of homogeneous fine-grained mud, uniformly gray-brown to olive-gray clayey silt. Using the geometric method of moments function in the GRADISTAT software, the sediment in both cores was classified as muddy fine silt, and was poorly sorted for the majority of both cores ( $2 \leq \sigma \leq 4$ ) (Blott and Pye, 2001). Noticeably poorer sorting is observed throughout core 680, with average values of  $\sigma = 3.32$ , as compared to the core 690 average of  $\sigma = 2.82$ . Core 680 also had a slightly larger average grain size, while core 690 exhibits uniformly fine sediment throughout the core, with the exception of the 20 cm mark, where a significant proportion of silt and a very small amount of sand are also observed (Figure 3). In core 690 a uniform, dark gray color is observed down the entire core (Munsell color value of 2.5Y 4/1). Color is relatively

uniform in core 680, varying from grayish brown (2.5Y 5/2) at the top of the core, to very dark gray (2.5Y 3/1), to gray (2.5Y 5/1), and finally returning to dark gray (2.5Y 4/1) near the base of the core. No distinct boundaries or rapid changes are visually observable, and furthermore the minor variations could be attributable to dried and altered condition of the core 680 u-channels, which made the judgment of color challenging. The overall uniformity of color in both cores is supported by spectrophotometry profiles. For example, changes in  $L^*$  vary between  $\approx 25$  and 45 for both cores, with the exception of large and small outlying values representing anomalous features such as shell fragments and cracks in the record. Traces of bioturbation are apparent regularly throughout both cores. No well-defined lithologic unit boundaries are apparent in either core (Figure 3). These color, grain size, and sorting characteristics are typical of Arctic postglacial shelf deposits (e.g., Syvitski, 1991; Darby et al., 2006; Keigwin et al., 2006), and the lithology is consistent with other post-glacial sediment cores sampled in the southern Beaufort Sea (e.g., Rochon et al., 2003; Barletta et al., 2008; Lisé-Pronovost et al., 2009; Bringué et al., 2012; Durantou et al., 2012).

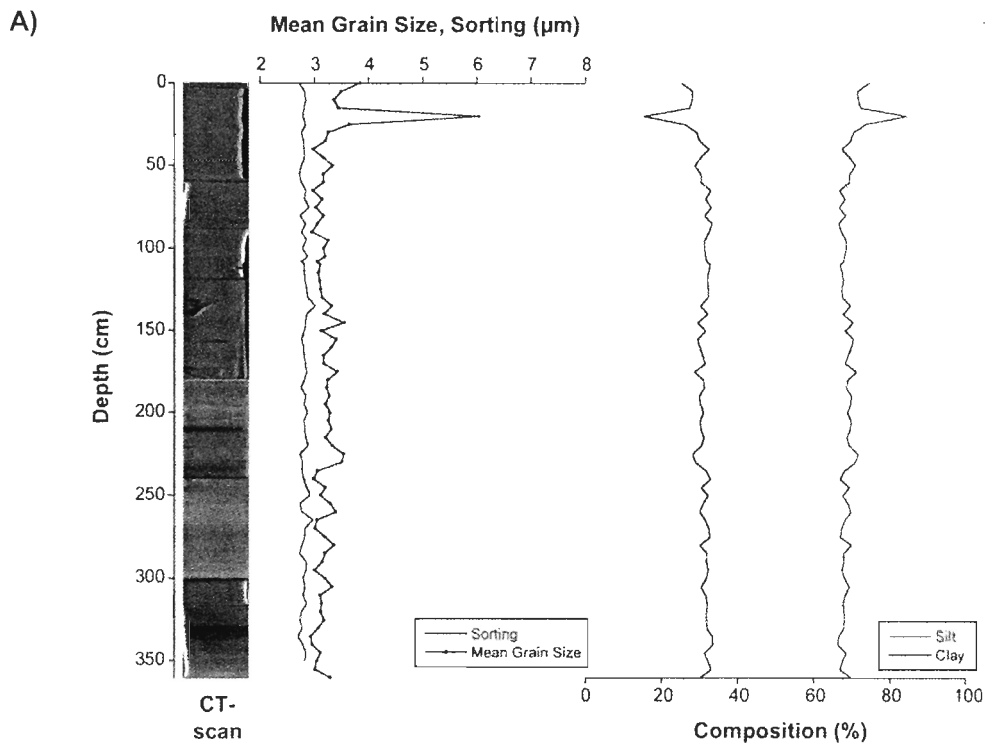


**Figure 3A:** CT-scan images, average grain size and sorting, and percentages of clay and silt for core 680.

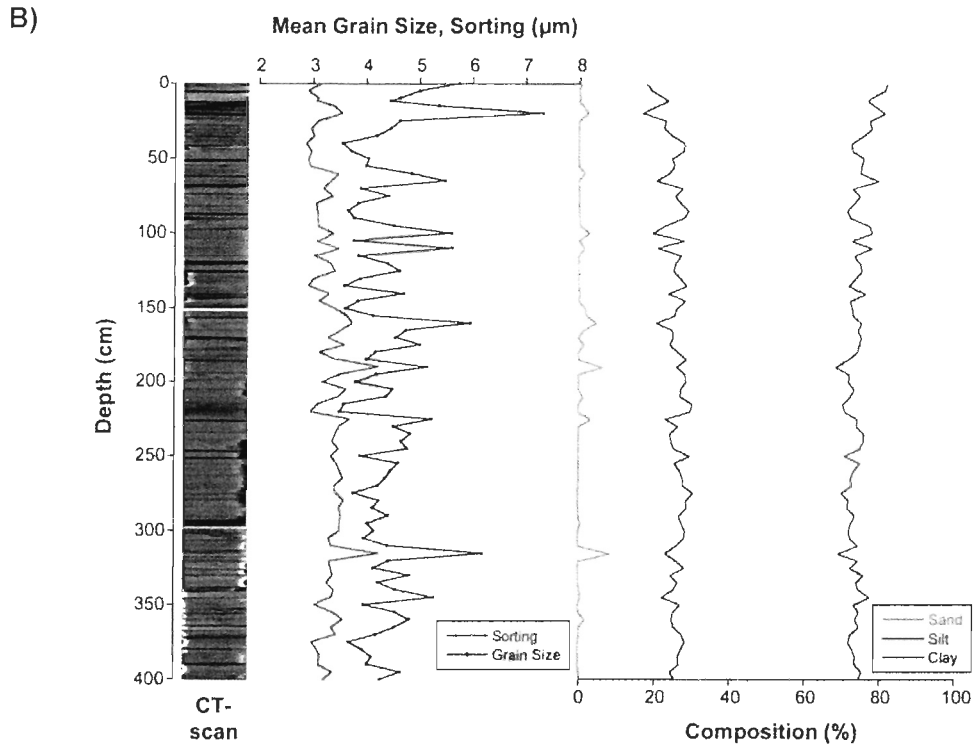


**Figure 3B:** CT-scan images, average grain size and sorting, and percentages of clay, silt, and sand for core 680.

The process of CASQ coring, unlike piston coring, is designed to preserve the sediment-water interface. Physical and magnetic properties were correlated between the CASQ cores and their corresponding box cores in order to confirm this. The successful preservation of the upper part of the sediment record in the CASQ cores is best demonstrated by the color spectrophotometry parameters  $L^*$ ,  $a^*$ , and  $b^*$ , of which  $L^*$  (lightness) is shown, and by the Ti content measured by XRF spectroscopy (Figure 4). In the case of core 690, since the top 10 cm of the CASQ core were too soupy for u-channel subsampling, correlation starts at a depth of 10 cm. The similarity of these data sets indicates that the sediment-water interface was indeed preserved in both cores. This is also consistent with the modern radiocarbon date obtained at the surface of the STN 690 box core, which can be fit linearly with the two dates obtained from the upper CASQ section.

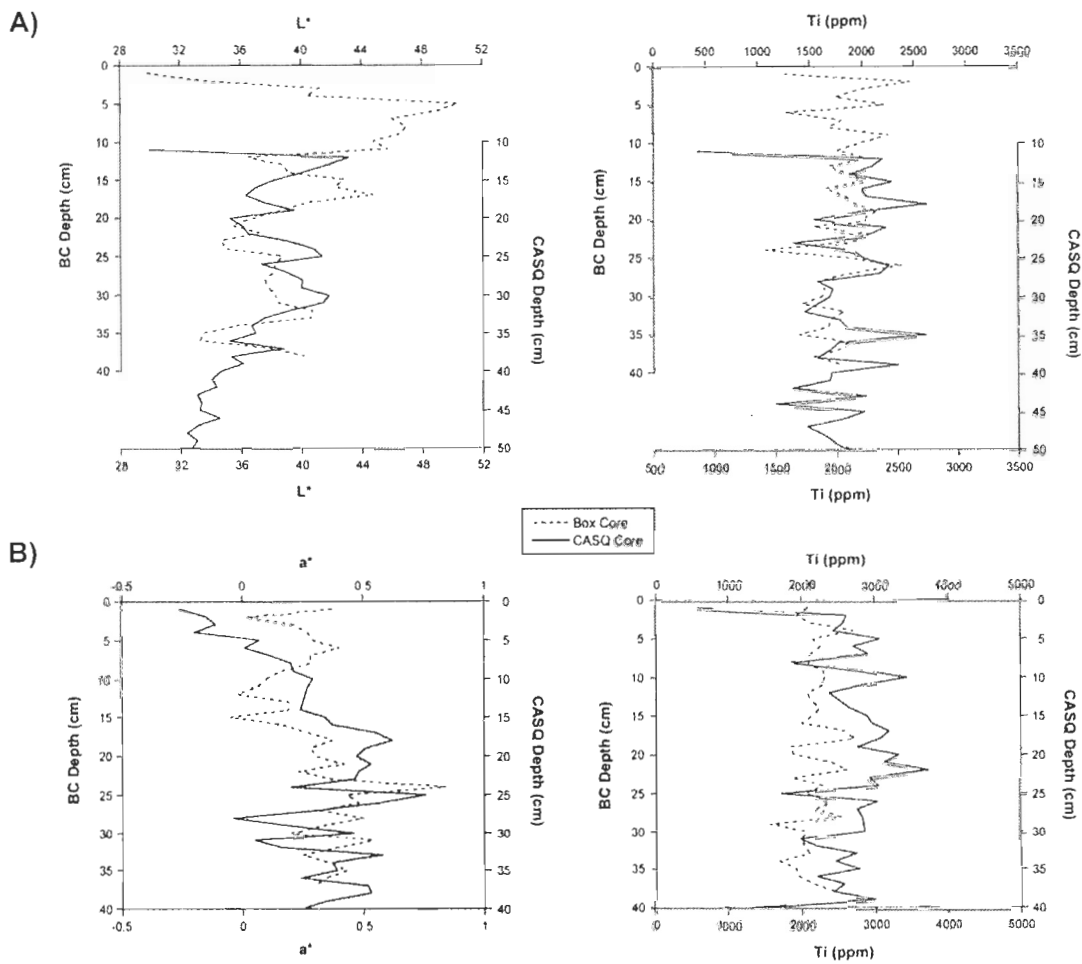


**Figure 4:** Core top correlation using  $L^*$ ,  $a^*$ , and Ti content, between the CASQ cores and their associated box cores for A) core 690 and B) core 680.

#### 4.2 Natural Remanent Magnetization

The NRM is characterized by a strong, stable ChRM, isolated between the AF demagnetization steps of 20 and 60 mT in both cores. A weak viscous remanent magnetization (VRM), which can be easily discerned in orthogonal projections of the total magnetization vector (Zijderveld, 1967), was removed by applying a maximum demagnetization field of 15 mT (Figures 5 and 6). The mean NRM prior to AF demagnetization was 0.010 A/m for core 690 and 0.015 A/m for core 680.

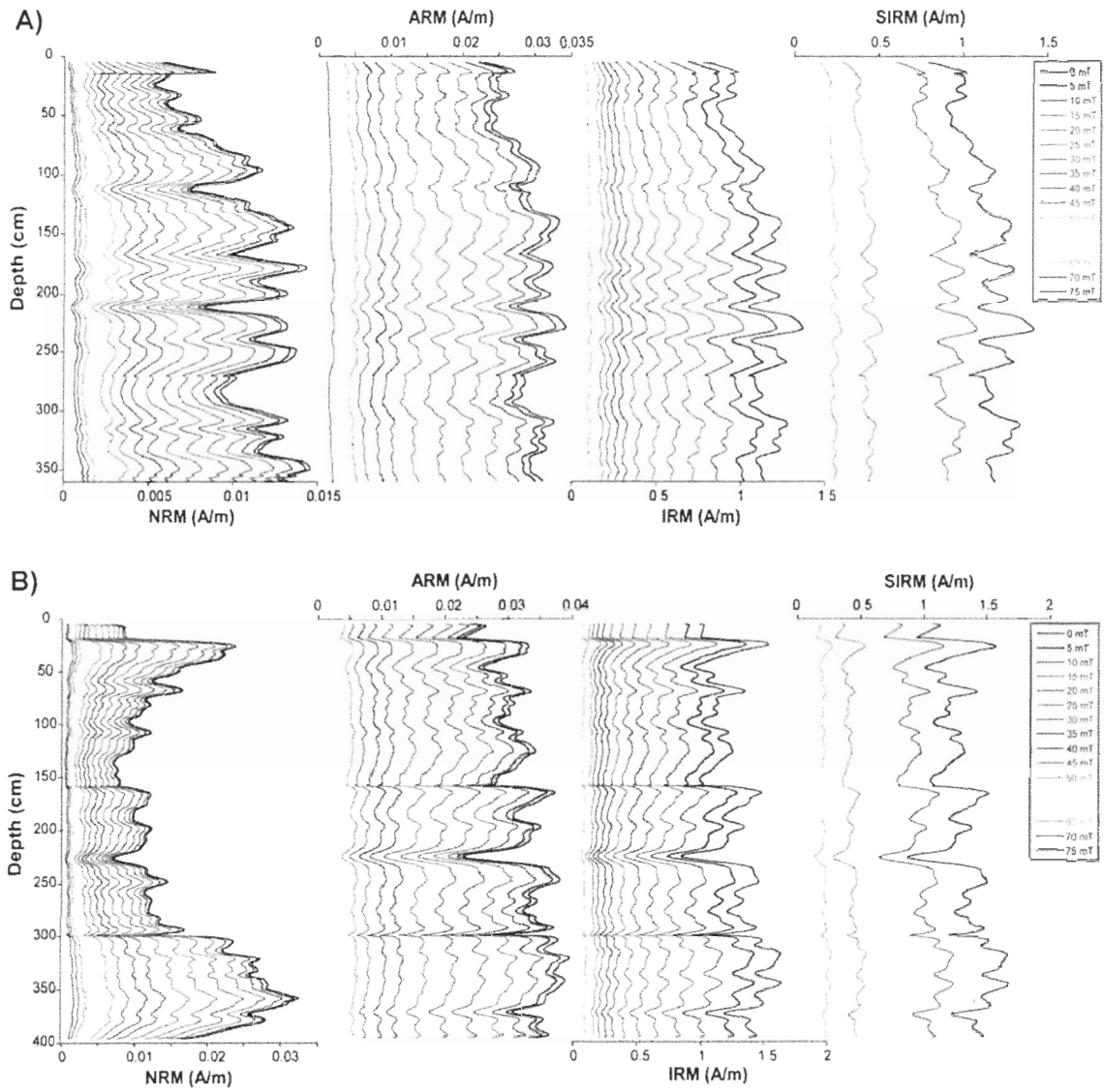
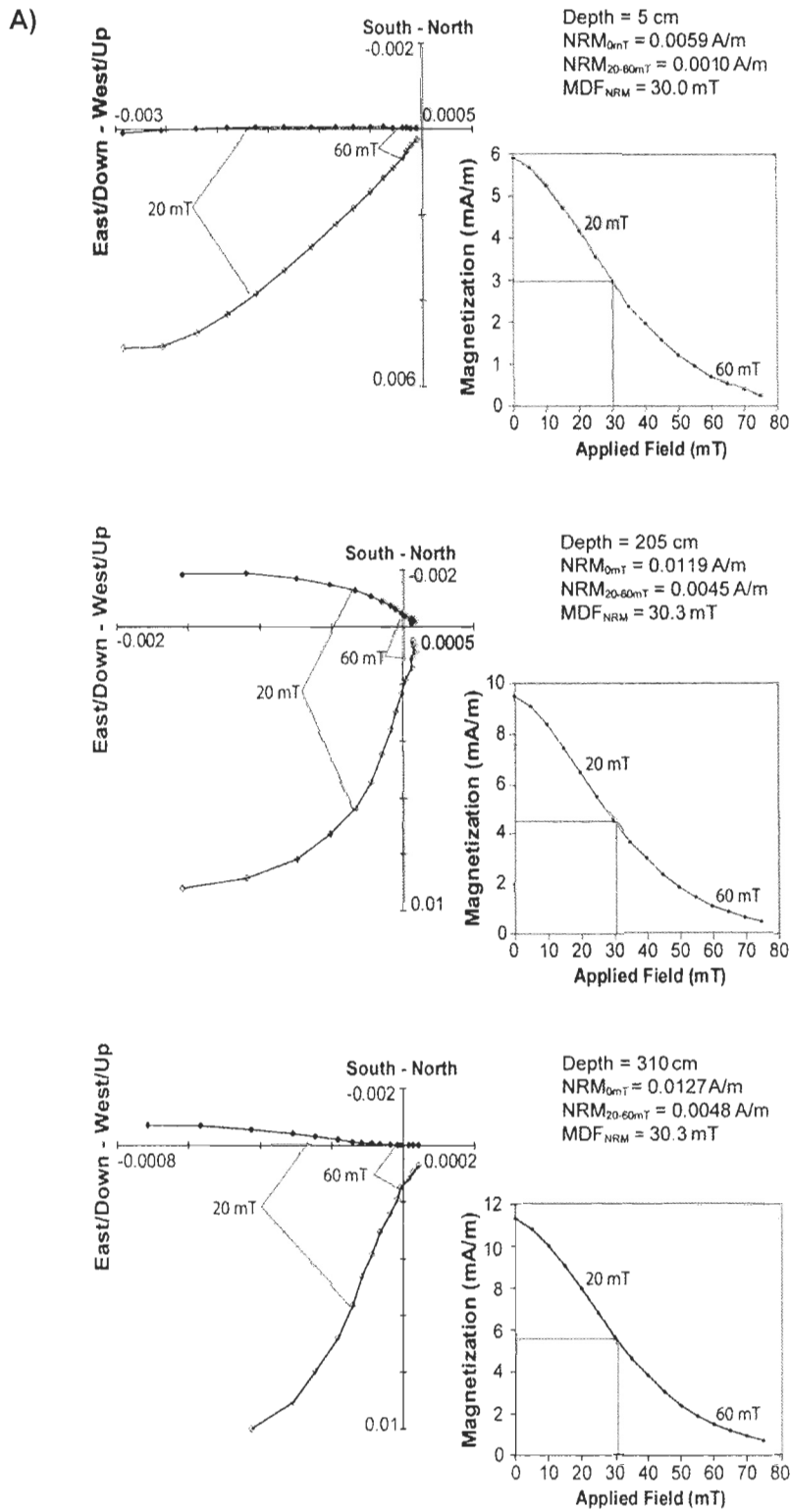
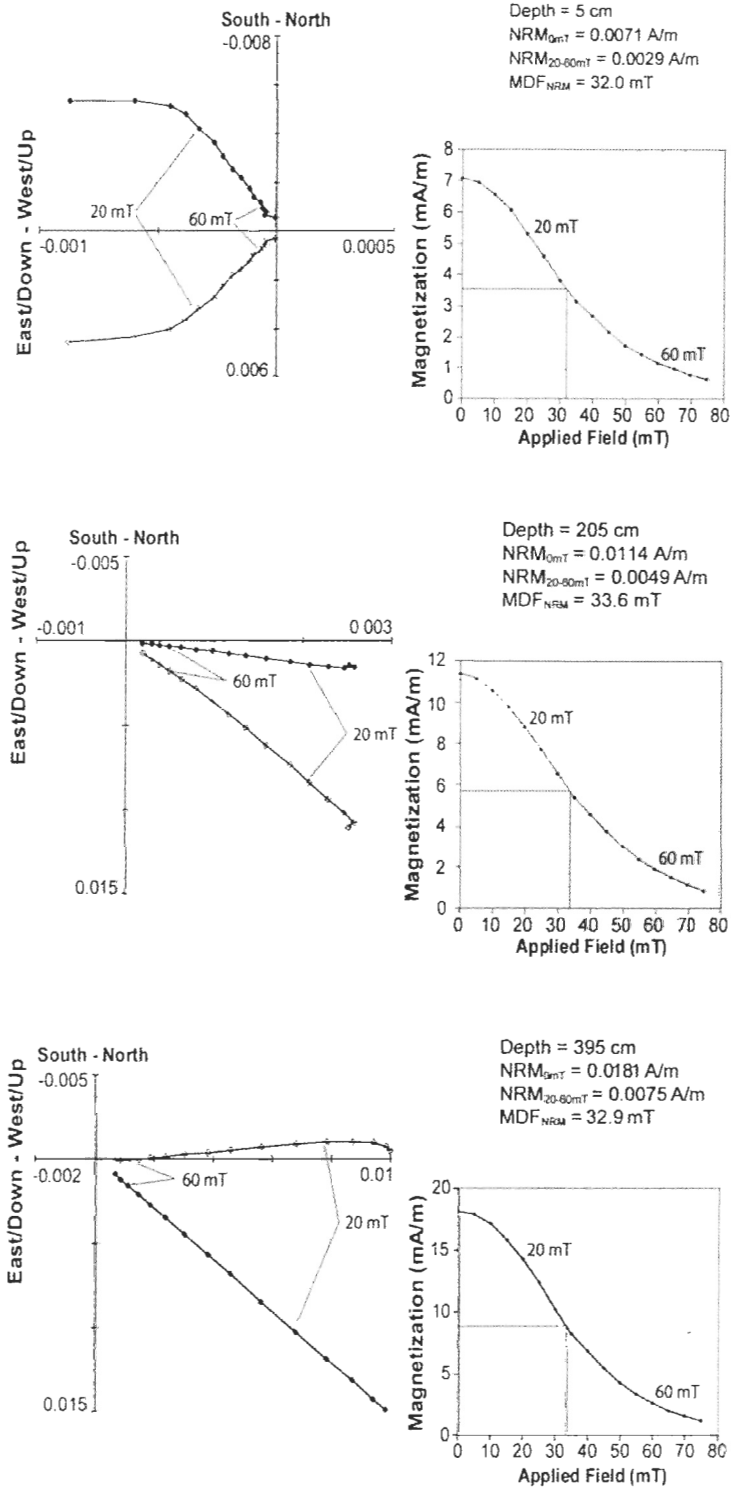


Figure 5: Demagnetization of NRM, ARM, IRM, and SIRM for A) core 690 and B) core 680.



**Figure 6A:** Orthogonal projections (Zijderveld diagrams) of demagnetization at various depths in core 690, with open diamonds representing the vertical projection of the magnetization vector and closed diamonds the horizontal projection. Also shown are AF demagnetization plots with the MDF indicated.

B)



**Figure 6B:** Orthogonal projections (Zijderveld diagrams) of demagnetization at various depths in core 680, with open diamonds representing the vertical projection of the magnetization vector and closed diamonds the horizontal projection. Also shown are AF demagnetization plots with the MDF indicated.

The ChRM inclination in core 690 varies about the geocentric axial dipole (GAD) inclination at the latitude of the site through the majority of the core. The mean inclination in core 690 is  $80.0^\circ$ , corresponding to a GAD of  $79.4^\circ$ . Slightly lower inclination values, some varying from the GAD by  $> 10^\circ$ , are recorded in the uppermost section of the core, from 10 to 60 cm. In core 680 the inclination deviates strongly from the GAD in both the upper and lower sections of the core (from the surface to  $\approx 125$  cm, and from 300 cm to the bottom), possibly due to the same coring problems that caused the implosion of the deepest section. The overall mean inclination in core 680 is  $44.5^\circ$ , while the GAD value at that location is  $79.5^\circ$ ; directional data from the u-channel sections spanning 0 to 150 cm and 300 to 400 cm were therefore excluded (Figure 7). Inclination approaches the expected range in the middle section of core 680, with an average value of  $66.4^\circ$ . However as this average value still varies from the GAD by  $> 10^\circ$ , the middle interval should similarly be treated with some caution.

Since the cores were not azimuthally oriented during sampling, ChRM declinations are relative. Declination values were therefore adjusted for rotation at section breaks and for circular values (e.g. 0 and  $360^\circ$ ). The top of the records were aligned to  $26.29^\circ$  for core 690 and  $26.28^\circ$  for core 680, the estimated declinations at those sites at the time of sampling as calculated from the International Geomagnetic Reference Field (IGRF) model (Figure 7). In core 680, an increase in declination of  $\approx 60^\circ$  is observed over the last  $\approx 20$  cm of the first section (136 to 156 cm). Such a jump suggests possible deformation of the directional record. Indeed, this sharp increase in relative declination also corresponds to the rapid return to GAD values observed in the inclination record. MAD values can be used to assess the quality of the directional record, with values  $< 5^\circ$  generally considered indicative of excellent data (Stoner and St-Onge, 2007).

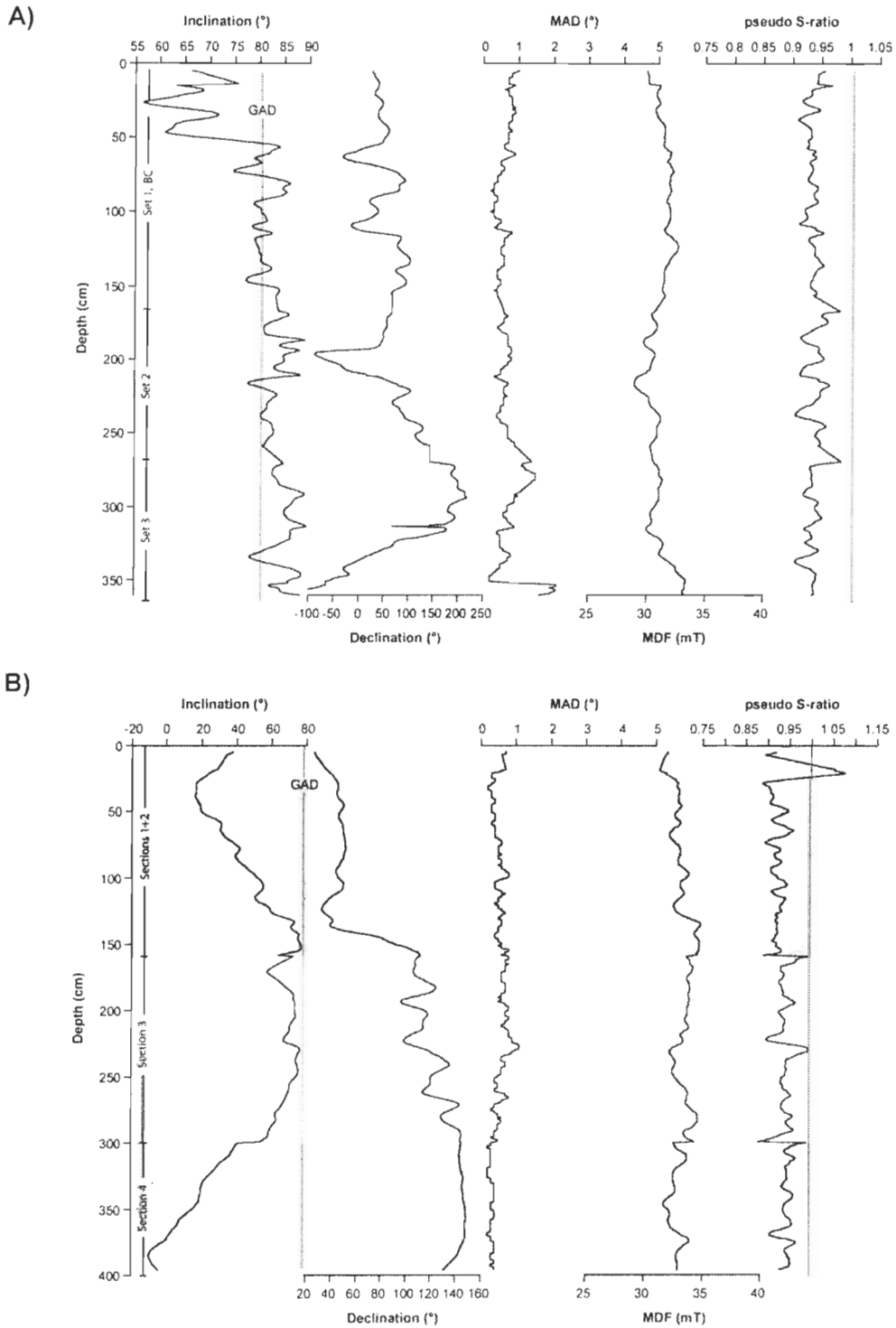


**Figure 7:** Measured inclination shown with the geocentric axial dipole (GAD), relative declination, maximum angular deviation (MAD), median destructive field (MDF), and  $IRM_{10mT}/SIRM_{10mT}$  (pseudo S-ratio) for A) core 690 and B) core 680. Unreliable intervals in core 680 are shaded in gray and correspond to the upper and lower sections of the core (see text for details).

### 4.3 Magnetic Mineralogy and Grain Size

In both cores MAD values do not exceed  $3^\circ$  in any section. Additionally, large variations in MDF and pseudo S-ratio values can be indicative of changes in magnetic mineralogy and grain size, respectively, that could adversely affect the paleomagnetic record. In both cores, MDF and pseudo S-ratio values are approximately constant downcore, suggesting uniform magnetic mineralogy and grain size (Figure 7). These rock-magnetic data support high-quality records of geomagnetic origin in both cores, including over intervals where the inclination deviates from the expected GAD values. Pseudo S-ratio values ( $IRM_{10mT}/SIRM_{10mT}$ ) are consistently close to 1 in both cores (Figure 7), with values of 0.94 for both cores 690 and 680, indicating that the bulk of the magnetic assemblage in the sediment is saturated in an applied field of 0.3 T, and is thus characterized primarily by low-coercivity minerals such as magnetite. The hysteresis parameters  $M_{rs}/M_s$  and  $H_{cr}/H_c$ , visualized in a Day plot (Figure 8), similarly demonstrate that magnetic grains in both cores are uniform in size downcore and lie within the pseudo-single domain (PSD) range, corresponding to a grain size of  $\approx 1$  to  $15 \mu\text{m}$  for magnetite (Day et al., 1977; King et al., 1983; Tauxe, 1993; Dunlop, 2002). Furthermore, the shape of magnetic hysteresis curves also suggests a magnetic assemblage dominated by low-coercivity, ferrimagnetic minerals such as magnetite (Figure 9) (Tauxe et al., 1996). Also typical of magnetite and titanomagnetite, all samples reach saturation in an applied field of  $\approx 0.2$  T and yield  $M_{rs}/M_s$  ratios between 0.1 and 0.3 (Day et al., 1977; Tauxe, 1993).

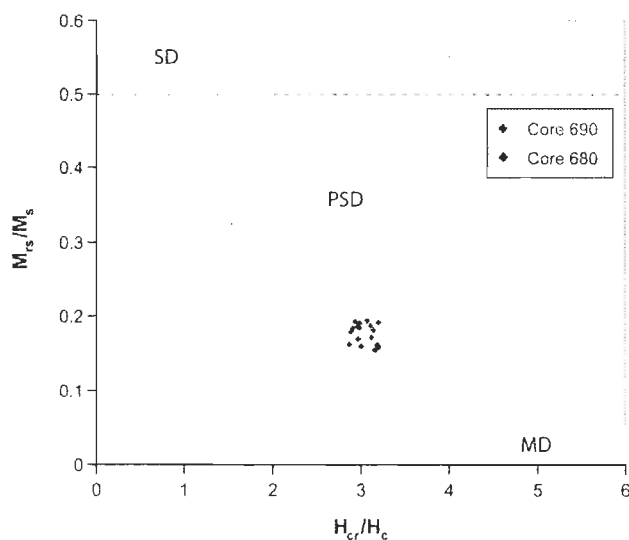


**Figure 8:** Day plot visualizing hysteresis parameters for core 690 (green) and core 680 (red), delimiting the single domain (SD), pseudo-single domain (PSD), and multi domain (MD) particle size ranges.

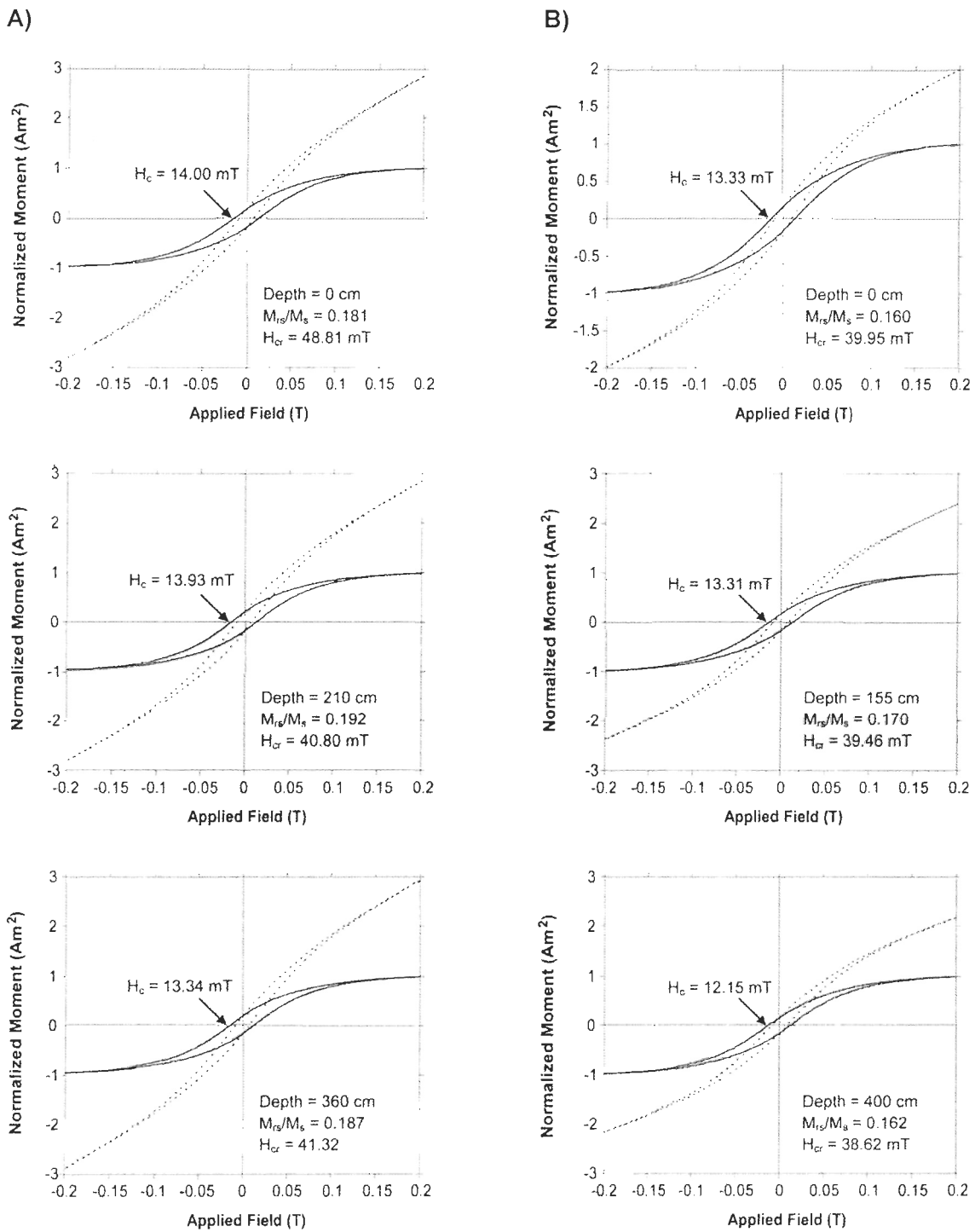


**Figure 9:** Magnetic hysteresis measurements (corrected to remove the paramagnetic component) from the top, near middle, and bottom of A) core 690 and B) core 680, with the raw measurement shown by the dashed curve. These examples are representative of hysteresis properties measured throughout the cores.

Finally, average MDF values of 31.21 mT in core 690 and 33.14 mT in core 680 are in agreement with the strong magnetite presence indicated by rock-magnetic data. For magnetic assemblages dominated by magnetite, MDF can also be regarded as a magnetic grain size indicator; in this case the uniformity of values downcore (Figure 7) reflects uniform magnetic grain sizes in both cores (Dankers, 1981). This mineralogy dominated by pseudo-single domain magnetite is similar to that observed in previous study from the area by Barletta et al. (2008).

#### *4.4 Environmental Magnetism*

The bulk magnetic properties of sediment are heavily dependent upon lithologic factors, including magnetic mineralogy, grain size, and concentration. The concentration of magnetic minerals supplied to the sediment strongly influences the intensity of natural and laboratory-induced remanences, and is particularly reflected by magnetic susceptibility. Therefore  $k_{LF}$  offers a means of assessing whether large variations in concentration may compromise the quality of the relative paleointensity (RPI) record;  $k_{LF}$  values varying by a factor greater than 10 are commonly considered suspect (Tauxe, 1993). In both cores variations in  $k_{LF}$  fall below a factor of 10, though smaller-scale variations, likely reflective of environmental processes, are observed (Figure 10). Additionally, with the mineralogy of remanence-carriers established as dominantly magnetite and the grain size determined to be relatively constant downcore (see section 4.3), NRM, ARM, IRM, SIRM, and  $k_{LF}$  can be regarded as primarily concentration dependent. However, the  $SIRM_{0mT}/k_{LF}$  and  $k_{ARM}/k_{LF}$  ratios could nevertheless reveal some fine variations in grain size (King et al., 1982; Thompson et al., 1986), in this case potentially connoting that periods of finer magnetic grains correspond to periods of lower concentrations of magnetic minerals (Figure 10).  $SIRM_{0mT}/k_{LF}$  is more specifically sensitive to larger grains, and  $k_{ARM}/k_{LF}$  to smaller ones (see section 3.4), thus the close similarity between these two ratios throughout the length of both cores could indicate a uniform distribution of intermediately-sized magnetic grains (Figure 10).

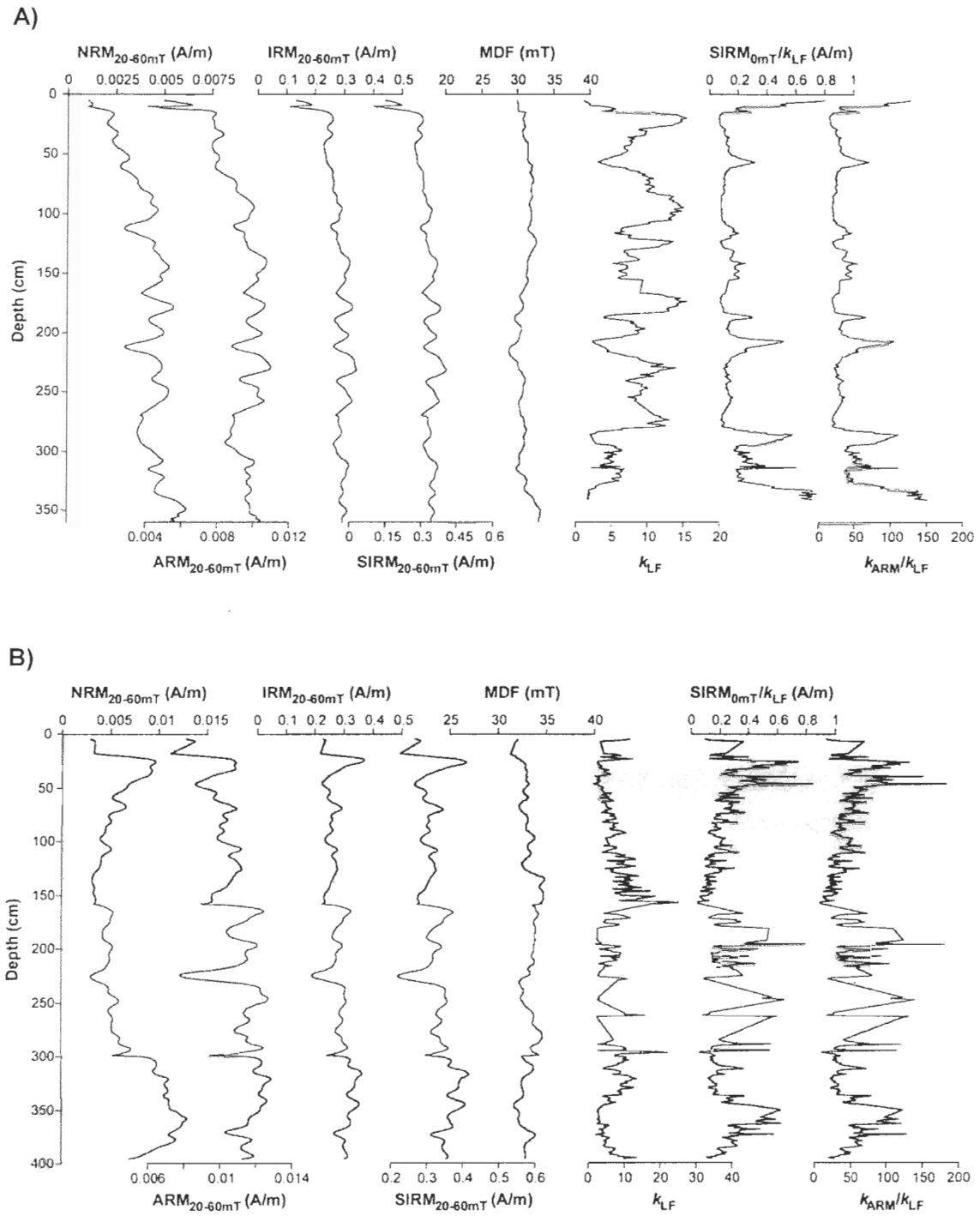


**Figure 10:** NRM, ARM, IRM and SIRM over the characteristic range (20-60 mT), median destructive field (MDF), low-field magnetic susceptibility ( $k_{LF}$ ), and grain size parameters  $SIRM_{30-50mT}/k_{LF}$  and  $k_{ARM}/k_{LF}$  for A) core 690 and B) core 680.

In core 690, a clear similarity can be discerned between the NRM, ARM, IRM, SIRM, MDF, and  $k_{LF}$  curves, illustrating the concentration and grain size dependencies of the paleomagnetic signal. These relationships are also visible in core 680; comparison to the  $k_{LF}$  record is more difficult due to the quality of that data (see section 2.2), although several corresponding peaks and troughs can nonetheless be discerned. The parallels between the NRM records and their three corresponding laboratory-induced magnetizations suggest that a RPI proxy may indeed be reliably normalized, and thereby isolated from the effects of changes in magnetic grain size and concentration. Conversely, such variations in magnetic properties, especially in concentration, can often reveal important environmental controls on sediment supply. Both the average values and magnitude of variations in  $k_{LF}$  are greater in core 680 than in core 690, suggesting that larger magnetic grains or a higher, more variable concentration of magnetic minerals may be present at the more distal site (Figure 10). It is also interesting to note that variations in the  $k_{LF}$  records appear to be quasi-periodic; this is particularly evident in core 690, with potential cyclical variations visible throughout most of the core. Several of these peaks can be visually correlated to less prominent ones in core 680, particularly in the higher-quality middle section (Figure 10). Such features are strongly reminiscent of potential climatic controls on deposition.

## 5. Discussion

### 5.1 Age Model

The age models of both cores were based on the radiocarbon ages obtained. In core 690, all available ages were used in the construction of the radiocarbon-based age model except for two shells. The excluded samples were bivalve fragments found at 189.5 cm and 276 cm that yielded ages outside of the margin of error of the overall age model. Their original presence at these depths would imply unlikely inversions in the sedimentation rate, thus they are considered to be too old, having most likely been remobilized. The three foraminifera samples from core 680 were excluded from its age model, since they were

composed of an unknown mix of benthic and planktonic species and yielded older apparent ages.

For core 690, three linear fits were used to construct the age model, the uppermost one comprising the surface of the core and the first radiocarbon date (at 14 cm), the lower one comprising all of the remaining selected dates, and the middle one joining them (Figure 11). This model results in an overall average sedimentation rate of 170 cm/ka, or an average rate of 246 cm/ka up to 25 cm (corresponding to the period from 2096 to 709 cal BP), followed by a rate of 33 cm/ka for the more recent segment (corresponding to the period from 709 cal BP to present). For core 680, a 4<sup>th</sup> order polynomial fit was applied to the entire set of bivalve dates (Figure 11). Here the average sedimentation rate is 192 cm/ka over the period from 2037 cal BP to present, though the youngest radiocarbon date and the polynomial fit also allow for a potentially lower sedimentation rate in recent years, as is observed to a greater degree in core 690.

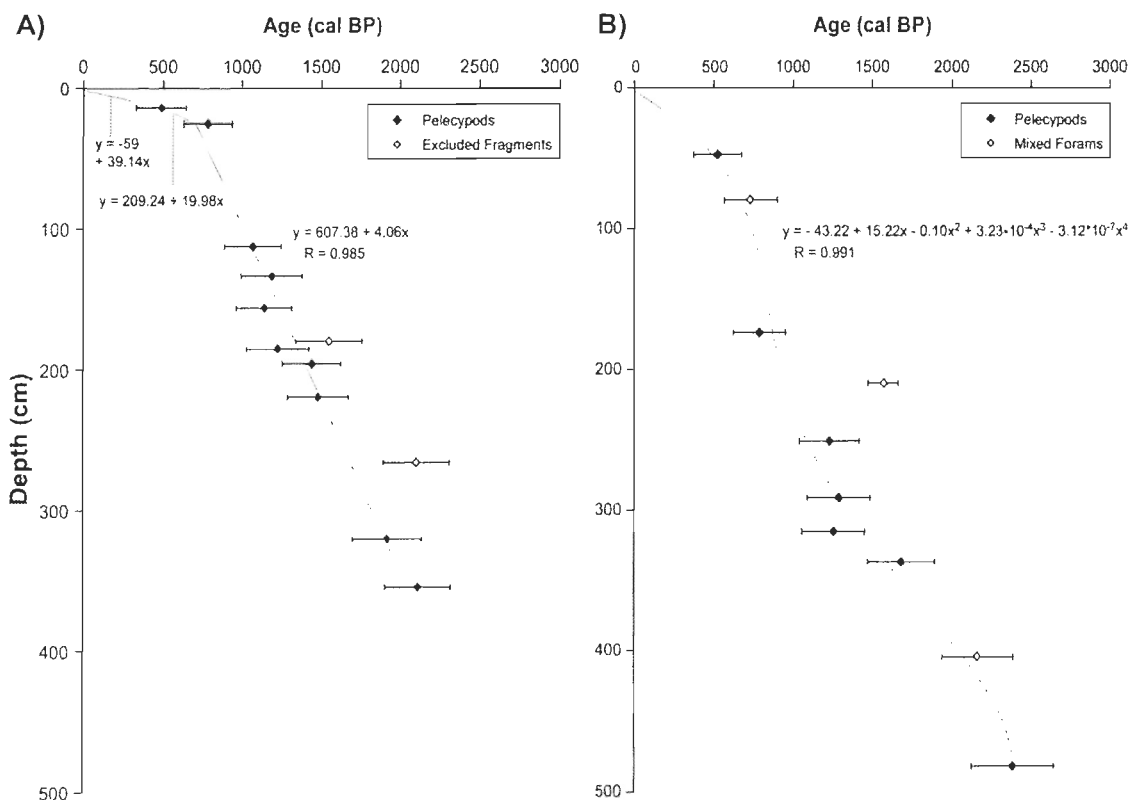


**Figure 11:** Age models, with A) three linked linear fits for core 690 and B) a 4th order polynomial fit for core 680. Open points represent excluded ages (see text for details).

Overall, these rates are comparable to others that have been measured in the Western Arctic over the same time period. Using magnetostratigraphy and radiocarbon ages, Lisé-Pronovost et al. (2009) determined an average sedimentation rate of  $\approx 120$  cm/ka on the Alaskan continental slope in the Chukchi Sea. Barletta et al. (2008) calculated a rate of  $\approx 140$  cm/ka on the western Mackenzie Shelf, close to the Mackenzie Trough, using several radiocarbon dates. Bringué and Rochon (2012) focused on the more recent part of the record, taking  $^{210}\text{Pb}$  measurements from the box core accompanying this study and again obtaining a sedimentation rate of  $\approx 140$  cm/ka. Finally, Durantou et al., 2012 conducted  $^{210}\text{Pb}$  and  $^{137}\text{Cs}$  analyses of the box core accompanying core 680 of this study and determined much higher rates, ranging from  $\approx 220$  to 330 cm/ka. Although slower rates, more similar to that suggested here by the uppermost part of the core 690 age model, are observed at certain localities in the Western Arctic (e.g., Lisé-Pronovost et al., 2009; Barletta et al., 2010a), there is little else to support such a drastic reduction in sedimentation in the Mackenzie Trough itself over the past several hundred years. To the contrary, the radiocarbon age model established here for core 680 and the box core model developed by Durantou et al. (2012) both suggest that high rates of sediment accumulation may have been maintained through the recent part of the record. This calls into question the accuracy of the radiocarbon age model for core 690, particularly the dates obtained for the uppermost two CASQ core shells.

### *5.2 Paleomagnetic Secular Variations*

In young, high-resolution paleomagnetic records, which do not encompass geomagnetic field excursions and reversals, paleomagnetic secular variations offer the primary means of investigating local geomagnetic field behavior and correlating between other records on regional scales. Here, the lack of physical signs of sediment deformation, the low MAD values, and the proximity of inclination measurements to the estimated GAD (for the majority of core 690 and the middle section of core 680) all suggest that a paleomagnetic secular variation (PSV) signal was reliably recorded and accurately measured. Comparison with geomagnetic field models and other nearby cores of similar resolution serves as a final means of assessing the quality of the directional record. Correlation of PSV records is achieved through both inclination (Figure 12) and relative

declination (Figure 13) between core 690, the middle section of core 680, the *CALS3K.4* geomagnetic field model (*Korte and Constable, 2011*), and several other records from the Western Arctic and high-latitude North America. The other records used are core 2004-804-803PC (803PC) from the Beaufort Sea, core HYL0501-05JPC (5JPC) from the Chukchi Sea (*Barletta et al., 2008*), core HYL0501-06JPC (6JPC) from the Chukchi Sea (*Lisé-Pronovost et al., 2009*), core 2005-804-006PC (006PC) from the Northwest Passage (*Ledu et al., 2010*), and a Mara Lake core from British Columbia, Canada (*Turner, 1987*). *Lisé-Pronovost et al. (2009)* proposed a correlation of the Chukchi Sea cores 5JPC and 6JPC, the Beaufort Sea core 803PC, and the Mara Lake core with PSVL, a compilation of PSV measurements from Western U.S. lava flows (*Hagstrum and Champion, 2002*). This tie-point appears to be consistent with the I-3 feature marked in the inclination record, which, in linking the records to one unaffected by reservoir effects, offers strong support of the two radiocarbon-based age models.

Three or four high-frequency PSV features can be tentatively correlated in inclination records between core 690 and the quality, middle section of core 680. The most prominent of these, here labeled I-1, appears to be paralleled in the relative declination record (D-1) (Figures 12 and 13). These features are potentially recorded in other records, namely core 803PC. In addition, some longer-term trends in inclination and declination may correlate with the *CALS3K.4* model calculations at the site of core 690, particularly a 5° to 10° increase in inclination values observed near the base of core 690 (I-3). This feature, along with what may be a matching one in the declination record, may also be correlated with the PSVL tie point established by *Lisé-Pronovost et al. (2009)* among cores 6JPC, 5JPC, 803PC and the Mara Lake core. In regarding the uppermost ≈ 700 yrs, the directional features of core 690 appear to be missing or distorted compared to the other records. This is likely the result of the stark reduction in apparent sedimentation rates dictated by the radiocarbon age model, and calls further into question the validity of the upper part of the model. Whether these longer-term features were also recorded in core 680 is difficult to judge due to the very limited span of time over which the PSV record was deemed reliable. Nonetheless, overall agreement between core 690, the middle section of core 680, and the other Western Arctic records confirm that these cores have likely accurately recorded regionally-coherent PSV features.

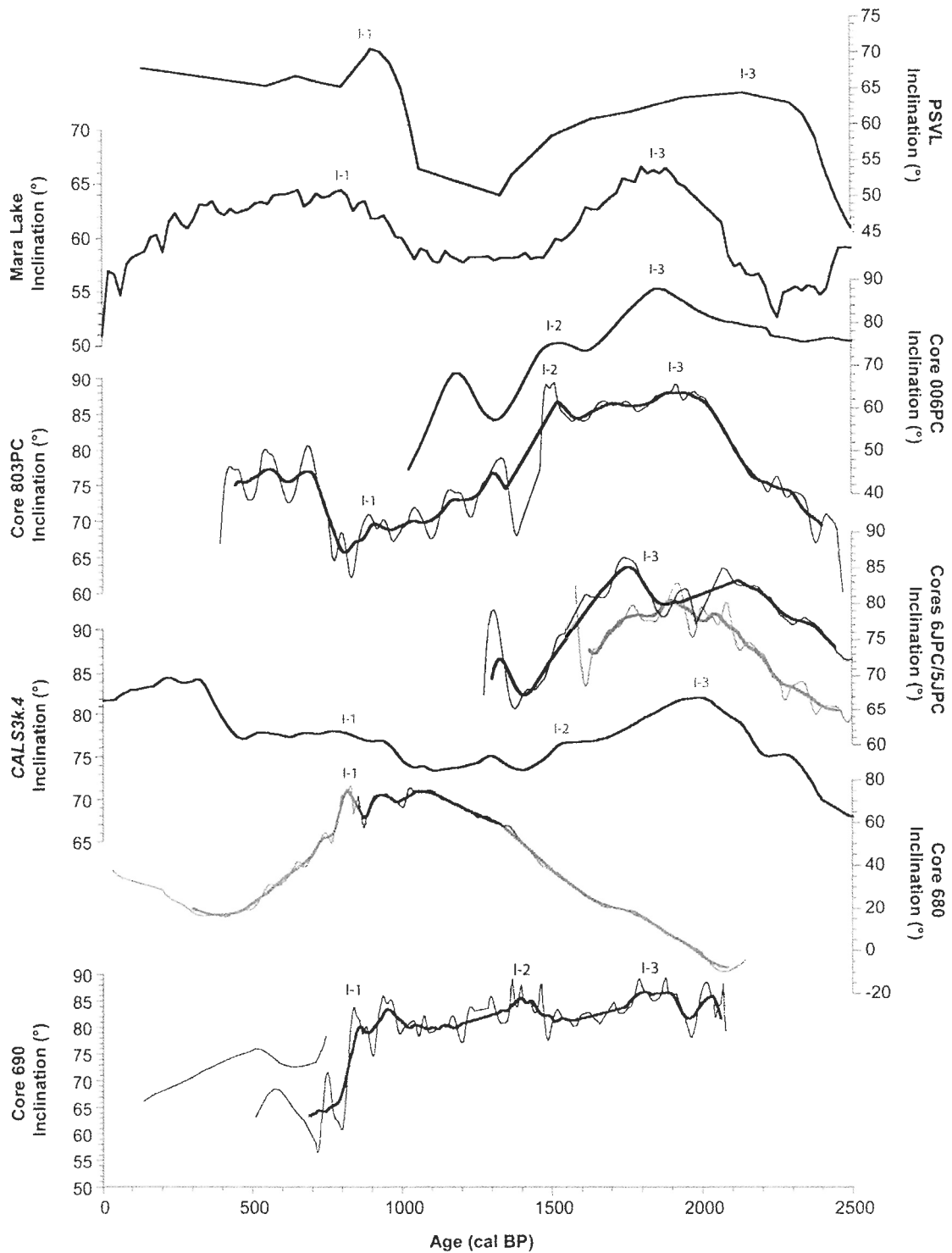


**Figure 12:** Inclination of core 690 and core 680 shown with the *CALS3k.4* geomagnetic field model output at station 690, as well as cores 5JPC and 6JPC from the Chukchi Sea, core 803PC from the Beaufort Sea, core 006PC from the Northwest Passage, and a core from Mara Lake in British Columbia. Also shown is the Western U.S. PSVL record.

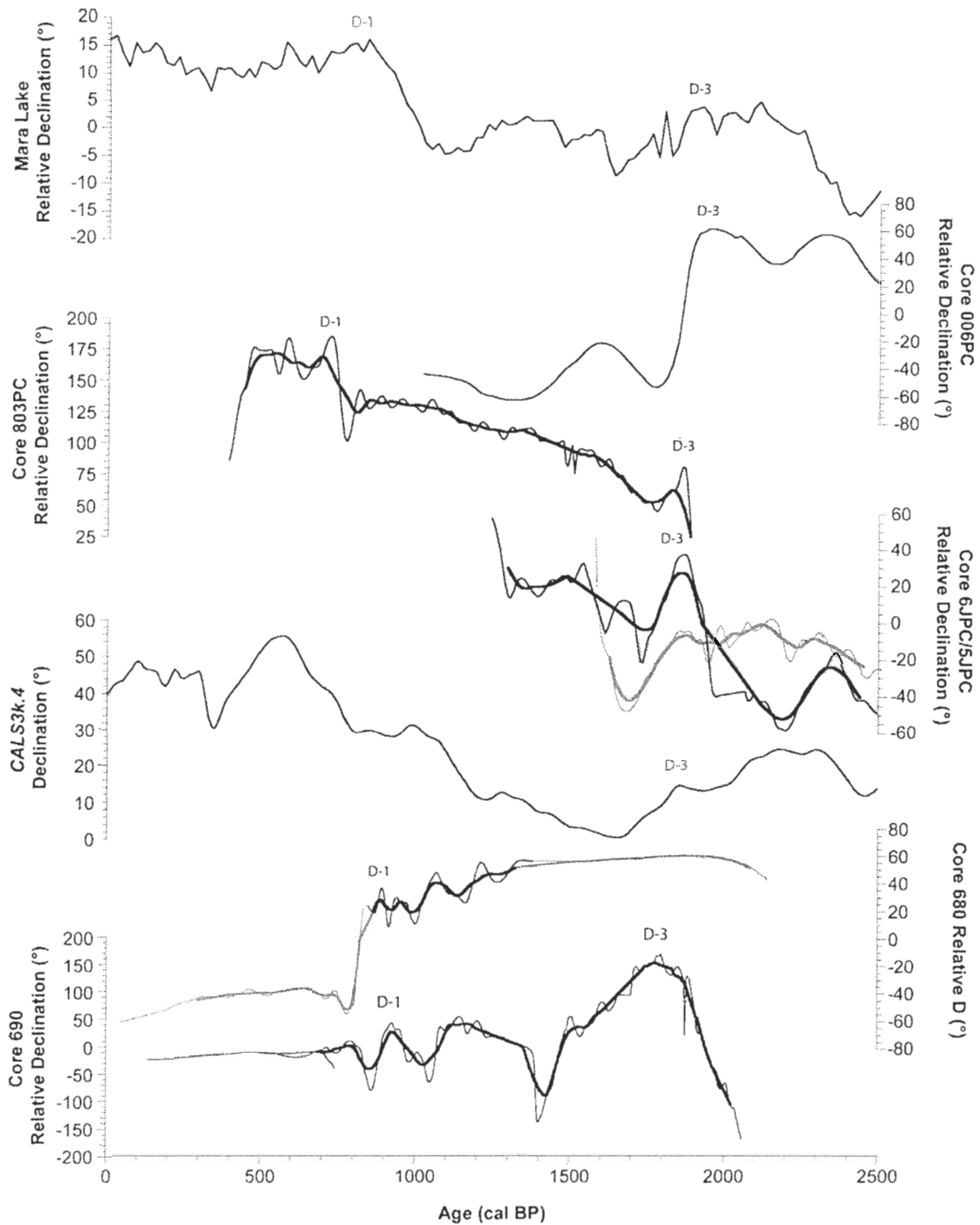


**Figure 13:** Relative declination of core 690 and core 680 shown with the *CALS3k.4* geomagnetic field model output at station 690, as well as cores 5JPC and 6JPC from the Chukchi Sea, core 803PC from the Beaufort Sea, core 006PC from the Northwest Passage, a core from Mara Lake in British Columbia, and the Western U.S. PSVL record.

### 5.3 Relative Paleointensity

Selected sections of both cores meet the established criteria for the determination of reliable PSV and relative paleointensity (RPI) records (e.g. King et al., 1983; Tauxe, 1993; Stoner and St-Onge, 2007). These criteria are: 1) a strong, stable, and single-component ChRM (see section 3.2, Figures 5 and 6); 2) MAD values below  $5^\circ$  and ChRM inclinations which vary about the GAD inclination of the site (see section 3.2, Figure 7); 3) a magnetic remanence carrier dominated by PSD magnetite (see section 3.3, Figures 7, 8 and 9); 4) a concentration of magnetic minerals that varies by less than a factor of 10 (see section 3.4, Figure 10). A quality sedimentary NRM record can be used to produce a proxy of RPI; it reflects changes in the concentration of magnetic grains present in addition to the intensity of the geomagnetic field, and must therefore be normalized by another magnetic parameter in order to isolate the desired information (e.g., Tauxe, 1993). Concentration-dependent parameters commonly used as normalizers include ARM, IRM, and SIRM (e.g., Tauxe, 1993; Valet, 2003; Stoner and St-Onge, 2007). The use of  $k_{LF}$  is not generally recommended, since it can be highly dependent on magnetic mineralogy and grain size in addition to the concentration of magnetic minerals. RPI proxies were constructed by two different procedures: the average ratio method and the slope method. In the commonly used average ratio method, the NRM measured at all demagnetization steps within the characteristic range (20-60 mT) is averaged and divided by the normalizer, averaged over the same range. In the slope method, also known as the pseudo-Thellier method, the slope of the NRM versus the normalizer is taken over the same range of demagnetization steps (Tauxe et al., 1995; Channell et al., 2002). No significant difference to the data was achieved by using the slope method, while coherence tests (see below) revealed slightly better success using the ratio method. The results presented hereafter are those calculated using the ratio method.

In Figure 10, the ARM, IRM, and SIRM, averaged over the characteristic range (20 to 60 mT), show similar features and variations for the greater part of both cores, suggesting that all three magnetizations activate the same assemblage of magnetic minerals. Various tests can be conducted to more precisely identify the most appropriate normalization parameter, or the one carried by the most similar assemblage as the NRM.

Comparing the demagnetization curves of the NRM, ARM, IRM, and SIRM at various intervals in each core offers one method of determining whether similar magnetic assemblages are responsible for carrying the different magnetizations. In both cores the demagnetization of ARM appears to behave relatively similarly to that of the NRM over the majority of steps. However in core 690 the SIRM curve more closely approaches the NRM curve over the characteristic range, which is effectively 30-50 mT in the case of SIRM (Figure 14A). In core 680 ARM remains the closest parameter throughout the demagnetization procedure (Figure 14B). This appears to be the case in both the middle section and the sections which recorded unreliable inclinations.

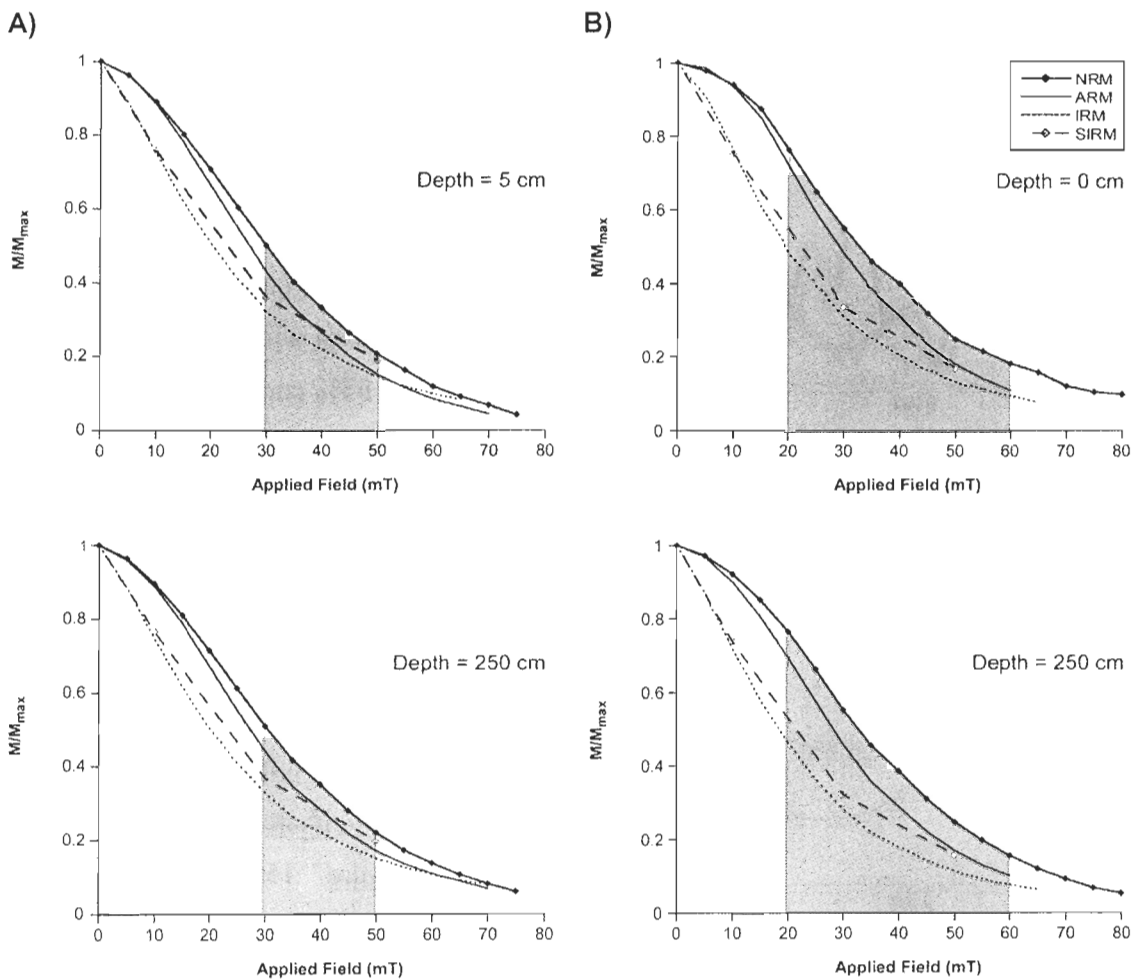


**Figure 14:** Demagnetization curves showing magnetization normalized by maximum magnetization for NRM, ARM, IRM, and SIRM versus the applied field.

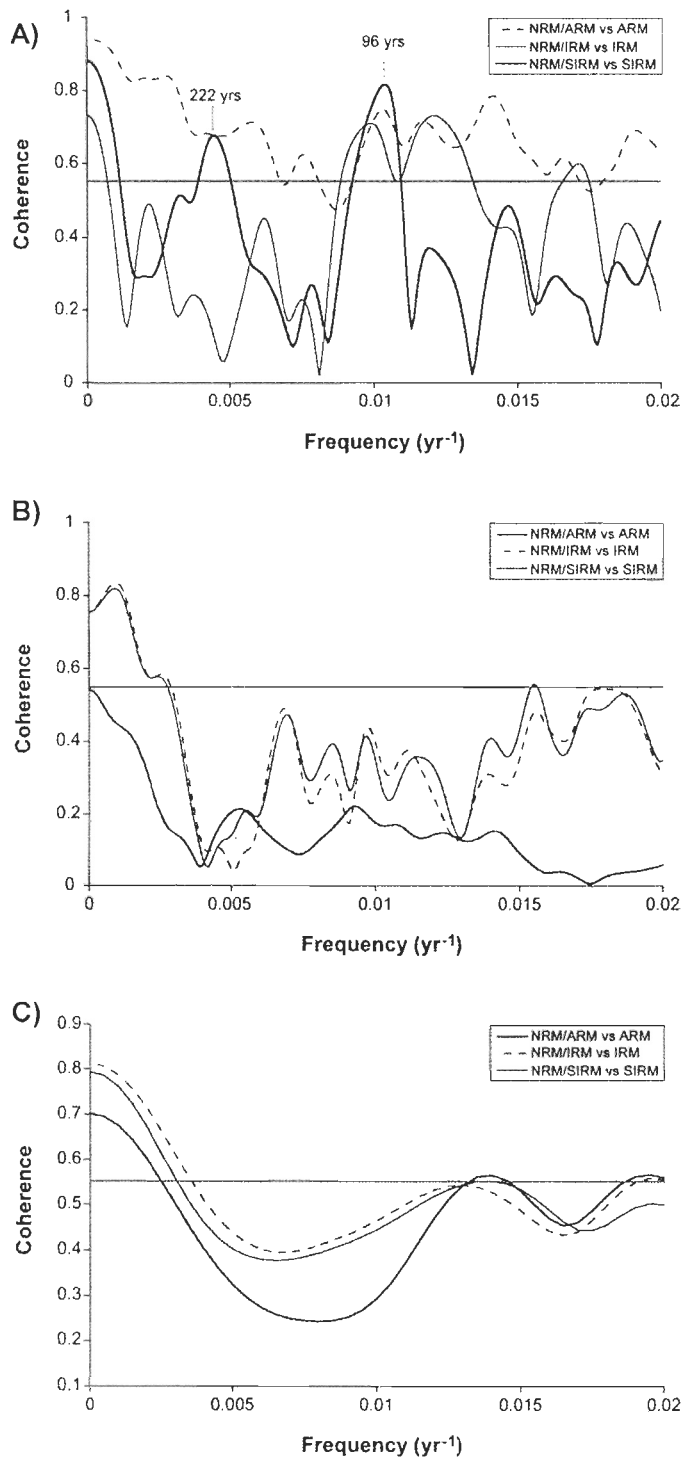


**Figure 15:** Coherence of different RPI calculations with their respective normalizers for A) core 690, B) core 680, and C) the middle section of core 680. The gray lines mark a confidence level of 95%.

As a means of further verifying the ideal normalizer, coherence tests, using a method of cross-spectral analysis previously proposed by Tauxe and Wu (1990), were carried out using the Analyseries software (Paillard et al., 1996) in order to determine the level of coherence between each RPI proxy and its normalizer. The results are similar to the ones revealed by comparing the demagnetization curves. In core 690, NRM/IRM and especially NRM/ARM were coherent with their normalizers at the 95% confidence interval over several frequencies. NRM/SIRM versus SIRM displayed the lowest overall level of coherence, exceeding the 95% confidence interval only at frequencies of 0.0045 and 0.0104 yr<sup>-1</sup> (corresponding to periods of approximately 222 and 96 yrs) (Figure 15A). In core 680, NRM/ARM is least coherent with its normalizer over most frequencies and is never coherent above the 95% confidence interval (Figure 15B). The results

are also favorable when only the middle section of the core (for which the measured inclination values agree with the GAD) is tested; here coherence is weakly demonstrated at frequencies of 0.0140 and 0.0195  $\text{yrs}^{-1}$  (corresponding to periods of approximately 71 and 51 yrs) (Figure 15C). Based on these analyses, and supported by the demagnetizations curves, NRM/SIRM was determined to be the most appropriate RPI proxy for core 690, and NRM/ARM for the middle section of core 680.

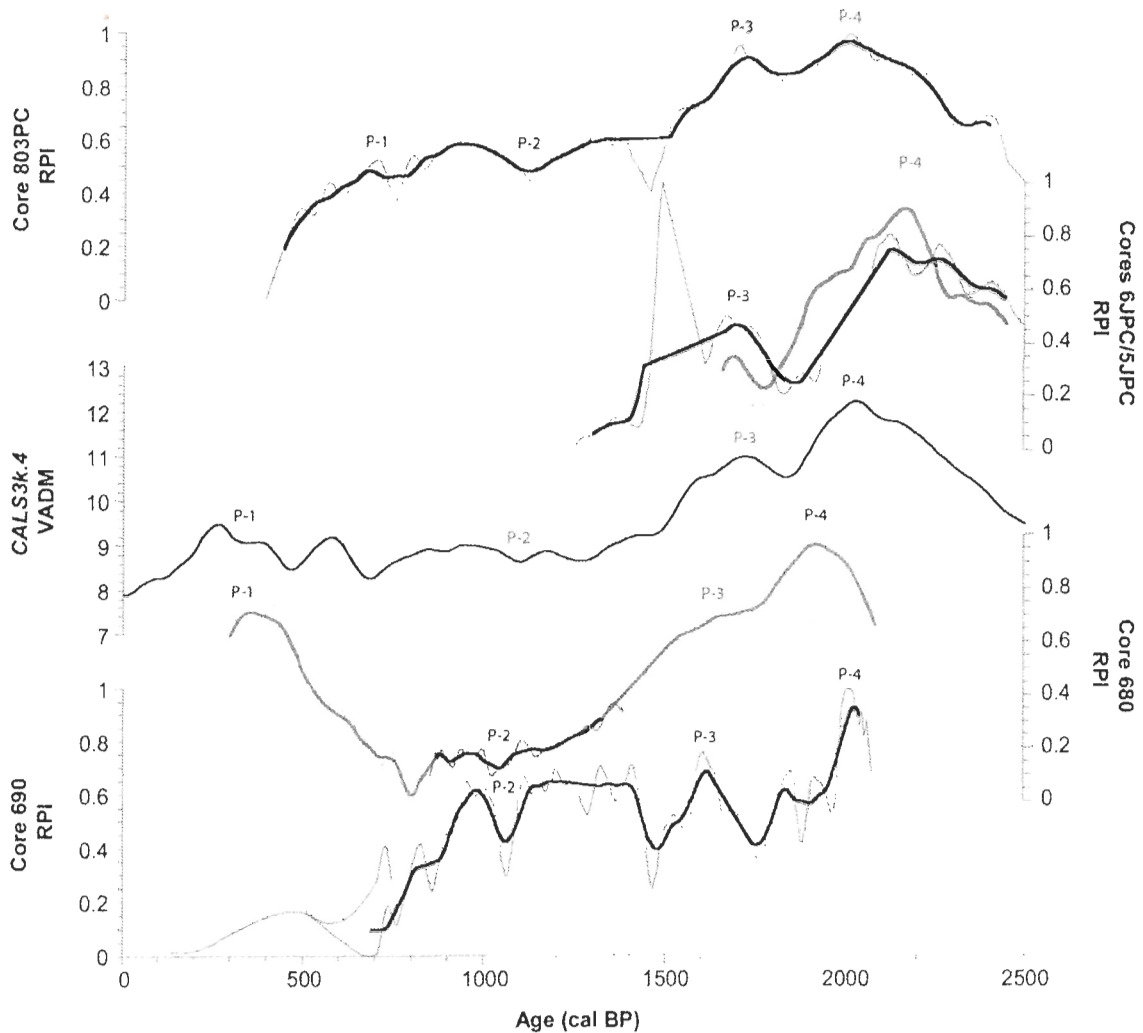


**Figure 16:** RPI of core 690 and core 680 shown with the *CALS3k.4* geomagnetic field model output at station 690, as well as cores 5JPC and 6JPC from the Chukchi Sea, and core 803PC from the Beaufort Sea.

Once established, the two RPI records were compared with one another and found to bear several high-frequency similarities throughout the length of the record, the most prominent of which are labeled P-1, P-2, P-3 and P-4 (Figure 16). It is likely that the first peak does not appear so vividly in core 690 because of the uppermost segment of its age model. To place the records in the appropriate regional magnetostratigraphic context, they were then compared with several other records in the Western Arctic, as well as the *CALS3K.4* geomagnetic field model (Korte and Constable, 2011). Of the directional records used for comparison in the previous section, RPI records were also available for core 2004-804-803 from the Beaufort Sea, and cores HYL-0501-05JPC and HYL-0501-06JPC from the Chukchi Sea (Barletta et al., 2008). Several of the same features identified in common between core 690 and core 680 potentially appear in the other records, and it is perhaps possible to link the P-4 feature in all the records. Furthermore, the longer-term trends observed in the two cores mirror the results of the *CALS3K.4* model closely, lending support to the quality of the RPI recorded in both (Figure 16).

#### *5.4 Geomagnetic Field Behavior*

High-latitude paleomagnetic records are also of great fundamental interest to geomagnetic field studies, as well as inspections on geodynamo workings. Though there are an insufficient number of such records available for study, existing ones have begun to allow the comparison of High Arctic, Low Arctic, and mid-latitude geomagnetic field characteristics. There is evidence to suggest that the geomagnetic field may behave uniquely in the High Arctic, which falls well within the hypothesized bounds of the tangent cylinder, while Low Arctic and mid-latitude records appear to correlate (e.g., Barletta et al., 2008; Benson et al., 2008; Cook et al., 2008; Francus et al., 2008; St-Onge and Stoner et al., 2011). The latitude of cores 690 and 680 is particularly interesting, as it is very near the proposed location of the tangent cylinder limits ( $\approx 69.5^\circ$  N). PSV features in both cores can indeed be tentatively linked to features in lower latitude records such as Mara Lake and PSVL, as shown in Figures 12 and 13, and may as well bear similarities to some continental U.S. lacustrine records not shown here (e.g., Lund and Banerjee, 1985; Verosub

et al., 1986). This is consistent with the findings of previous studies from the region (e.g., Barletta et al., 2008; Lisé-Pronovost et al., 2009). Conversely, these broader features do not correlate with High Arctic records, namely from Murray and Sawtooth Lakes on Ellesmere Island, Nunavut (Besonen et al., 2008; Cook et al., 2008). In addition to contributing information regarding the spatial influence of the tangent cylinder, this further supports the possibility of using reliably dated, mid-latitude paleomagnetic records to strengthen magnetostratigraphy-based chronologies of Arctic studies.

More high-resolution paleomagnetic studies are also needed in order to investigate uniquely mid- to high-latitude geomagnetic field dynamics, including the behavior of flux lobes and, possibly related, the rapid migration of the North Magnetic Pole and concurrent decline in field intensity observed over the past  $\approx 100$  yrs (Olsen and Mandeia, 2007). The long directional record obtained from core 690 exhibits several large changes in relative declination, suggesting that the recent migration of the North Magnetic Pole, though an extraordinary feature in historical records, may not be atypical in a longer context (Figure 13). This is consistent with the inference of other past migrations from virtual geomagnetic pole (VGP) reconstructions, such as one from the Fram Strait toward North America occurring over  $\approx 50$  yrs in the 15th century (St-Onge and Stoner, 2011).

### *5.5 Mackenzie Shelf Environmental Setting*

The physical and magnetic properties of the two cores are largely homogeneous and exhibit no distinctive trends or rapid changes, and thus it appears that the two cores fall within one major lithologic unit. This surface unit, characteristic of postglacial shelf deposits (see section 3.1), most likely comprises sediment eroded from the North American continent by the Mackenzie River. These fine-grained, continental sediments are generally rich in quality magnetic recorders such as magnetite and titanomagnetite, and commonly occur in deposits on Arctic shelves (Bischof and Darby, 1997, 1999; Darby, 2003; Darby and Bischof, 2004; Stoner and St-Onge, 2007). Here, magnetite is indeed demonstrated to be the primary remanence carrier in both cores (see section 3.3). Magnetic grain size varies

little downcore and is comparable between the two cores, based on uniform MDF values and similar magnetic hysteresis parameters (Figures 7, 8, and 9).

Both mean physical grain size (Figure 3) and magnetic grain size (Figures 7 and 9) are marginally larger in core 680 than in core 690. This is unexpected since core 690 is  $\approx$  17 km closer to the mouth of the river, and suggests that other circulation patterns may be active in transporting larger grained sediments in or across the Mackenzie Trough. One possibility is the extension of the eastward-flowing Beaufort Undercurrent, proposed by Aagaard (1984) and Hill et al. (1991). This bottom current begins to play a stronger role relative to that of the Mackenzie river outflow at depths  $>$  60 m, thus over a regime that encompasses the core 680 site but not the core 690 site. Site 680 is also in more direct alignment with two other potential sediment sources: coastal erosion from Herschel Island via eastward wind and surface currents, and fluvial transport from the Babbage River (Figure 1). Any of these factors could impose a contributing control on deposition, most likely acting to a greater degree at site 680 than at site 690, and thereby reducing the relative influence of the Mackenzie River itself. This could potentially explain not only the larger overall grain size in core 680, but also the higher degree of sorting and more erratic variations in granulometry and magnetic susceptibility downcore (Figures 3 and 10).

### *5.6 Late Holocene Environmental Changes*

When regarded on their independent age scales, possible stratigraphic correlation between the two sites is observed in the  $k_{LF}$  records (and  $k_{ARM}/k_{LF}$  ratios) (Figure 17). The major peaks in the  $k_{LF}$  record of core 690 appear to be matched by peaks in core 680, though in core 680 these features are less prominent either due to the greater degree of natural variation in grain size or the quality of the magnetic susceptibility record. Once again, the uppermost feature in core 690 appears to be dilated due to its age model.

In order to further assess the possibility of periodic or quasi-periodic changes in concentration, and thus sediment supply, wavelet analysis was conducted on  $k_{LF}$  and other magnetic parameters in both cores using MATLAB. Wavelet analysis revealed little from

NRM, ARM, and IRM records, but for  $k_{LF}$  a strong signal was exhibited at a period of  $\approx 200$  yrs throughout the length of core 690 (Figure 18). A higher frequency also appears in core 690, with a period of  $\approx 95$ -115 yrs. The  $\approx 200$  yr periodicity is also registered in core 680, though with a significantly weaker signal than in core 690 (Figure 19). The higher frequency features observed in core 690 do not appear in core 680; one weak peak is recorded at a period of  $\approx 70$  yrs, but it is largely diminished by a low degree of smoothing ( $sf = 3$ ). This signal only appears in the record between about 740 and 1740 cal BP.

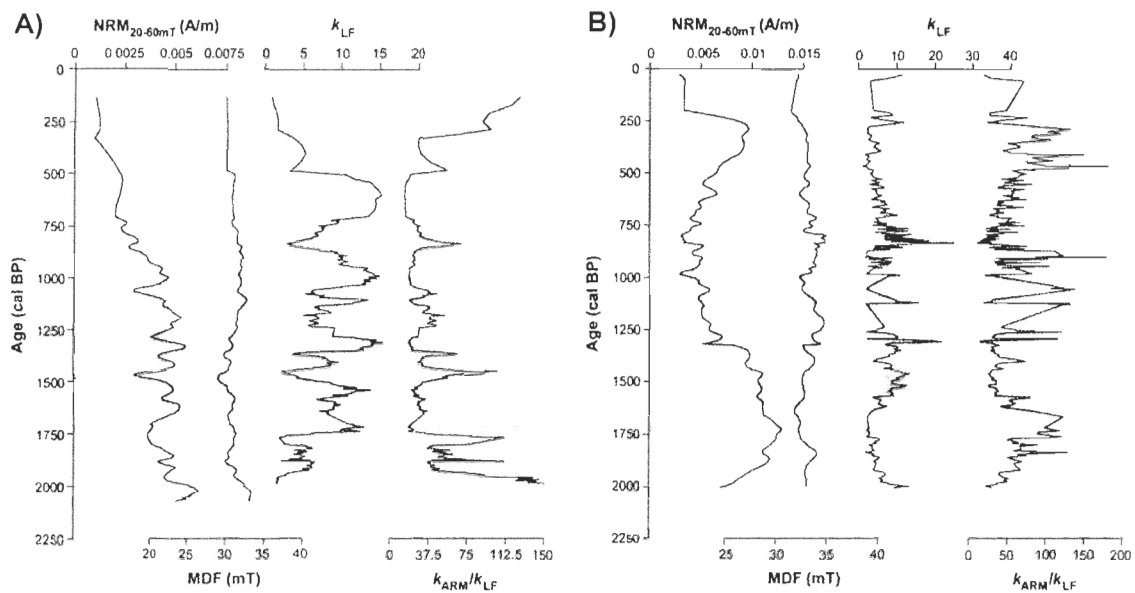


**Figure 17:** NRM, MDF,  $k_{LF}$ , and  $k_{ARM}/k_{LF}$  versus age for A) core 690 and B) core 680. Corresponding bands of higher magnetic susceptibility between the two cores are suggested by shaded intervals.

Cross-wavelet coherence tests of both smoothed and unsmoothed data confirm that the same major features are indeed recorded at both sites (Figure 20). The  $\approx 200$  yr period exhibits strong coherence between the two cores, gaining power relative to other signals when smoothed datasets are used. A weaker coherence in the  $\approx 100$  yr signal is also measured, despite being difficult to independently identify in core 680 (probably due to masking by the more prominent signals). The high frequency ( $\approx 70$  yr period) feature observed in core 680 is not seen in coherence tests, confirming that it was not recorded, or only very weakly recorded, in core 690.

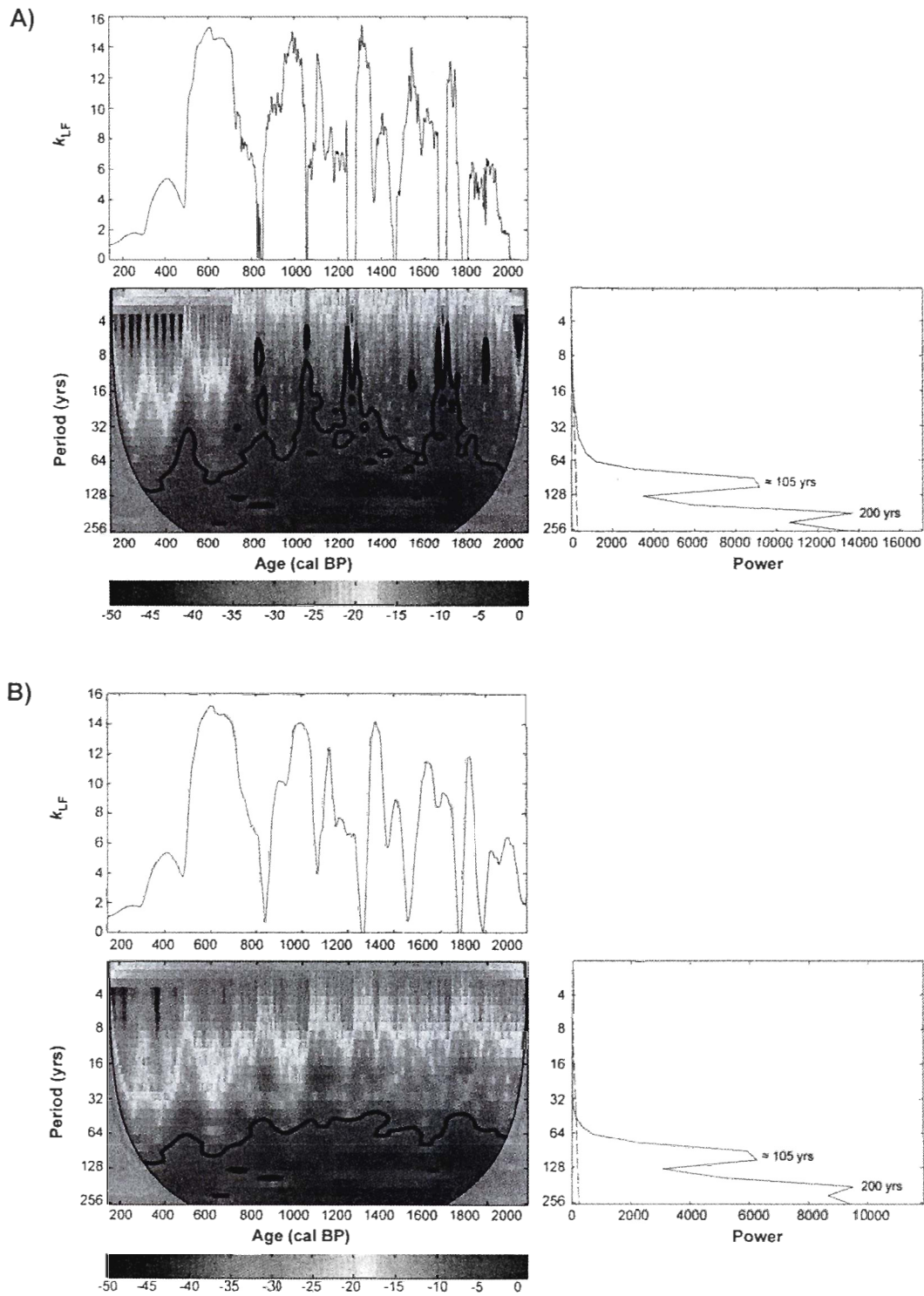


Figure 18: Wavelet analysis of A) unsmoothed and B) smoothed ( $sf=3$ )  $k_{LF}$  in core 690.

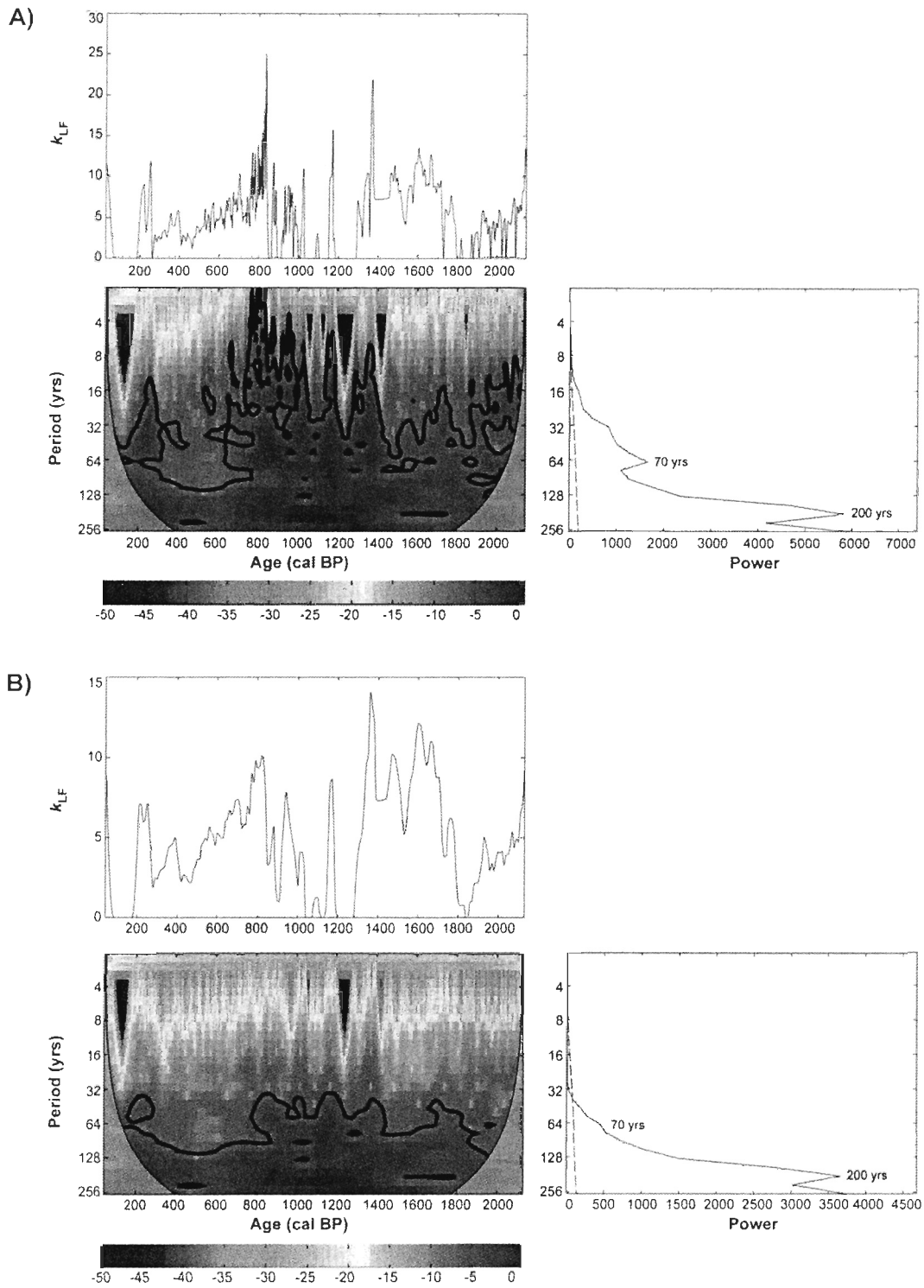
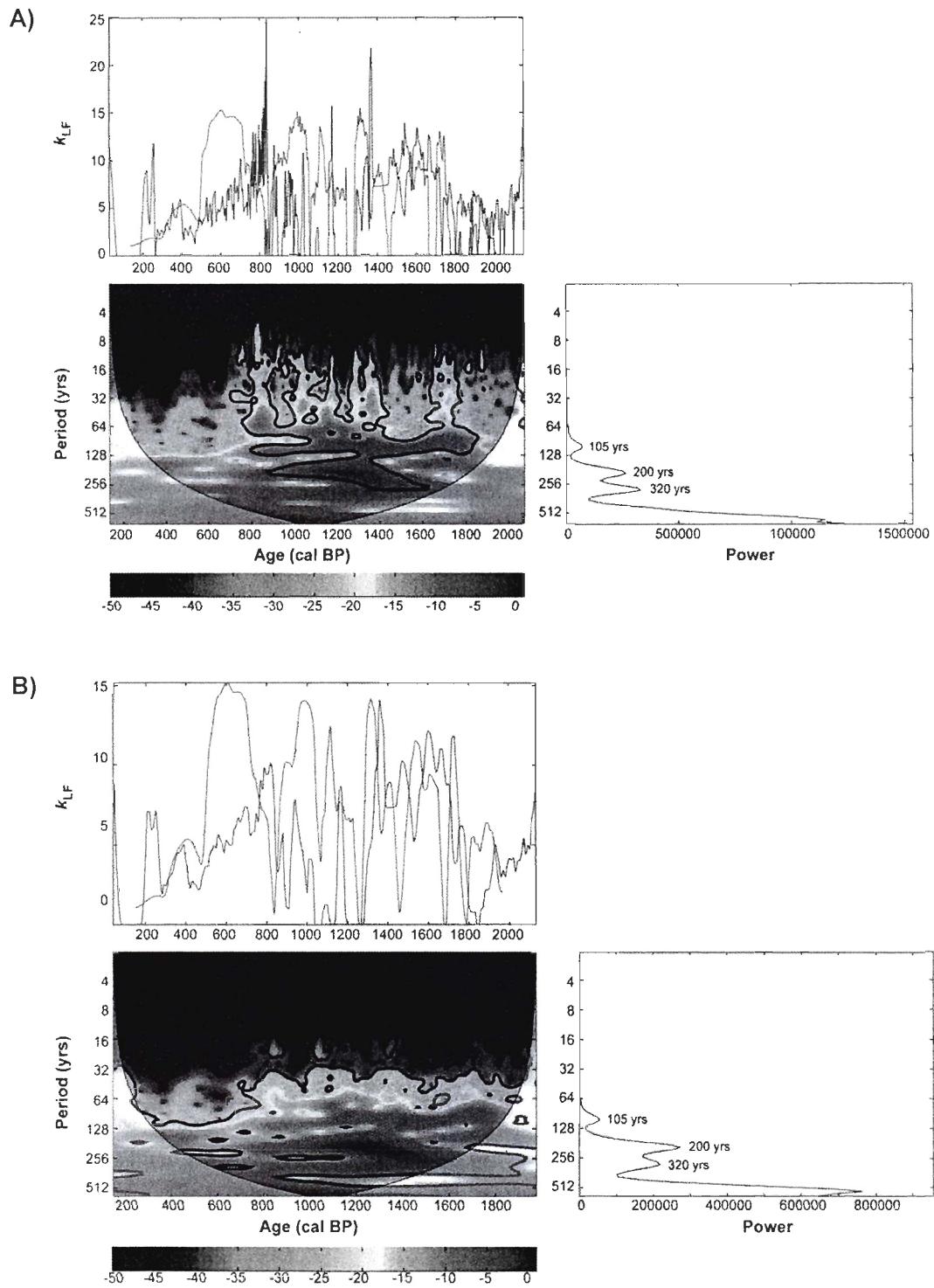


Figure 19: Wavelet analysis of A) unsmoothed and B) smoothed ( $sf = 3$ )  $k_{LF}$  in core 680.



**Figure 20:** Cross-wavelet coherence between core 690 and 680 for A) unsmoothed and B) smoothed  $k_{LF}$ .

The 200 yr feature observed in both records is potentially related to a 200 yr solar cycle known as the Suess (or de Vries) cycle (Damon and Sonnett, 1991). A model developed by Shindell et al. (2001) suggests that decreases in solar irradiance could trigger surface climate changes similar to those observed during the low index/negative phase of the Arctic Oscillation (AO) and North Atlantic Oscillation (NAO), demonstrating this specifically for the example of the  $\approx 0.25\%$  decrease in solar activity during the Maunder Minimum. By the same principle, it is possible that the  $\approx 100$  yr period observed in both cores could be a reflection of the Geissberg Cycle, an 88 yr amplitude modulation of the 11 yr Schwabe Cycle in solar activity (Sonnett and Finney, 1990). Solar activity could indirectly affect the AO and NAO either by controlling atmospheric circulation patterns, or by influencing North Atlantic Deep Water (NADW) formation through its controls on sea ice (Haigh, 1996; Shindell et al., 1999; Bond et al., 2001). Simulations conducted by Shindell et al. (2001) have shown that the reduction of solar irradiance led to dryer conditions in the Western Arctic through the resultant effects on the AO/NAO, while Schiller et al. (1997) demonstrated that a reduction in NADW formation would be similarly manifested in the water vapor budget of the North Pacific. In either case, these claims concerning atmospheric moisture supply are supported by Alaskan proxy records (Bond et al., 2001; Hu et al., 2003), as well as by box core proxy data from the site of core 680, in which freshwater palynomorph fluxes increased during the positive phase of the AO beginning around AD 1970 (Durantou et al., 2012). Dryer conditions would likely result in reduced precipitation in the Mackenzie River watershed, and thus reduced runoff. Decreases in both the contribution and size of sediments due to continental runoff can be expected to register in the sedimentary record as periods of relatively low magnetic susceptibility, or relatively high  $SIRM_{0mT}/k_{LF}$  and  $k_{ARM}/k_{LF}$  values, respectively (e.g., Liu et al., 2012).

Higher frequency decadal to multi-decadal variations in magnetic susceptibility, such as the  $\approx 70$  yr feature transiently observed in the core 680 record, could also be occurring due to the influence of the Pacific Decadal Oscillation (PDO). Also at play as a modulating influence may be the El Niño Southern Oscillation (ENSO), which has been linked to the

PDO through modeling studies, observational data, and various proxy records (Alexander et al., 2002; Newman et al., 2003; Vimont, 2005; Di Lorenzo et al., 2010; as cited in Steinman et al., 2012). The PDO has been proposed as a one of the most prominent regional controls on climate in the Western Arctic; it notably affects the Aleutian Low, which in turn governs both precipitation to the Mackenzie River watershed and the advection of Pacific waters through the Bering Strait (Zhao et al., 2006; Cassano and Cassano, 2010; Danielson et al., 2011). Indeed, the aforementioned young proxy records developed by Durantou et al. (2012) from the box core sampled at site 680 also reflect the strong influence of the PDO in this area, which modulates the advection of relatively warm, saline Pacific waters into the Arctic Ocean and eastward over the Beaufort Shelf. Furthermore, Burn (2008) has successfully modeled a link between the PDO and the timing of variations in runoff in the Mackenzie River watershed. The 20-30 yr cycles of the PDO cannot however explain the longer-term periodic features observed in the records of this study. Nevertheless, the PDO has also been shown to co-vary with the AO (Hetzinger, 2011), while a teleconnection has been demonstrated between the AO and other Canadian watersheds, such as those of the Hudson Bay (Déry and Wood, 2004), making this another mechanism by which solar variability could influence the hydrology of the western North American continent. The fact that this multi-decadal feature does not appear to be recorded in core 690 raises questions, particularly concerning differing degrees of fluvial and marine influence on sedimentation at the two sites, though the dubious age model over the upper segment of core 690 is also a likely contributor to the loss of higher frequency signals.

These conjectures are supported by the comparison of the magnetic susceptibility records with various proxy reconstructions representing PDO dynamics during the Holocene (Figure 21). Peaks in magnetic susceptibility are shown to correlate with peaks in two  $\delta^{18}\text{O}$  records from the U.S. Southwest, obtained from speleothems in New Mexico and alpine lakes in Colorado (Asmerom et al., 2007; Anderson, 2012). In these records,  $\delta^{18}\text{O}$  maxima are interpreted to reflect periods of decreased precipitation in the region, corresponding to increased solar activity and enhanced PDO/ENSO dynamics (Asmerom et

al., 2007; Anderson, 2012). In the northwestern U.S. and southwestern Canada, the same PDO phase results instead in increased precipitation, reflected by a Washington reconstruction based on lake sediment  $\delta^{18}\text{O}$  and  $\delta^{13}\text{C}$  records (Steinman et al., 2012).

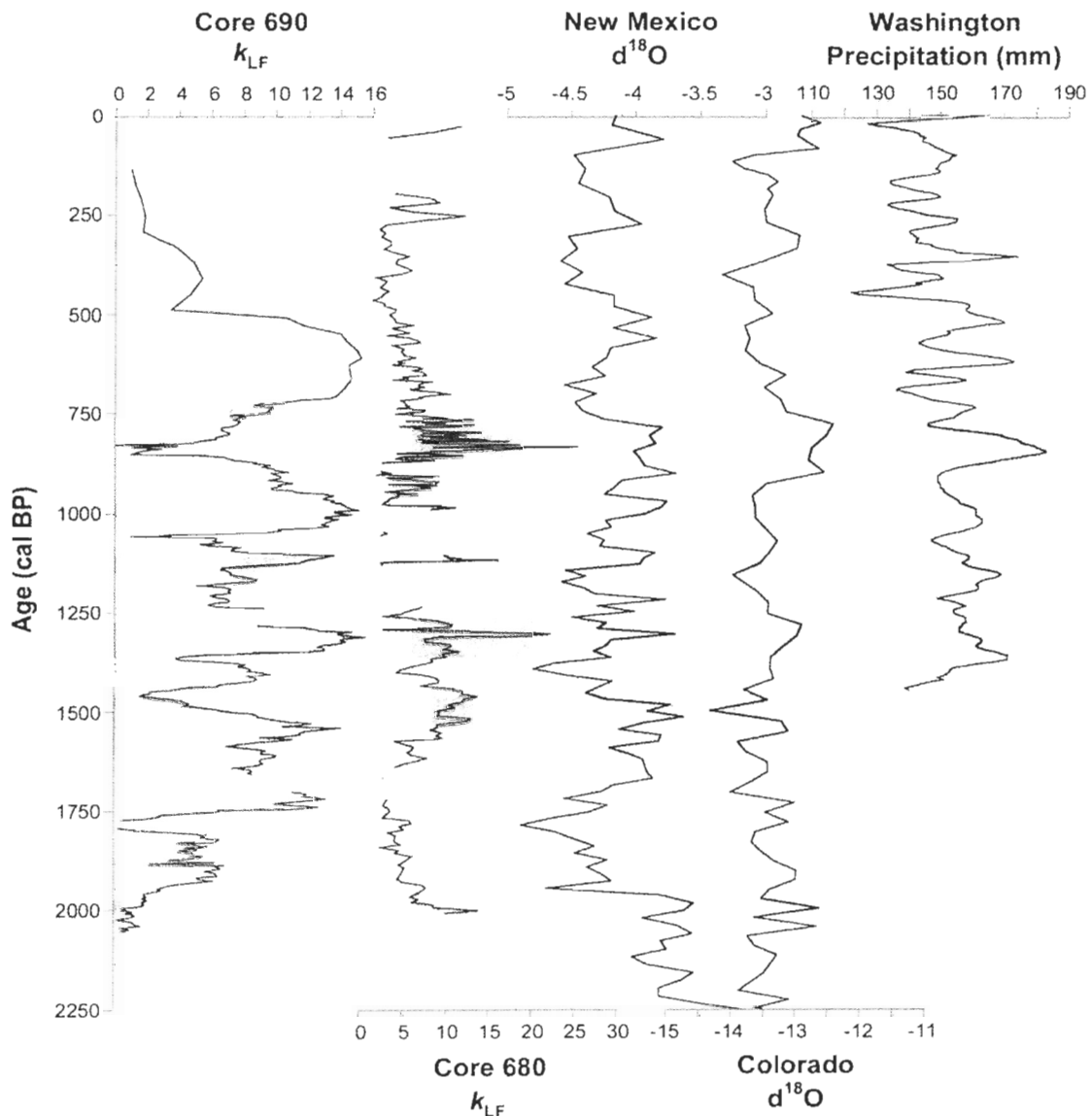


**Figure 21:** Comparison of  $k_{LF}$  with  $\delta^{18}\text{O}$  records from New Mexico and Colorado, and a precipitation reconstruction from Washington.

## 6. Conclusions

Full-vector paleomagnetic records were successfully developed for core 690 and part of core 680 representing the Late Holocene in the Beaufort Sea. A relatively large number of shells sampled from each core allowed for the establishment of two radiocarbon age models, which were verified using the full-vector paleomagnetic correlation of both cores with the *CALS3K.4* geomagnetic field model and several other regional paleomagnetic records. The high sedimentation rates of the Mackenzie River Trough permit an exceptionally high-resolution paleomagnetic and paleoclimatic record by Arctic standards. Granulometric properties demonstrate a mild difference in depositional regimes between the two cores despite their proximity to one another, suggesting that at greater distances from the Mackenzie River ocean and surface currents, as well as other potential sediment sources in the vicinity, also contribute to sedimentation. In addition, quasi-periodic variations in-phase with known solar cycles (such as the Suess and Geissberg) were observed particularly in the magnetic susceptibility records of both cores, and suggest a possible linkage between solar activity and atmospheric oscillations such as the Arctic and North Atlantic Oscillations, and, most notably, the Pacific Decadal Oscillation, which may modulate the hydrologic budget of the Mackenzie River.

## **7. Acknowledgements**

We extend great thanks to ArcticNet and the captain, officers, crew and scientists aboard the CCGS Amundsen during the Malina Arctic expedition of 2009. We are also grateful to Jacques Labrie (ISMER) for his help with laboratory work and wavelet analysis, and to Guillaume Massé (Takuvik) for sharing four radiocarbon dates. This study was supported by the Natural Sciences and Engineering Research Council of Canada through Discovery and Northern Supplement grants to G.S. and A.R., and by a scholarship from the GEOTOP research center to E.B. Finally, we thank Canada Economic Development for Quebec Regions for the purchase of the CASQ corer, and the Canadian Foundation for Innovation for financial support in the acquisition and operation of the cryogenic magnetometer.



## CONCLUSION

Les carottes 690 et 680 présentent deux nouveaux enregistrements paléomagnétiques de l'Holocène récent dans l'ouest de l'Arctique. Chaque enregistrement a une chronologie basée sur plusieurs dates au radiocarbone et soutenue par la corrélation temporelle complète du vecteur paléomagnétique (inclinaison, déclinaison et intensité), établie pour toute la longueur de la carotte 690 et la partie intermédiaire de la carotte 680, avec d'autres enregistrements de l'Arctique ainsi qu'avec le modèle géomagnétique *CALS3K.4* (Korte et al., 2011). De plus, les similarités entre ces archives et d'autres enregistrements provenant des moyennes latitudes, ainsi que les différences avec les enregistrements du haut Arctique, permettent de spéculer sur l'influence du cylindre tangent qui devrait influencer certaines caractéristiques du champ uniquement dans le haut Arctique.

En plus de l'étude paléomagnétique, ces deux carottes offrent une perspective sur l'histoire climatique et environnementale de la région pendant les deux derniers millénaires. La granulométrie démontre que le sédiment au site 680 est moins bien trié et de plus grande taille moyenne par rapport au site 690 (ce dernier étant le plus près de l'embouchure du fleuve Mackenzie). Ceci suggère que la sédimentation au site le plus distal subit l'influence du courant profond de Beaufort, ou qu'il y aurait possiblement une autre source de sédiment provenant de l'île de Herschel ou du fleuve Babbage.

Finalement, des variations cycliques observées dans les données de la susceptibilité magnétique des deux carottes indiquent un possible contrôle climatique sur l'apport de sédiment. Le cycle le plus important se manifeste à la même échelle de temps que le cycle solaire de Suess de  $\approx 200$  ans (Damon and Sonnett, 1991). Ce cycle pourrait avoir une influence sur les oscillations atmosphériques de l'Arctique et du nord de l'Atlantique et sur la formation des eaux profondes de l'Atlantique Nord (e.g., Haigh et al., 1996; Shindell et al., 2001; Bond et al., 2001). La compréhension des processus solaires, atmosphériques et

océaniques est au cœur de la mise en contexte des changements climatiques qui sont observés aujourd'hui et les enregistrements environnementaux de l'Arctique fournissent de l'information de grande valeur à la compréhension de la dynamique de tels processus.

Malgré son importance pour la compréhension du champ géomagnétique et des changements climatiques modernes, l'Arctique reste aujourd'hui une région insuffisamment étudiée et sous-échantillonnée. Grâce à ce projet de maîtrise, certaines réponses ont pu être apportées. Toutefois, il n'est pas encore possible de répondre à l'ensemble des questions préalablement présentées. Une meilleure évaluation de l'influence spatiale du cylindre tangentiel et des lobes de flux aurait nécessité un plus grand nombre d'échantillons espacés spatialement. Du côté environnemental, des études plus détaillées des courants marins, de la bathymétrie et de la sédimentation moderne dans la Fosse du Mackenzie seraient nécessaires pour vérifier les sources secondaires de sédiments et les processus marins qui les contrôlent. Finalement, pour mieux comprendre le rôle joué par les oscillations atmosphériques dans les variations climatiques et environnementales actuelles en Arctique, une fois de plus, des enregistrements sédimentaires supplémentaires de haute résolution couvrant tout l'Holocène seraient essentiels. Néanmoins, les deux archives présentées dans ce mémoire offrent une perspective préliminaire de grande valeur sur quelques processus qui pourraient agir dans l'ouest de l'Arctique et confirment la capacité de la Fosse du Mackenzie à enregistrer et à bien préserver les variations géomagnétiques et climatiques avec une résolution temporelle remarquable pour l'Arctique.



## RÉFÉRENCES BIBLIOGRAPHIQUES

- Aagaard, K., 1984. The Beaufort Undercurrent. *The Alaskan Beaufort Sea: ecosystems and environments*, 47-71.
- Alexander, M.A., Bladé, I., Newman, M., Lazante, J.R., Lau, N.C., Scott, J.D., 2002. The Atmospheric Bridge: The influence of ENSO teleconnections on air-sea interaction over the global ocean. *Journal of Climate* 15, 2205-2231.
- Ambaum, M.H.P., Hoskins, B.J., Stephenson, D.B., 2001. Arctic Oscillation or North Atlantic Oscillation? *Journal of Climate* 14, 3495-3507.
- Anderson, L., 2012. Rocky Mountain Hydroclimate: Holocene variability and the role of insolation, ENSO and the North American Monsoon. *Global and Planetary Change*, 92-93, 198-208. doi:10.1016/j.gloplacha.2012.05.012.
- Andrews, J.T., Jennings, A.E., 1990. Geomagnetic secular variations (inclination) of high latitude fiord cores: eastern Canadian Arctic. *Polar Research* 8, 245-259.
- Andrews, J.T., Mothersill, J.S., Tabrez, A.R., 1986. Paleomagnetic record, texture, and mineralogy of Late Quaternary sediments, Baffin Island Fjords, N.W.T., Canada. *Arctic and Alpine Research* 18 (4), 361-376.
- Asmerom, Y., Polyak, V., Burns, S., Rasmussen, J., 2007. Solar forcing of Holocene climate: New insights from a speleothem record, southwestern United States. *Geology* 35 (1), 1-4. doi: 10.1130/G22865A.1.
- Barletta, F., St-Onge, G., Channell, J.E.T., Rochon, A., Polyak, L., Darby, D.A., 2008. High-resolution paleomagnetic secular variation and relative paleointensity records from the western Canadian Arctic: implication for Holocene stratigraphy and geomagnetic field behavior. *Canadian Journal of Earth Sciences* 45, 1265-1281.

- Barletta, F., St-Onge, G., Channell, J.E.T., Rochon, A., 2010. Dating of Holocene western Canadian Arctic sediments by matching paleomagnetic secular variation to a geomagnetic field model. *Quaternary Science Reviews* 29, 2315-2324.
- Barletta, F., St-Onge, G., Stoner, J.S., Lajeunesse, P., Locat, J., 2010. A high-resolution Holocene paleomagnetic secular variation and relative paleointensity stack from eastern Canada. *Earth and Planetary Science Letters* 298, 162-174.
- Batchelor, C.L., Dowdeswell, J.A., Pietras, J.T., 2013. Seismic stratigraphy, sedimentary architecture and palaeo-glaciology of the Mackenzie Trough: evidence for two Quaternary ice advances and limited fan development on the western Canadian Beaufort Sea margin. *Quaternary Science Reviews* 65, 73-87.
- Besonen, M.R., Patridge, W., Bradley, R.S., Francus, P., Stoner, J.S., Abbot, M.B., 2008. A record of climate over the last millennium based on varved lake sediments from the Canadian High Arctic. *The Holocene* 18 (1), 169-180.
- Bischof, J.A., Darby, D.A., 1997. Mid to Late Pleistocene ice drift in the western Arctic Ocean: evidence for a different circulation in the past. *Science* 277, 74-78.
- Bischof, J.A., Darby, D.A., 1999. Quaternary ice transport in the Canadian Arctic and extent of Late Wisconsinian glaciations in the Queen Elizabeth Islands. *Canadian Journal of Earth Sciences* 36, 2007-2022.
- Blasco, S.M., Fortin, G., Hill, P.R., O'Conner, M.J., Brigham-Grette, J.K., 1990. The Late Neogene and Quaternary stratigraphy of the Canadian Beaufort continental shelf. In: Grantz, A., Johnson, L., Sweeney J.F. (Eds.), *The Arctic Ocean region, The Geology of North America*, vol. L, Geological Society of America, pp. 491-502.
- Blott, S.J., Pye, K., 2001. GRADISTAT: a grain size distribution and statistics package for the analysis of unconsolidated sediments. *Earth Surface Processes and Landforms* 26, 1237-1248.
- Bloxham, J., Gubbins, D., 1985. The secular variation of Earth's magnetic field. *Nature* 317, 777-781.

- Bond, G., Kromer, B., Beer, J., Muscheler, R., Evans, M.N., Showers, W., Hoffman, S., Lotti-Bond, R., Hajdas, I., Bonani, G., 2001. Persistent solar influence on North American climate during the Holocene. *Science* 294 (5549), 2130-2136.
- Boyer-Villemare, U., St-Onge, G., Bernatchez, P., Lajeunesse, P., Labrie, J., 2012. High-resolution multiproxy records of sedimentological changes induced by dams in the Sept-Îles area (Gulf of St. Lawrence, Canada). *Marine Geology* 338, 17-29.
- Brachfeld, S., Banerjee, S.K., 2000. A new high-resolution geomagnetic relative paleointensity record for the North American Holocene: a comparison of sedimentary and absolute intensity data. *Journal of Geophysical Research* 105, 821-834.
- Bringué, M., Rochon, A., 2012. Late Holocene paleoceanography and climate variability over the Mackenzie Slope (Beaufort Sea, Canadian Arctic). *Marine Geology* 291-294, 83-96.
- Burn, D.H., 2008. Climatic influences on streamflow timing in the headwaters of the Mackenzie River Basin. *Journal of Hydrology* 352, 225-238.
- Carmack, E.C., Barber, D., Christensen, J., Macdonald, R., Rudels, B., Sakshaug, E., 2006. Climate variability and physical forcing of the food webs and the carbon budget on panarctic shelves. *Progress in Oceanography* 71 (2-4), 145-181.
- Carmack, E.C., Macdonald, R.W., 2002. Oceanography of the Canadian Shelf of the Beaufort Sea; a setting for marine life. *Arctic* 55, 29-45.
- Carmack, E.C., Macdonald, R.W., Jasper, S., 2004. Phytoplankton productivity on the Canadian Shelf of the Beaufort Sea. *Marine Ecology, Progress series* 277, 37-50.
- Carson, M.A., Jasper, J.N., Conly, F.M., 1998. Magnitude and sources of sediment input to the Mackenzie Delta, Northwest Territories, 1974-94. *Arctic* 51, 116-124.
- Cassano, E.N., Cassano, J.J., 2010. Synoptic forcing of precipitation in the Mackenzie and Yukon River basins. *International Journal of Climatology* 30, 658-674.

- Channell, J.E.T., Mazaud, A., Sullivan, P., Turner, S., Raymo, M.E., 2002. Geomagnetic excursions and paleointensities in the 0.9-0.15 Ma interval of the Matuyama Chron at ODP site 983 and 984 (Iceland Basin). *Journal of Geophysical Research* 107 (B6), 1-11.
- Cook, T.L., Bradley, R.S., Stoner, J.S., Francus, P., 2008. Five thousand years of sediment transfer in a High Arctic watershed recorded in annually laminated sediments from Lower Murray Lake, Ellesmere Island, Nunavut, Canada. *Journal of Paleolimnology*, doi: 10.1007/s10933-008-9252.
- Creer, K.M., Tucholka, P., 1982. Construction of type curves of the geomagnetic secular variation for dating lake sediments from east central North America. *Canadian Journal of Earth Sciences* 19, 1106-1115.
- Damon, P.E., Sonnett, C.P., 1991. Solar and terrestrial components of the atmospheric  $^{14}\text{C}$  variation spectrum. In: Sonnett, C.P., Giampapa, M.S., Matthews, M.S., (Eds.), *The Sun in Time*, The University of Arizona Press, pp. 360-388.
- Danielson, S., Eisner, L., Weingartner, T., Aagaard, K., 2011. Thermal and haline variability over the central Bering Sea shelf: Seasonal and interannual perspectives. *Continental Shelf Research* 31, 539-554.
- Dankers, P., 1981. Relationship between median destructive field and coercive forces for dispersed natural magnetite, titanomagnetite and hematite. *Geophysical Journal of the Royal Astronomical Society* 64, 447-461.
- Darby, D.A., 2003. Sources of sediment found in sea ice from the western Arctic Ocean, new insights into processes of entrainment and drift patterns. *Journal of Geophysical Research* 108, 13-1:13-10.
- Darby, D.A., Bischof, J.F., 2004. A Holocene record of changing Arctic Ocean ice drift analogous to the effects of the Arctic Oscillation. *Paleoceanography* 19, PA1027.
- Darby, D.A., Polyak, L., Bauch, H.A., 2006. Past glacial and interglacial conditions in the Arctic Ocean and marginal seas - a review. *Progress in Oceanography* 71, 129-144.

- Day, R., Fuller, M., Schmidt, V.A., 1977. Hysteresis properties of titanomagnetites: grain-size and compositional dependence. *Physics of Earth and Planetary Interiors* 13, 260-267.
- Dean, E.T., 1997. Rates, timing, and cyclicity of Holocene eolian activity in north-central United States: Evidence from varved lake sediments. *Geology* 25 (4), 331-334.
- Déry, S.J., Wood, E.F., 2004. Teleconnection between the Arctic Oscillation and Hudson Bay river discharge. *Geophysical Research Letters* 31, L18205.
- Di Lorenzo, E., Cobb, K.M., Furtado, J.C., Schneider, N., Anderson, B.T., Bracco, A., Alexander, M.A., Vimont, D.J., 2010. Central Pacific El Niño and decadal climate change in the North Pacific Ocean. *Nature Geoscience* 3, 762-765.
- Dittmar, T., Kattner, G., 2003. The biogeochemistry of the river and shelf ecosystem of the Arctic Ocean: a review. *Marine Chemistry* 83, 103-120.
- Doraxan, D., Ehn, J., Bélanger, S., Matsuoka, A., Hooker, S., Babin, M., 2012. Optical characterization of suspended particles in the Mackenzie River plume (Canadian Arctic Ocean) and implications for ocean colour remote sensing. *Biogeosciences* 9, 3213-3229. doi: 10.5194/bg-9-3213-2012.
- Dowdeswell, J.A., Kenyon, N.H., Laberg, J.S., 1997. The glacier-influenced Scoresby Sund Fan, East Greenland continental margin: evidence from GLORIA and 3.5 kHz records. *Marine Geology* 35, 359-362.
- Durantou, L., Rochon, A., Ledu, D., Massé, G., Schmidt, S., Babin, M., 2012. Quantitative reconstruction of sea-surface conditions over the last ~ 150 yr in the Beaufort Sea based on dinoflagellate cyst assemblages: the role of large scale atmospheric circulation patterns. *Biogeosciences* 9, 5391-5406. doi: 10.5194/bg-9-5391-2012.
- Elverhøi, A., Lieston, O., Nagy, J., 1980. Glacial Erosion, Sedimentation and Microfauna in the Inner Part of Kongsfjorden, Spitsbergen. *Norsk Polar-institutt Skrifter* 172, 28-61.
- Francus, P., Bradley, R.S., Lewis, T., Abbott, M.B., Retelle, M., Stoner, J.S., 2008. Limnological and sedimentary processes at Sawtooth Lake, Canadian High Arctic, and

their influence on varve formation. *Journal of Paleolimnology*. doi: 10.1007/s10933-008-9210-x.

Gallet, Y., Genevey, A., LeGoff, M., 2002. Three millennia of directional variation of the Earth's magnetic field in Western Europe as revealed by archeological artefacts. *Physics of the Earth and Planetary Interiors* 131, 81-89.

Geiss, C.E., Banerjee, S.K., 2003. A Holocene-Late Pleistocene geomagnetic inclination record from Grandfather Lake, SW Alaska. *Geophysical Journal International* 153, 497-507.

Genevey, A., Gallet, Y., Constable, C., Korte, M., Hulot, G., 2008. ArcheoInt: an upgraded compilation of geomagnetic field intensity data for the past ten millennia and its application to the recovery of the past dipole moment. *Geochemistry Geophysics Geosystems* 9, Q03048.

Gogorza, C.S.G., Sinito, A.M., Vilas, J.F., Creer, K.M., Nuñez, H., 2000. Geomagnetic secular variations over the last 6500 years as recorded by sediments from the lakes of south Argentina. *Geophysical Journal International* 143, 787-798.

Haberzettl, T., St-Onge, G., Lajeunesse, P., 2010. Multi-proxy records of environmental changes in Hudson Bay and Strait since the final outburst flood of Lake Agassiz-Ojibway. *Marine Geology* 271, 93-105.

Haberzettl, T., St-Onge, G., Behling, H., Kirleis, W., 2012. Evaluating Late Holocene radiocarbon-based chronologies by matching the palaeomagnetic secular variations to geomagnetic field models: an example from Lake Kalimpaa (Sulawesi, Indonesia). In: Jovane, L., Herrero-Bervera, E., Hinnov, L.A., Housen, B.A., (Eds.), *Magnetic Methods and the Timing of Geologic Processes*, Geologic Society, London, Special Publications 373.

Hagstrum, J.T., Champion, D.F., 2002. A Holocene paleosecular variation record from <sup>14</sup>C-dated volcanic rocks in western North America. *Journal of Geophysical Research* 107 (B1), 8-1:8-14.

- Haigh, J.D., 1996. The impact of solar variability on climate. *Science* 272 (5264), 981, 984.
- Harper, J.R., Penland, S., 1982. Beaufort Sea sediment dynamics, Woodward-Clyde Consultants.
- Hetzinger, S., Halfar, J., Mecking, J.V., Keenlyside, N.S., Kronz, A., Steneck, R.A., Adey, W.H., Lebednik, P.A., 2011. Marine proxy evidence linking decadal North Pacific and Atlantic climate. *Climate Dynamics* 39, 1447-1455, doi: 10.1007/s00382-011-1229-4.
- Hill, P.R., Blasco, S.M., Harper, J.R., Fissel, D.B., 1991. Sedimentation on the Canadian Beaufort Shelf. *Continental Shelf Research* 11 (8-10), 821-841.
- Hill, P.R., 1996. Late Quaternary sequence stratigraphy of the Mackenzie Delta. *Canadian Journal of Earth Sciences* 33, 1064-1074.
- Hill, P.R., Lewis, C.P., Desmarais, S., Kaupaymuthoo, V., Rais, H., 2001. The Mackenzie Delta: Sedimentary processes and facies of a high-latitude, fine-grained delta. *Sedimentology* 48, 1047-1078.
- Hu, F.S., Kaufman, D., Yoneji, S., Nelson, D., Shemesh, A., Huang, Y., Tian, J., Bond, G., Clegg, B., Brown, T., 2003. Cyclic Variation and Solar Forcing of Holocene Climate in the Alaskan Subarctic. *Science* 301, 1890-1893.
- Jerosch, K., 2012. Geostatistical mapping and spatial variability of surficial sediment types on the Beaufort Shelf based on grain size data. *Journal of Marine Systems*, in press.
- Keigwin, L.D., Donnelly, J.P., Cook, M.S., Driscoll, N.W., Brigham-Grette, J., 2006. Rapid sea-level rise and Holocene climate in the Chukchi Sea., *Geology* 34, 861-864.
- King, J.W., Banerjee, S.K., Marvin, J.A., Özdemir, Ö., 1982. A comparison of different magnetic methods for determining the relative grain size of magnetite in natural materials: some results from lake sediments. *Earth and Planetary Science Letters* 59, 404-419.

- Kleiber, H.P., Knies, J., Niessen, F., 2000. The Late Weichselian glaciation of the Franz Victoria Trough, northern Barents Sea: ice sheet extent and timing. *Marine Geology* 168, 25-44.
- Knudsen, M.F., Riisager, P., Donadini, F., Snowball, I., Muscheler, R., Korhonen, K., Pesonen, L.J., Jacobsen, B.H., 2008. Variations in the geomagnetic dipole moment during the Holocene and the past 50 kyr. *Earth and Planetary Science Letters* 272, 319-329.
- Koch, J., Clague, J.J., Osborn, G.D., 2007. Glacier fluctuations during the past millennium in Garibaldi Provincial Park, southern Coast Mountains, British Columbia. *Canadian Journal of Earth Sciences* 44, 1215-1233.
- Kono, M., Roberts, P.H., 2003. Recent geodynamo simulation and observations of the geomagnetic field. *Reviews of Geophysics* 40. doi: 10.1029/2000RG000102.
- Korte, M., Constable, C., 2005. The geomagnetic dipole moment over the last 7000 years: new results from a global model. *Earth and Planetary Science Letters* 236, 348-358.
- Korte, M., Genevey, A., Constable, C., Frank, U., Schnepp, E., 2005. Continuous geomagnetic field models for the past 7 millennia: 1. A new global data compilation. *Geochemistry Geophysics Geosystems* 6, Q02H15.
- Korte, M., Constable, C., Donadini, F., Holme, R., 2011. Reconstructing the Holocene geomagnetic field. *Earth and Planetary Science Letters* 312, 497-505.
- Korte, M., Constable, C., 2011. Improving geomagnetic field reconstructions for 0-3 ka. *Physics of the Earth and Planetary Interiors* 188 (3-4), 347-259.
- Korte, M., Muscheler, R., 2012. Centennial to millennial geomagnetic field variations. *Journal of Space Weather and Space Climate* 2, A08.
- Lantuit, H., and Pollard, W.H., 2008. Fifty years of coastal erosion and retrogressive thaw slump activity on Herschel Island, southern Beaufort Sea, Yukon Territory, Canada. *Geomorphology* 95, 84-102.

- Lawrence, K.P., Tauxe, L., Staudigel, H., Constable, C.G., 2009. Paleomagnetic field properties at high southern latitude. *Geochemistry, Geophysics, Geosystems* 10, Q01005, doi: 10.1029/2008GC002072.
- Lean, J., Rind, D., 1999. Evaluating sun-climate relationships since the Little Ice Age. *Journal of Atmospheric and Solar-Terrestrial Physics* 61, 25-36.
- Ledu, D., Rochon, A., de Vernal, A., St-Onge, G., 2008. Palynological evidence of Holocene climate change in the eastern Arctic: a possible shift in the Arctic oscillation at the millennial time scale. *Canadian Journal of Earth Sciences* 45, 1363-1375.
- Lewis, C.P., 1988. Mackenzie Delta sedimentary environments and processes. Contract report. Environment Canada, Water Resources Branch, Ottawa.
- Lisé-Pronovost, A., St-Onge, G., Brachfeld, S., Barletta, F., Darby, D., 2009. Paleomagnetic constraints on the Holocene stratigraphy of the Arctic Alaskan margin. *Global and Planetary Change* 68, 85-99.
- Liu, Q., Roberts, A.P., Larrasoaña, C.J., Banerjee, S.K., Guyodo, Y., Tauxe, L., Oldfield, F., 2012. *Environmental Magnetism: Principles and Applications*. *Reviews of Geophysics* 50, RG4002.
- Lund, S.P., 1996. A comparison of Holocene paleomagnetic secular variation records from North America. *Journal of Geophysical Research* 101, 8007-8024.
- Lund, S.P., Banerjee, S.K., 1985. Late Quaternary paleomagnetic field variations from two Minnesota lakes. *Journal of Geophysical Research* 90, 803-825.
- Macdonald, R.W., Solomon, S.E., Cranston, R.E., Welch, H.E., Yunker, M.B., Gobeil, C., 1998. A sediment and organic carbon budget for the Canadian Beaufort Shelf. *Marine Geology* 144, 255-273.
- Macdonald, R.W., McLaughlin, F.A., Carmack, E.C., 2002. Fresh water and its sources during the SHEBA drift in the Canada Basin of the Arctic Ocean. *Deep Sea Research Part I: Oceanographic Research Papers* 49 (10), 1769-1785.

- Macdonald, R.W., Harner, T., Fyfe, J., 2005. Recent climate change in the Arctic and its impact on contaminant pathways and interpretation of temporal trend data. *Science of the Total Environment* 342, 5-86.
- Maher, A.B., Thompson, R., Hounslow, M.E., 1999. Introduction. In: Maher, A.B., Thompson, R. (Eds.), *Quaternary Climates, Environments and Magnetism*. Cambridge University press, United Kingdom.
- Mazaud, A., 2005. User-friendly software for vector analysis of the magnetization of long sediment cores. *Geochemistry Geophysics Geosystems* 6, Q12006.
- Newman, M., Compo, G.P., Alexander M.A., 2003. ENSO-forced variability of the Pacific Decadal Oscillation. *Journal of Climate* 16, 3853-3857.
- Niebauer, H.J., Day, R.H., 1989. Causes of interannual variability in the sea ice cover of the eastern Bering Sea. *GeoJournal* 18, 45-59.
- Ólafsdóttir, S., Geirsdóttir, Á., Miller, G.H., Stoner, J.S., Channell, J.E.T., 2013. Synchronizing Holocene lacustrine and marine sediment records using paleomagnetic secular variation. *Geology* 41 (5), 535-538.
- Olsen, N., Manda, M., 2007. Will the Magnetic North Pole move to Siberia. *Eos, Transactions, American Geophysical Union* 88, 293-294.
- Overland, J., Adams, J., Bond, N., 1999. Decadal variability of the Aleutian Low and its relation to high-latitude circulation. *Journal of Climate* 12, 1542-1548.
- Paillard, D., Labeyrie, L., Yiou, P., 1996. Macintosh program performs time-series analysis. *Eos Trans. AGU* 77, 379.
- Pelletier, B.R., 1984. Marine science atlas of the Beaufort Sea sediments. Geological Survey of Canada, Miscellaneous Report 38.
- Pickart, R.S., 2004. Shelfbreak circulation in the Alaskan-Beaufort Sea: mean structure and variability. *Journal of Geophysical Research* 109, C04024. doi: 10.1029/2003JC001912.

- Richerol, T., Rochon, A., Blasco, S., Scott, D.B., Schell, T.M., Bennett, R.J., 2008. Distribution of dinoflagellate cysts in surface sediments of the Mackenzie Shelf and Amundsen Gulf, Beaufort Sea (Canada). *Journal of Marine Systems* 74, 825-839.
- Roberts, A.P., Tauxe, L., Heslop, D., 2013. Magnetic paleointensity stratigraphy and high-resolution Quaternary geochronology: successes and future challenges. *Quaternary Science Reviews* 61, 1-16.
- Rochon, A., de Vernal, A., 1994. Palynomorph distribution in recent sediments from the Labrador Sea. *Canadian Journal of Earth Sciences* 31, 115-127.
- Rochon, A., Blasco, S., Travaglini, P., 2003. Cruise MR02-K05 on board the RV Mirai: Joint Western Arctic Climate Study (JWACS) 2002 Geoscience Program - Leg 2 - Tuktoyaktuk (Northwest Territories) to Dutch Harbor (Alaska) September 20 - October 10, 2003. Geologic Survey of Canada, open file 1781.
- Sagnotti, L., Macri, P., Lucchi, R., Rebesco, M., Camerlenghi, A., 2011. A Holocene paleosecular variation record from the northwestern Barents Sea continental margin. *Geochemistry Geophysics Geosystems* 12 (11).
- Schiller, A., Mikolajewicz, U., Voss, R., 1997. The stability of the North Atlantic thermohaline circulation in a coupled ocean-atmosphere general circulation model. *Climate Dynamics* 13, 325.
- Schipp, S.S., Anderson, J.B., Domack, E.W., 1999. Late Pleistocene-Holocene retreat of the West Antarctic Ice-Sheet system in the Ross Sea: Part 1 - Geophysical results. *Geological Society of America Bulletin* 111, 1486-1516.
- Scott, D.B., Schell, T., St-Onge, G., Rochon, A., Blasco, S., 2009. Foraminiferal assemblage changes over the last 15,000 years on the Mackenzie-Beaufort Sea Slope and Amundsen Gulf, Canada: Implications for past sea-ice conditions.
- Shindell, D.T., Rind, D., Balachandran, N., Lean, J., Lonergan, P., 1999. Solar cycle variability, ozone, and climate. *Science* 284, 305.

- Shindell, D.T., Schmidt, G.A., Mann, M.E., Rind, D., Waple, A., 2001. Solar forcing of regional climate change during the Maunder Minimum. *Science* 294 (5549), 2149-2152.
- Simon, Q., Hillaire-Marcel, C., St-Onge, G., Andrews, J.T., 2013. North-eastern Laurentide, western Greenland, and southern Inuitian ice stream dynamics during the last glacial cycle. *Journal of Quaternary Science*. doi: 10.1002/jqs.2648.
- Snowball, I., Sandgren, P., 2002. Geomagnetic field variations in northern Sweden during the Holocene quantified from varved lake sediments and their implications for cosmogenic nuclide production rates. *The Holocene* 12, 517-530.
- Snowball, I., Sandgren, P., 2004. Geomagnetic field intensity changes in Sweden between 9000 and 450 cal BP: extending the record of "archeomagnetic jerks" by means of lake sediments and the pseudo-Thellier technique. *Earth and Planetary Science Letters* 227, 361-376.
- Snowball, I., Zillén, L., Ojala, A., Saarinen, T., Sandgren, P., 2007. FENNOSTACK and FENNORPIS: varve dated Holocene paleomagnetic secular variation and relative paleointensity stacks from Fennoscandia. *Earth and Planetary Science Letters* 255, 106-116.
- Sonnett, C.P., and Finney, S.A., 1990. The spectrum of radiocarbon. *Philosophical Transactions of the Royal Society of London* 30A, 413-426.
- Steinman, B.A., Abbott, M.B., Mann, M.E., Stansell, N.D., Finney, B.P., 2012. 1,500 year quantitative reconstruction of winter precipitation in the Pacific Northwest. *Proceedings of the National Academy of Sciences*, 109 (29), 11619-11623. doi: 10.1073/pnas.1201083109.
- Stoner, J.S., St-Onge, G., 2007. Magnetic stratigraphy in paleoceanography: reversals, excursions, paleointensity, and secular variation. In: Hillaire-Marcel, C., de Vernal, A., (Eds.), *Proxies in Late Cenozoic Paleoceanography (Developments in Marine Geology)*, vol. 1. Elsevier, pp. 99-138.

- Stoner, J.S., Jennings, A., Kristjánsdóttir, G.B., Dunhill, G., 2007. A paleomagnetic approach toward refining Holocene radiocarbon-based chronologies: Paleoceanographic records from the north Iceland (MD99-2269) and east Greenland (MD99-2322) margins. *Paleoceanography* 22, PA1209.
- St-Onge, G., Stoner, J.S., Hillaire-Marcel, C., 2003. Holocene paleomagnetic records from the St-Lawrence Estuary, eastern Canada: centennial- to millennial-scale geomagnetic modulation of cosmogenic isotopes. *Earth and Planetary Science Letters* 209, 113-130.
- St-Onge, G., Mulder, T., Francus, P., Long, B., 2007. Continuous physical properties of cored marine sediment. In: Hillaire-Marcel, C., de Vernal, A., (Eds.), *Proxies in Late Cenozoic Paleoceanography (Developments in Marine Geology)*, vol. 1, Elsevier, pp. 99-138.
- St-Onge, G., and Stoner, J.S., 2011. Paleomagnetism near the North Magnetic Pole: A Unique Vantage Point for Understanding the Dynamics of the Geomagnetic Field and Its Secular Variations. *Oceanography* 24 (3), 42-50.
- St-Onge, G., St-Onge, M.-P., in press. Environmental changes in Baffin Bay during the Holocene based on physical and magnetic properties of sediment cores. *Journal of Quaternary Science*.
- Syvitski, J.P.M., 1991. Towards an understanding of sediment deposition on glaciated continental shelves. *Continental Shelf Research* 11 (8-10), 821-842.
- Tauxe, L., 1993. Sedimentary records of relative paleointensity: theory and practice. *Reviews of Geophysics* 31, 319-354.
- Tauxe, L., Wu, G., 1990. Normalized remanence in sediments of the Western Equatorial Pacific: relative paleointensity of the geomagnetic field? *Journal of Geophysical Research* 95 (B8), 12337-12350.
- Thompson, D.W.J., Wallace, J.M., 1998. The Arctic Oscillation signature in the wintertime geopotential height and temperature fields, *Geophysical Research Letters* 25, 1297-1300.

- Thompson, R., Oldfield, F., 1986. Environmental magnetism. George Allen and Unwin Ltd, London.
- Turner, G.M., 1987. A 5000 year geomagnetic paleosecular variation record from western Canada. *Geophysical Journal International* 91 (1), 103-121.
- Turner, G.M., Thompson, R., 1981. Lake sediment record of the geomagnetic secular variation in Britain during Holocene times. *Geophysical Journal of the Royal Astronomical Society* 65, 703-725.
- Valet, J.-P., 2003. Time variations in geomagnetic intensity. *Reviews of Geophysics* 41 (1), 4.1-4.44.
- Verosub, K.L., Mehringer, P.L., Waterstraat, P., 1986. Holocene secular variation in Western North America: paleomagnetic record from Fish Lake, Harney county, Oregon. *Journal of Geophysical Research* 91 (B3), 3609-3623.
- Vilks, G., Wagner, F.J.E., Pelletier, B.R., 1979. The Holocene marine environment of the Beaufort Shelf. Geological Survey of Canada.
- Vimont, D., 2005. The contribution of the interannual ENSO cycle to the spatial pattern of decadal ENSO-like variability. *Journal of Climate* 18, 2080-2092.
- Weeks, R., Laj, C., Endigoux, L., Fuller, M., Roberts, A., Manganne, R., Blanchard, E., Goree, W., 1993. Improvements in long-core measurements techniques: applications in paleomagnetism and paleoceanography. *Geophysical Journal International* 114, 651-662.
- Wiles, G.C., D'Arrigo, R.D., Villalba, R., Calkin, P.E., Barclay, D.J., 2004. Century-scale solar variability and Alaskan temperature change over the past millennium. *Geophysical Research Letters* 31, L15203. doi: 10.1029/2004GL020050.
- Zachos, J., Pagani, M., Sloan, L., Thomas, E., Billups, K., 2001. Trends, Rhythms, and Aberrations in Global Climate 65 Ma to Present. *Science* 292, 686-693.

Zhao, J.P., Cao, Y., Shi, J.X., 2006. Core region of the Arctic Oscillation and the main atmospheric events impact on the Arctic. *Geophysical Research Letters* 33, L22708, doi: 10.1029/2006GL027590.

Zijderveld, J.D.A., 1967. AC Demagnetization of rocks: analysis of results. In: Collinson, D.W., Creer, K.M., Runcorn, S.K. (Eds.), *Methods in Paleomagnetism*. Elsevier, pp. 254-286.



